



저작자표시-비영리-변경금지 2.0 대한민국

이용자는 아래의 조건을 따르는 경우에 한하여 자유롭게

- 이 저작물을 복제, 배포, 전송, 전시, 공연 및 방송할 수 있습니다.

다음과 같은 조건을 따라야 합니다:



저작자표시. 귀하는 원저작자를 표시하여야 합니다.



비영리. 귀하는 이 저작물을 영리 목적으로 이용할 수 없습니다.



변경금지. 귀하는 이 저작물을 개작, 변형 또는 가공할 수 없습니다.

- 귀하는, 이 저작물의 재이용이나 배포의 경우, 이 저작물에 적용된 이용허락조건을 명확하게 나타내어야 합니다.
- 저작권자로부터 별도의 허가를 받으면 이러한 조건들은 적용되지 않습니다.

저작권법에 따른 이용자의 권리는 위의 내용에 의하여 영향을 받지 않습니다.

이것은 [이용허락규약\(Legal Code\)](#)을 이해하기 쉽게 요약한 것입니다.

[Disclaimer](#)

공학박사학위논문

슬릿을 이용하여 횡방향 충격을 받는 원형
튜브의 변형을 줄이는 방법에 대한 연구

A study on reducing the deflection of circular tubes under
transverse impact through slits

2023 년 2 월

서울대학교 대학원

기계항공공학부

도영경

슬릿을 이용하여 횡방향 충격을 받는 원형 튜브의 변형을 줄이는 방법에 대한 연구

A study on reducing the deflection of circular tubes under transverse impact through slits

지도교수 김도년

이 논문을 공학박사 학위논문으로 제출함

2022년 10월

서울대학교 대학원

기계항공공학부

도영경

도영경의 공학박사 학위논문을 인준함

2022년 12월

위원장 : 김윤영 (인)

부위원장 : 김도년 (인)

위원 : 윤병동 (인)

위원 : 노건우 (인)

위원 : Dhadwal, Manoj Kumar (인)

Abstract

Recently, with the development of transportation, the number of vehicles is increasing and the number of traffic accidents is also increasing. Accordingly, the issue of securing collision safety for passengers is rapidly emerging as a key issue. To ensure the passenger's safety, the structure under impact must absorb the impact energy and minimize structural deformation that threaten the safety of passengers. Thin-walled structures are most widely used for structures subjected to impact loads and are used in airplanes, automobiles and trains.

The deformation caused by the crash of thin-walled tube of a cowl cross bar used in a vehicle is investigated. The cowl cross bar causes permanent deflection due to transverse impact, which deflects towards the occupant and causes injury. The safety of the occupants can be ensured by reducing the permanent deflection towards the occupants. The material or geometry must be improved for thin-walled tubes to perform better in crashes. Existing research methods are all focused on the axial loading, and most of them improve collision performance, but bring additional weight increase. A recent trend in the automotive industry is to reduce weight and improve fuel economy.

In this study, the tube deformation subjected to transverse loading was investigated through finite element analysis. Slit patterns are etched between the tube center and the impact plate to decrease the maximum displacement. By adjusting the aspect ratio, the number of slits, and the range of the patterned area, we investigated how the slits affect the tube's maximum deflection. We find that the thin longitudinal slits are effective in reducing the maximum displacement by making the impact energy dissipated by the cross-section into an elliptical shape. Carving slit patterns into the surface of the tube has the additional benefit of not significantly changing the bending rigidity and not increasing the weight.

Keyword : Thin-walled tubes, Finite element analysis, Side impact, Slit pattern

Student Number : 2014-21878

Contents

Abstract	1
Contents	2
List of Figures	5
List of Tables	12
Chapter 1 Introduction	13
1.1 Background and objectives.....	13
1.2 Research outline	15
Chapter 2 Problem definition and design concept	17
2.1 Introduction	17
2.2 Thin-walled structure of the vehicle body	19
2.3 Role of thin-walled tube structure of Cowl Cross Bar (CCB) in collision	20
2.4 Idealized model of thin-walled tube	21
2.5 Design concept for decreasing deflection.....	22
2.6 Collapse mechanism of thin-walled tube under 3-point bending	23
2.6.1 Elastic behavior and ovalisation plateau	25
2.6.2 Structural collapse	27
2.7 Expected collapse mechanism	29
2.8 Plastic deformation	32
Chapter 3 Deformation of the tube without slit patterns	35
3.1 Introduction	35
3.2 Simulation set-up.....	36
3.3 Deformed shape of the tube from finite element analysis	38
3.3.1 Deformed shape of the half tube without slit patterns	38
3.3.2 Deformed shape of full tube without slit patterns	45

3.4 Selection of the part to be engraved with slit patterns.....	48
Chapter 4 Deformation of the tube with single slit	49
4.1 Introduction	49
4.2 Finite element modeling	50
4.2.1 Definition of the sub-domain	50
4.2.2 Definition of the slit pattern on a sub-domain.....	51
4.3 Deformed shape of the tube with different aspect ratio.....	52
4.3.1 Deformed shape of the tube	52
4.3.2 The effect of aspect ratio	56
4.3.3 Energy absorption of the tube	63
4.3.4 The local deformation effect of the slit	65
4.4 Conclusion.....	69
Chapter 5 Deformation of the tube with multiple slits on each sub-	
 domain	70
5.1 Introduction	70
5.2 Deformed shape of the tube with different division direction.....	73
5.2.1 Deformed shape of the tube	73
5.2.2 The effect of different division direction	78
5.2.3 The effect of uniformly arranged slit patterns.....	86
5.2.4 The effect of slit pattern under different loading conditions.....	89
5.3 Deformed shape of the tube with different height.....	93
5.3.1 Deformed shape of the tube	93
5.3.2 The effect of different height	97
5.4 Deformed shape of the tube with different pattern range.....	105
5.4.1 Deformed shape of the tube	105
5.4.2 The effect of different pattern range	111

5.5 Stress concentration in the deformed tube caused by the slit pattern	118
5.5.1 Stress concentration in the thin-walled tube with slit patterns	118
5.5.2 Slit pattern design to reduce stress concentration	121
5.6. The effect of slit pattern on thin-walled tubes of different shapes ...	125
5.7. Conclusion.....	128
Chapter 6 Concluding remark.....	129
Bibliography	131
국 문 초 록	136

List of Figures

- Figure 2.1.** Traffic accident death rate by frontal crash and side crash. Traffic Accident Analysis System.
- Figure 2.2.** Crumple zone and safety zone of the vehicle body.
- Figure 2.3.** Schematic diagram of cowl cross bar of vehicle body.
- Figure 2.4.** Schematic diagram of thin-walled tube structure subjected to transverse impact loading.
- Figure 2.5.** Collapse mechanism of thin-walled tube structure subjected to 3-point bending load. (a) Isometric view. (b) Side view.
- Figure 2.6.** Deformation mechanism of a simply supported cylindrical tube subjected to 3-point bending collapse. (a) Top view. (b) Cross-section I-I of (a). (c) Cross-section II-II of (a).
- Figure 2.7.** The cross section of the thin-walled tube structure in elastic behavior phase.
- Figure 2.8.** The cross section of the thin-walled tube structure in ovalisation plateau phase.
- Figure 2.9.** The cross section shape of the thin-walled tube structure in structural collapse and schematic representation of collapse mode.
- Figure 2.10.** Theoretical model of collapse behavior of thin-walled tube structure subjected to 3-point bending load. (a) Star model. (b) Diamond model.
- Figure 2.11.** Schematic representation of expected deformation shape of thin-walled tube structure subjected to 3-point bending load. (a) Isometric view. (b) Side view. (c) Top view.
- Figure 2.12.** Schematic representation of expected deformation shape of thin-walled tube structure subjected to 4-point bending load. (a) Isometric view. (b) Side view. (c) Top view.
- Figure 2.13.** Expected deformation shape of thin-walled tube structure from impact point to clamped end and cross-section of the center of impact point.
- Figure 2.14.** Expected deformation shape of thin-walled tube structure from the center of the tube structure to impact point and cross-section of the

center of impact point.

Figure 2.15. Expected deformation shape of thin-walled tube structure subjected to 4-point bending load with design concept. The design concept is to apply slit patterns to take more deformation of the tube structure and reduce the center deflection.

Figure 3.1. Problem definition of the thin-walled tube structure subjected to 4-point bending load. (a) Tube structure of cowl cross bar. (b) Idealized model.

Figure 3.2. Finite element model of half thin-walled tube structure with symmetric condition.

Figure 3.3. Isometric view of deformed shape and undeformed shape of thin-walled tube structure under impact loading from nonlinear dynamic finite element analysis.

Figure 3.4. Deformed shape and undeformed shape of thin-walled tube structure under impact loading from nonlinear dynamic finite element analysis. (a) Side view. (b) Top view.

Figure 3.5. Isometric view of deformed shape with effective stress of thin-walled tube structure under impact loading from nonlinear dynamic finite element analysis.

Figure 3.6. Deformed shape with effective stress of thin-walled tube structure under impact loading from nonlinear dynamic finite element analysis. (a) Side view. (b) Top view.

Figure 3.7. Deformed shape and undeformed shape of thin-walled tube structure under impact loading from nonlinear dynamic finite element analysis. Calculated the ellipticity and maximum center deflection.

Figure 3.8. Deformed shape with plastic strain-yy of thin-walled tube. (a) Isometric view. (b) Side view. (c) Top view.

Figure 3.9. Deformed shape with plastic strain-zz of thin-walled tube. (a) Isometric view. (b) Side view. (c) Top view.

Figure 3.10. Deformed shape of thin-walled tube structure with meshes. Two white

squares are rigid plate and impact point.

Figure 3.11. Deformed shape of thin-walled tube structure with smoothed plastic strain-yy. (a) Isometric view. (b) Side view. (c) Top view.

Figure 3.12. Deformed shape of thin-walled tube structure with smoothed plastic strain-zz. (a) Isometric view. (b) Side view. (c) Top view.

Figure 3.13. Selection of the part to be engraved with slit patterns. The blue line represents central plastic hinges, the red line represents, and the black dashed line represents the selected design area.

Figure 4.1. Finite element model with slit patterns and subdivision on the half tube model. (a) Sub-domain. (b) Sub-tube. (c) Half tube.

Figure 4.2. Definition of the slit pattern on a sub-domain.

Figure 4.3. Deformed shape with effective stress of thin-walled tube with a longitudinal slit on each sub-domain. Longitudinal slit consists of A/A_D is 0.023, H/H_D is 0.036, W/W_D is 0.64, and aspect ratio is 0.0625. (a) Isometric view. (b) Side view. (c) Top view.

Figure 4.4. Deformed shape with effective stress of thin-walled tube with a square slit on each sub-domain. Square slit consists of A/A_D is 0.023, H/H_D is 0.146, W/W_D is 0.16, and aspect ratio is 1. (a) Isometric view. (b) Side view. (c) Top view.

Figure 4.5. Deformed shape with effective stress of thin-walled tube with a circumferential slit on each sub-domain. Circumferential slit consists of A/A_D is 0.023, H/H_D is 0.582, W/W_D is 0.04, and aspect ratio is 16. (a) Isometric view. (b) Side view. (c) Top view.

Figure 4.6. Contour map of the non-dimensional maximum center deflection.

Figure 4.7. Contour map of the non-dimensional ellipticity of center cross-section.

Figure 4.8. Contour map of the non-dimensional bending rigidity.

Figure 4.9. Contour map of the non-dimensional torsional rigidity.

Figure 4.10. Force – displacement curve for un-patterned tube and tubes with longitudinal and circumferential slits under transverse impact loading.

Figure 4.11. Reaction force graph as a function of time at the impact point of the

tube without slit patterns. Plastic deformation of the tube occurs in the red region.

Figure 4.12. Reaction force graph as a function of time at the impact point of the tube without slit patterns and the tube with longitudinal and circumferential slits.

Figure 4.13. Deformation shape over time of tubes with longitudinal slits. The red box represents the local deformation shape of the longitudinal slit.

Figure 4.14. Deformation shape over time of tubes with circumferential slits. The red box represents the local deformation shape of the circumferential slit.

Figure 5.1. Definition of slit pattern division from the reference rectangular slit. Six cases of P_N are created for each division. (a) Circumferential division. (b) Longitudinal division.

Figure 5.2. Deformed shape with effective stress of thin-walled tube with a reference slit on each sub-domain. The reference single rectangular slit consists of A/A_D is fixed at 0.058, H/H_D is 0.073, W/W_D is 0.800, and the number of slits on a sub-domain is 1. (a) Isometric view. (b) Side view. (c) Top view.

Figure 5.3. Deformed shape with effective stress of thin-walled tube with the circumferential division slit on each sub-domain. The circumferential division slit consists of A/A_D is fixed at 0.058, H/H_D is 0.018, W/W_D is 0.800, and the number of slits on a sub-domain is 4. (a) Isometric view. (b) Side view. (c) Top view.

Figure 5.4. Deformed shape with effective stress of thin-walled tube with the longitudinal division slit on each sub-domain. The longitudinal division slit consists of A/A_D is fixed at 0.058, H/H_D is 0.073, W/W_D is 0.200, and the number of slits on a sub-domain is 4. (a) Isometric view. (b) Side view. (c) Top view.

Figure 5.5. Non-dimensional maximum center deflection of the tube with respect to the division direction and P_N .

- Figure 5.6.** Non-dimensional ellipticity of the center cross-section of the tube with respect to the division direction and P_N .
- Figure 5.7.** Non-dimensional bending rigidity of the tube with respect to the division direction and P_N .
- Figure 5.8.** Non-dimensional torsional rigidity of the tube with respect to the division direction and P_N .
- Figure 5.9.** Conceptual explanation of tube sections drawn assuming stiff and hinge elements.
- Figure 5.10.** Definition of Part 1 ~ 4 on half sub-tube. Reference refers to a model in which two slits are uniformly arranged in one sub-domain.
- Figure 5.11.** Definition of G1 ~ G6 models designed to have different slit pattern arrangements.
- Figure 5.12.** Definition of boundary condition change according to impact point movement.
- Figure 5.13.** Center deflection of the tube with respect to the position of the impact point and the number of slit patterns (P_N).
- Figure 5.14.** Non-dimensional center deflection of the tube with respect to the position of the impact point and the number of slit patterns (P_N).
- Figure 5.15.** Ellipticity of the tube cross-section with respect to the position of the impact point and the number of slit patterns (P_N).
- Figure 5.16.** Deformed shape with effective stress of thin-walled tube with the thin slit on each sub-domain. The thin reference single rectangular slit has H/H_D of 0.012, W/W_D of 0.800, and the number of slit on a sub-domain is 6. (a) Isometric view. (b) Side view. (c) Top view.
- Figure 5.17.** Deformed shape with effective stress of thin-walled tube with the medium slit on each sub-domain. The medium reference single rectangular slit has H/H_D of 0.024, W/W_D of 0.800, and the number of slit on a sub-domain is 6. (a) Isometric view. (b) Side view. (c) Top view.
- Figure 5.18.** Deformed shape with effective stress of thin-walled tube with the thick

slit on each sub-domain. The thick reference single rectangular slit has H/H_D of 0.036, W/W_D of 0.800, and the number of slit on a sub-domain is 6. (a) Isometric view. (b) Side view. (c) Top view.

Figure 5.19. Non-dimensional maximum center deflection of the tube with respect to the height of the slits and P_N .

Figure 5.20. Non-dimensional ellipticity of the center cross-section of the tube with respect to the height of the slits and P_N .

Figure 5.21. Non-dimensional bending rigidity of the tube with respect to the height of the slits and P_N .

Figure 5.22. Non-dimensional torsional rigidity of the tube with respect to the height of the slits and P_N .

Figure 5.23. Definition of pattern range (2 sub-tubes, 3 sub-tubes, and 4 sub-tubes) on the finite element tube model with sub-domains. (a) Isometric view. (b) Side view.

Figure 5.24. Deformed shape with effective stress of thin-walled tube with the reference slits on 2 sub-tubes. The pattern range is 2 sub-tubes, H/H_D of the reference slit is 0.012, W/W_D is 0.800, the number of slit on a sub-domain is 4, and the number of total slits is 64. (a) Isometric view. (b) Side view. (c) Top view.

Figure 5.25. Deformed shape with effective stress of thin-walled tube with the reference slits on 3 sub-tubes. The pattern range is 3 sub-tubes, H/H_D of the reference slit is 0.012, W/W_D is 0.800, the number of slit on a sub-domain is 4, and the number of total slits is 96. (a) Isometric view. (b) Side view. (c) Top view.

Figure 5.26. Deformed shape with effective stress of thin-walled tube with the reference slits on 4 sub-tubes. The pattern range is 4 sub-tubes, H/H_D of the reference slit is 0.012, W/W_D is 0.800, the number of slit on a sub-domain is 4, and the number of total slits is 128. (a) Isometric view. (b) Side view. (c) Top view.

Figure 5.27. Non-dimensional maximum center deflection of the tube with respect

to the different pattern ranges and P_N .

Figure 5.28. Non-dimensional ellipticity of the center cross-section of the tube with respect to the different pattern ranges and P_N .

Figure 5.29. Non-dimensional bending rigidity of the tube with respect to the different pattern ranges and P_N .

Figure 5.30. Non-dimensional torsional rigidity of the tube with respect to the different pattern ranges and P_N .

Figure 5.31. The stress distribution of the deformed shape of the tube without slit patterns. A red triangle indicates where the maximum effective stress occurs.

Figure 5.32. The stress distribution of the deformed shape of the tube with slit patterns. A red triangle indicates where the maximum effective stress occurs.

Figure 5.33. Original slit pattern means a rectangle slit pattern. Modified slit pattern is a form in which holes are drilled at both ends of the slit pattern, and the blue border line means the final shape of the modified slit pattern.

Figure 5.34. The stress distribution of the deformed shape of the tube with modified slit patterns. A red triangle indicates where the maximum effective stress occurs.

Figure 5.35. Non-dimensional center deflection of the tube with respect to the different slit pattern and P_N .

Figure 5.36. Non-dimensional maximum effective stress of the tube with respect to non-dimensional center deflection and different slit pattern.

Figure 5.37. Undeformed and deformed shapes of un-patterned thin-walled tubes with different cross-section shapes subjected to transverse impact. (a) Circle. (b) Rectangle. (c) Hexagon.

Figure 5.38. Undeformed and deformed shapes of patterned thin-walled tubes with different cross-section shapes subjected to transverse impact. (a) Circle. (b) Rectangle. (c) Hexagon.

List of Tables

- Table 4.1.** Cross-section shape, maximum deflection, ellipticity of center cross-section, bending and torsional rigidity of the tube engraved with longitudinal, square, circumferential slit. All values are calculated as percent with reference to the value of the tube without patterns.
- Table 4.2.** Energy absorption, tube volume, and specific energy absorption for un-patterned tube, longitudinal and circumferential slit patterned tubes.
- Table 5.1.** Cross-section shape, maximum deflection, ellipticity of center cross-section, bending and torsional rigidity of the tube engraved with single, circumferential division, longitudinal division slits. All values are calculated as percent with reference to the value of the tube without patterns.
- Table 5.2.** Number of slits on part 1, 2, 3, 4, maximum deflection, and ellipticity of center cross-section of the tube engraved with slits. All values are calculated as percentage along with the tube without patterns.
- Table 5.3.** Cross-section shape, maximum deflection, ellipticity of center cross-section, bending and torsional rigidity of the tube engraved with thin, medium, thick slits. All values are calculated as percent with reference to the value of the tube without patterns.
- Table 5.4.** Cross-section shape, maximum deflection, ellipticity of center cross-section, bending and torsional rigidity of the tube with pattern range of 2, 3, 4 sub-tubes. All values are calculated as percent with reference to the value of the tube without patterns.
- Table 5.5.** Maximum deflection, cross-section width and height for circle, rectangle and hexagon shaped thin-walled tube. All values were calculated as % based on each tubes without patterns.

Chapter 1

Introduction

1.1 Background and objectives

With the recent advancement of automobile industry, vehicle collision safety, which secures passenger safety in the vehicle crash situation, is becoming more important. In addition, as social awareness of rapid climate change and environmental pollution increases, the importance of vehicle weight reduction technology is increasing for the purpose of improving fuel efficiency and reducing harmful gas emissions in the automobile industry. According to this trend, many studies are being conducted in the automobile industry to improve the existing performance while reducing the weight of the existing body. Recently, the death rate due to traffic accidents is increasing, and passenger safety is a key issue.

The body of a vehicle is largely composed of a crumple zone and a safety zone. Body components of the vehicle's front and rear, excluding the interior area for passengers, are called crumple zones. The crumple zone absorbs the energy of collision and reduces the amplitude of the collision energy. In the event of a collision, the crumple zone is intended to distort as much as possible and lessen the impact energy that is transmitted to the occupants. However, in order to prevent the car's structure from actually affecting the occupants, the safety zone prevents deformation. Specifically, the safety zone absorbs the residual impact with little structural deformation to securely secure the occupant area after the impact is reduced while passing through the crumple zone because of substantial structural deformation.

Numerous studies on various impact traits have been done depending on the structure's purpose. In many automotive parts, thin-walled frameworks are

employed to improve crash resistance [1-5]. One such structure important for the vehicle's crashworthiness is the cowl cross bar [6], which is located between the safety and crumple zone. Its main purpose is to ensure passenger safety by minimizing deformation under side impact. Many studies [7] have been performed to enhance the crashworthiness of structures by changing their geometrical configuration [8-17] or materials [18-22]. However, as additional materials are used, the structure's weight inevitably rises, reducing fuel efficiency and increasing harmful gases in many cases.

This study presents another method to improve the crashworthiness of thin-walled circular tube by carving slits on the tube's surface without putting on more weight. There have been related studies [23-28], but they are primarily biased with respect to the axial impact of the structure. Here, we observe the structure of thin-walled tube subjected to transverse impact and examine ways to decrease the permanent deflection through various slit designs etched into the tube surface. To confirm the outcomes, nonlinear finite element analysis is also performed out.

1.2 Research outline

In Chapter 2, we introduce the thin-walled structure of a vehicle body and the role of thin-walled tube of cowl cross bar under impact loading. Also, we introduce the problem definition of thin-walled tube under impact loading. We study the deformation process of thin-walled structure under 3-point bending. Then, we expand deformation mechanism to the collapse process of thin-walled structure subjected to 4-point bending using the theoretical model established in plastic deformation process of thin-walled tube under bending load. Also, we introduce the advantages of engraving patterns on the structure and present the design concept for reducing the highest center displacement under impact loading.

In Chapter 3, we present idealized model of thin-walled tube of cowl cross bar subjected to transverse impact load. We expand the idealized model and impact situations to the finite element half tube model using geometric symmetry. In addition, we introduce the impact simulation set-up and establish the material properties, boundary and loading conditions for the simulation model of thin-walled tube subjected to transverse impact loading. Then, we perform finite element analysis using un-patterned half tube and full tube models and present the deformation mechanism under impact. We present the selection of the location where the slit patterns will be engraved on the tube for the design concept using the results of nonlinear dynamic analysis.

In Chapter 4, we introduce a method to change the configuration of simulation model of half tube to engrave slit patterns on the selected location. Along the longitudinal axis, we separate the half tube model into 15 sub-tubes, each sub-tube is further divided into 8 sub-domains. Also, we introduce the definition of the rectangular slit pattern on a sub-domain. Then, we present the tube deformation with a rectangular slit on a sub-domain. We select slit patterns with different aspect ratio and compare the deformed tube shape with effective stress to which slit patterns are applied. We introduce the effect of slit patterns with different aspect ratios on the deformation of the tube under transverse impact. The outcomes show that a longitudinal slit pattern is beneficial in reducing the maximum tube center

displacement.

In Chapter 5, we introduce the tube deformation with multiple slit patterns on a sub-domain. We present the method of dividing a single longitudinal slit pattern based on the results and insights obtained in Chapter 4 to investigate the influence of the number of slits on the tube deformation. We divide a single longitudinal slit pattern with respect to both the longitudinal and circumferential axes and investigate the deformation according to the division directions. Also, we expand the effect of the quantity of slit patterns to the effect of the slit's height on the deformation. Furthermore, we expand the effect of the number of slits to the effect of the pattern range on the tube deformation to locally make the plastic deformation of the tube wider. The results in this chapter show that the more the rectangle pattern is divided in the circumferential direction, the thinner the slit pattern, and the wider the pattern range is, the more effective it is to decrease the maximum center displacement.

Chapter 2

Problem definition and design concept

2.1 Introduction

In modern society, the demand for high-tech transportation is increasing every day. Due to this demand, the number of vehicles is continuously increasing, and traffic accidents are inevitably increasing. As a result, passenger safety has become a key issue. For passenger safety, the vehicle structure should be able to convert impact energy into other energies in a collision, thus ensuring the safety of the passengers. Therefore, the structure must absorb impact energy and minimize structural deformations that cause injury to passengers. Among the structures that play this role, the most widely used are thin-walled structures. The reason is that it has many advantages such as cost effective, excellent performance under dynamic loading, and high efficiency. The direction of the advancement of the collision behavior of the thin-walled tube is the direction of material improvement and geometrical improvement. In terms of material improvement, it is a method of replacing existing materials with reinforcing materials such as CFRP. In terms of geometrical improvement, additional materials are added such as rib structures.

However, researches related to the impact performance of thin-walled structures have mostly focused on axial impact loading. The reason for this is that the focus is on situations in which the impact energy is maximally absorbed in the impacted structure in relation to human casualties. In other words, many studies have been conducted from the perspective of maximizing impact absorption. However, it can

be seen that future research is needed by examining the death rate of occupants due to traffic accidents in vehicles in which thin plate structures are widely used. The death rate from side crashes has always been higher than that from frontal crashes.

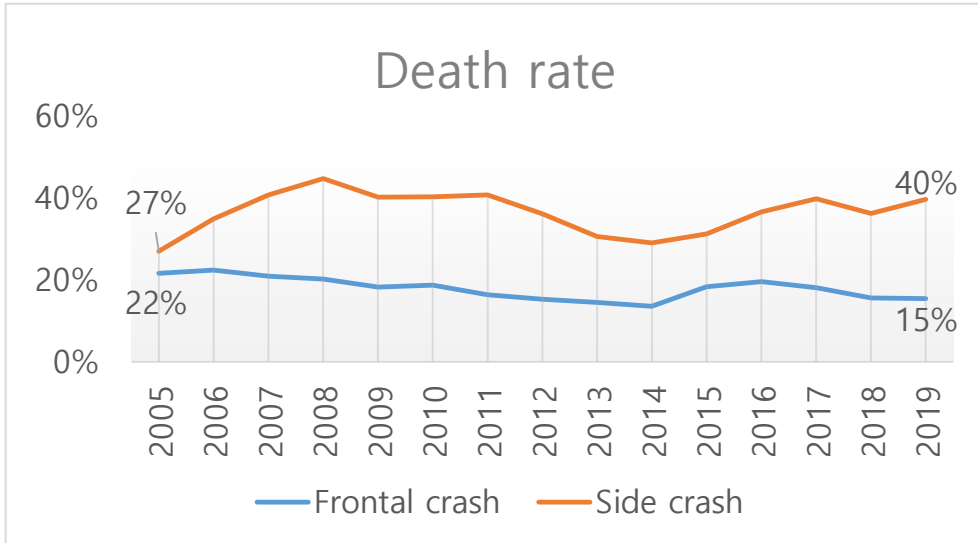


Figure 2.1. Traffic accident death rate by frontal crash and side crash. Traffic Accident Analysis System.

The impact loading conditions of thin-walled structure include axial, oblique, lateral, and bending loading cases. In four impact loading conditions, side crash of vehicle accidents is a kind of lateral or transverse loading. Therefore, we started to study thin-walled structure under transverse loading. Since this study concentrates on the thin-walled tube structure used in vehicles, it is essential to understand the structural role.

In this chapter, we introduce the definition of the problem. Then, we expand the finite element modeling of the problem structure to analysis with deformation shape and physical properties. Also, we present material model, boundary conditions, and contact conditions for nonlinear dynamic finite element analysis of thin-walled tube deformation under transverse impact.

2.2 Thin-walled structure of the vehicle body

The body frame of an automobile consists of a variety of structures, but the most used structures are the thin-walled structures. Before defining the problem, it is important to understand the structural role of each part in the event of a crash to the body frame. A safety zone and crumple zone in general make up a car's body.

The front and back portions of the car's body, not including the cabin, are referred to as the crumple zone. It controls the amount of deceleration and absorbs the force of a frontal or rear strike. To reduce the impact energy transmitted to passengers during the crash, it is designed to deform as much as possible. However, to prevent serious effects from the car body on passengers, the safety zone withstands deformation. To put it another way, when a collision occurs, the safety zone primarily absorbs the residual impact while the crumple zone reduces the impact by large structural deformation.

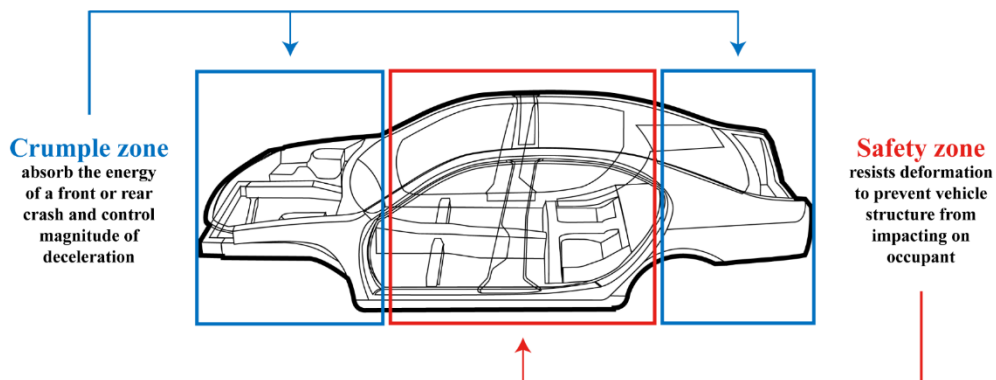


Figure 2.2. Crumple zone and safety zone of the vehicle body.

2.3 Role of thin-walled tube structure of Cowl Cross Bar (CCB) in collision

A steering system, audio system, airbag module, and air conditioning system are supported by a cowl cross bar. The CCB connects to the vehicle body and incorporates these parts into the cockpit module. The front crumple zone's end and the safety zone's beginning are where the cowl cross bar is loaded. When a collision occurs, the thin-walled tube structure of the cowl crossbar absorbs the impact energy and deflects it towards the driver. In particular, since the cowl cross bar has a steering wheel attached to it, deflection occurs in this part and may injure a person. When viewed from the side, the space for the driver is reduced compared to before the collision due to deflection after the collision. Therefore, in terms of collision performance, the objective is to absorb reduced impact force and to decrease the deformation caused by the collision to protect the safety of the occupants.

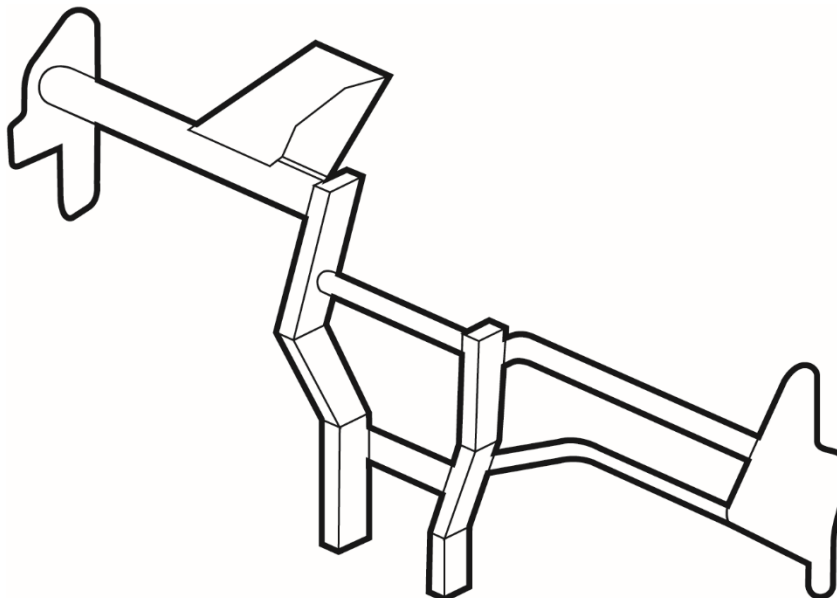


Figure 2.3. Schematic diagram of cowl cross bar of vehicle component.

2.4 Idealized model of thin-walled tube

Although many modules are combined in the thin-walled tube structure of the cowl cross bar, we needed to simplify it to analyze the deformation behavior due to collision. Among cowl cross bars, the most deformed part due to collision occurs and the most important part is where the steering system is attached. Steering system is attached by welding at 1/3 point from both ends of thin-walled tube structure of cowl cross bar. And the thin-walled tube structure has to combine various modules and is attached to the dash board. Therefore, the two points welded to the tube structure are assumed to be the impact points to which the impact energy is transmitted during impact. Also, the thin-walled tube structure's ends are assumed to be clamped. In other words, the schematic diagram of the cowl cross bar of the collision process is a shape in which impact loading is applied to 2 impact points on the thin-walled tube with both ends fixed.

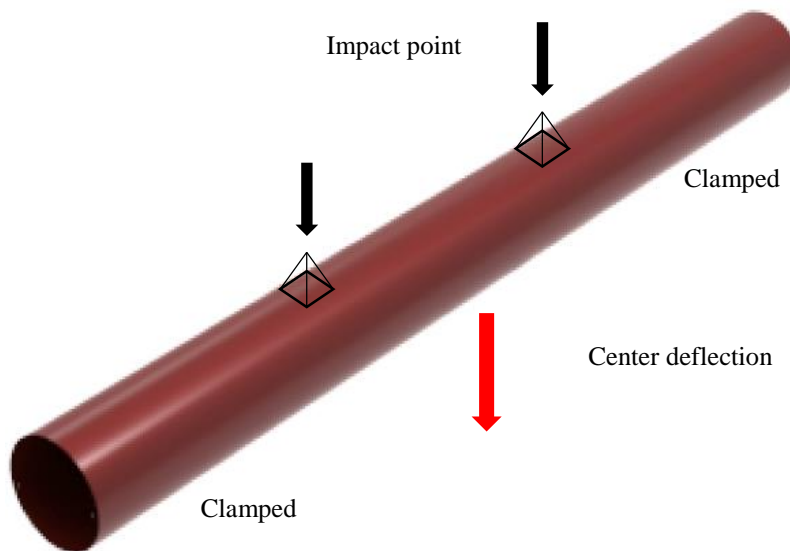


Figure 2.4. Schematic diagram of thin-walled tube structure subjected to transverse impact loading.

2.5 Design concept for decreasing deflection

We introduce the design concept for decreasing the maximum deflection of the thin-walled structure under transverse impact. We have simplified the collision process for cowl crossbars to one where the thin tube is subjected to a 4-point bending type of collision. Therefore, studies on 3-point bending similar to 4-point bending of thin walled tube structures are investigated. Also, we present a description of the collapse mechanism experienced by thin-walled tube structures when there is only one point of impact. Then, we present expected description of the collapse mechanism of the problem which is consist of thin-walled tube and 2 impact points. We present the application of patterns to the tube structure to broaden the range of existing mechanical designs. By applying patterns to a thin walled tube structure without patterns, bending and torsional rigidities can be controlled, thereby expanding the mechanical design area. In particular, by engraving patterns on a structure without patterns, it is possible to realize the new movement that could not be expressed with a structure without patterns. In addition, according to the shape, height, number, and arrangement of the patterns, it is possible to artificially give deformation to a local region of the structure. Also, since the pattern means cut-out of the existing material, it also reduces the bending and torsional rigidities of the structure. However, even if the same area is cut-out, the deformation of the structure can be significantly changed by controlling various parameters of the pattern.

Therefore, this study aimed to reduce the maximum deflection of a thin tube under transverse impact by utilizing the advantages of this patterned structure. Consequently, we present a design concept to decrease the maximum tube deflection under the given conditions.

2.6 Collapse mechanism of thin-walled tube under 3-point bending

There has been extensive use of slender structures as structural members in many engineering applications such as aircraft subfloor, trains, and vehicles. Therefore, there have been numerous studies on thin-walled structures, and most of them are focused on the characteristics of mechanisms that absorb energy and collapse. In particular, to forecast how the thin-walled tube structure will collapse, computer simulation codes such as finite elements have been used or experiments have been relied on. However, these methods took a long time to calculate or were not economical. As a result, many researchers have begun to develop theoretical models based on analysis of computer simulations and experimental findings. With the efforts of many researchers, a theoretical model for thin-walled tube structure under pure or 3-point bending has been established.

Based on the following experimental conditions, a theoretical model for the thin-walled tube structure's collapse mechanism was developed. A thin walled tube structure is placed horizontally and an impact loading or pure bending is applied to the center of the tube with both ends fixed. It is a theoretical forecast of the mechanism by which the thin-walled tube structure collapses in that situation. The theoretical model mainly concentrates on the overall collapse mechanism of slender tube structure and the cross-section at the impact plate and deformation shape in the longitudinal direction. In overall collapse process of the thin-walled tube, it presents how input energy is distributed and dissipated when loading is applied to the slender tube, and how the entire tube's deformation occurs. Cross-sectional deformation at the impact point, it presents how the cross-section undergoes changes when the thin-walled circular tube is subjected to loading.

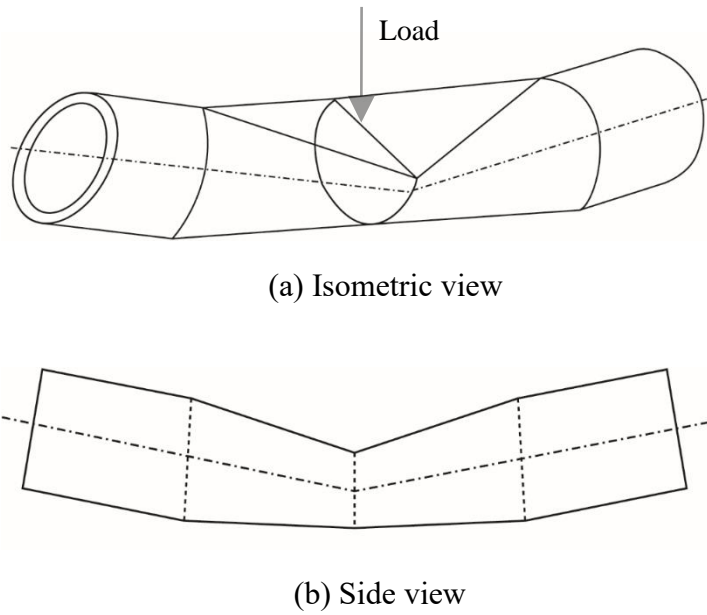


Figure 2.5. Collapse mechanism of thin-walled tube structure subjected to 3-point bending load. (a) Isometric view. (b) Side view.

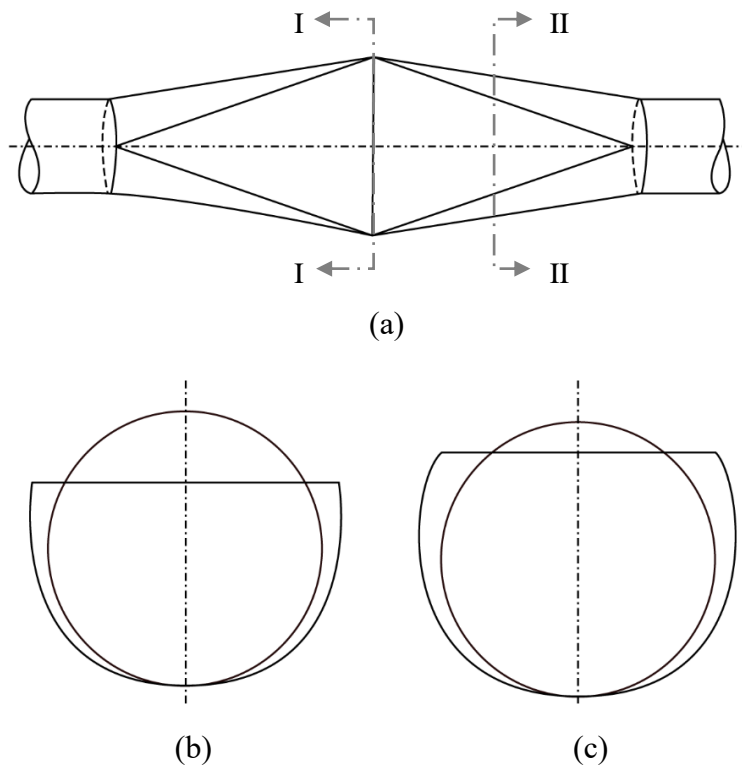


Figure 2.6. Deformation mechanism of a simply supported cylindrical tube subjected to 3-point bending collapse. (a) Top view. (b) Cross-section I-I of (a). (c) Cross-section II-II of (a).

2.6.1 Elastic behavior and ovalisation plateau

Three phases, namely elastic behavior, ovalisation plateau, and structural collapse, generally comprise the mechanism by which thin-walled tube structures collapse [29-42]. There are various deformation modes for each phase.

In elastic behavior, until a spinning at the yield moment, the moment gradually increases with a slope equal. Each phase's analytical model is described.

$$M_y = \frac{2\sigma_y I}{D_0} \quad (2.1)$$

$$\theta_y = \frac{M_y L_0}{EI} \quad (2.2)$$

where L_0 , E , M_y , σ_y , I , D_0 , and θ_y are pure moment length, elastic modulus, yield moment, measured yield stress, second moment of area, outside diameter, and yield rotation angle, respectively.

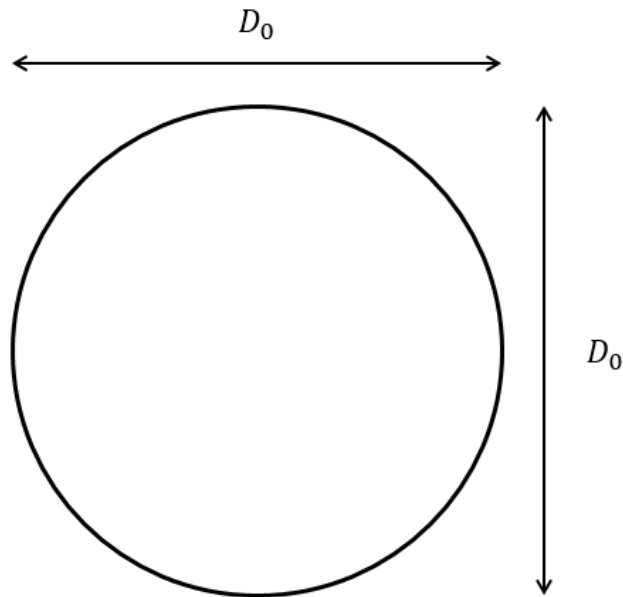


Figure 2.7. The cross section of the thin-walled tube structure in elastic behavior phase.

In ovalisation plateau phase, the thin-walled tube structure's initial circular cross-section changes into an elliptical one. Also, in this ovalisation plateau phase, the substance exhibits mild kinematic hardening. As the bending rotation increases, it is presumed that the bending moment will stay unchanged.

$$M_{ovalised} = S_{ovalised} \sigma_y = \frac{4}{3} (R_v^2 R_h - R_{vi}^2 R_{hi}) \sigma_y \quad (2.3)$$

where R_h , R_v , R_{hi} , R_{vi} , $S_{ovalised}$, and σ_y are external horizontal radius, external vertical radius, internal horizontal radius, internal vertical radius, ovalised tube's plastic section modulus, and ovalised tube's measured yield stress.

$$R_h = \frac{D_h}{2} = 0.55D_0 \quad \text{and} \quad R_v = \frac{D_v}{2} = 0.45D_0 \quad (2.4)$$

$$R_{hi} = (R_h - t) \quad \text{and} \quad R_{vi} = (R_v - t) \quad (2.5)$$

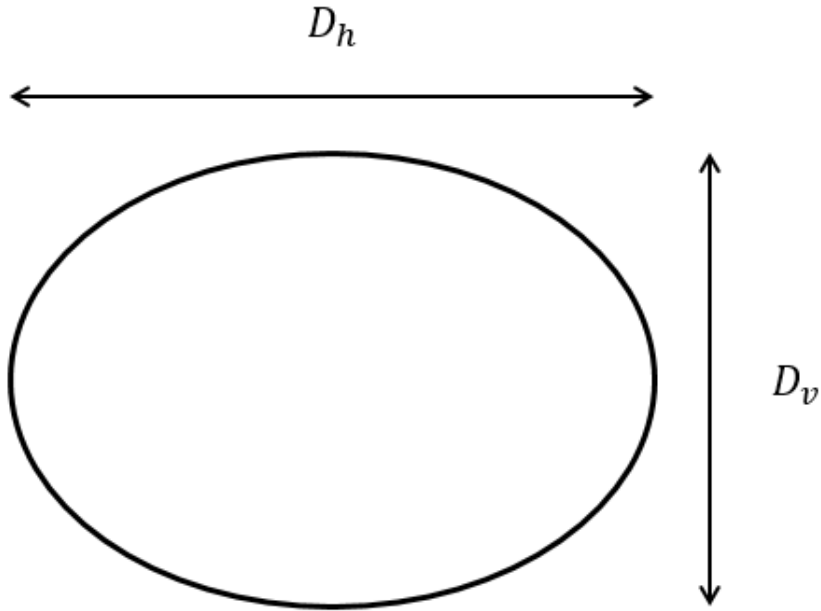


Figure 2.8. The cross section of the thin-walled tube structure in ovalisation plateau phase.

2.6.2 Structural collapse

In the structural collapse phase [43-54], the tube structure starts to crumble and the load capability decreases rapidly. In particular, plastic folding occurs in the plastic zone. The plastic zone consists of central plastic hinges and curved plastic hinges, and is divided into flattened regions and circular regions by these hinges. In general, the central plastic hinge is created in the middle of the impact point, and the oblique curved plastic hinge is formed in the tube's longitudinal direction starting from the central plastic hinge.

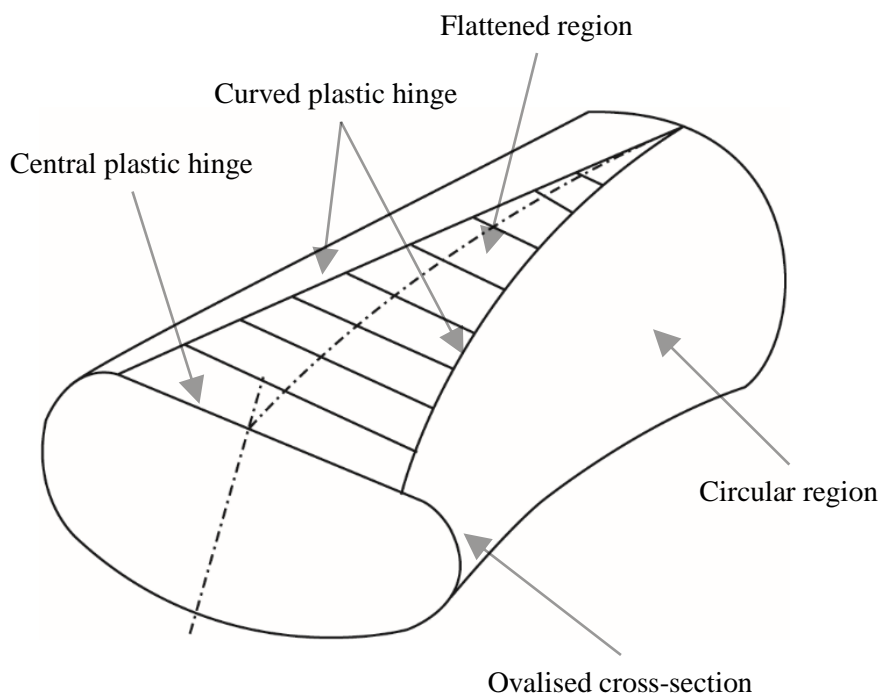
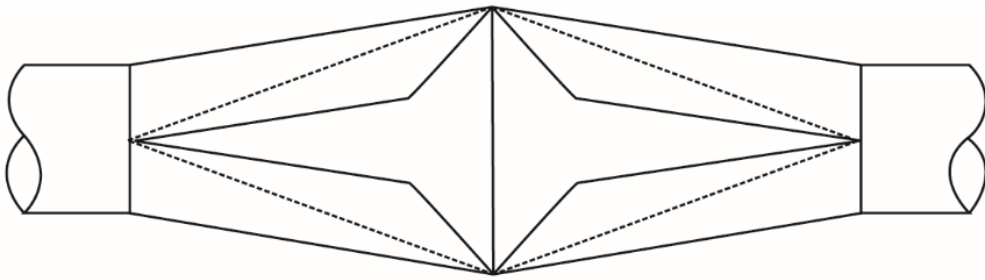
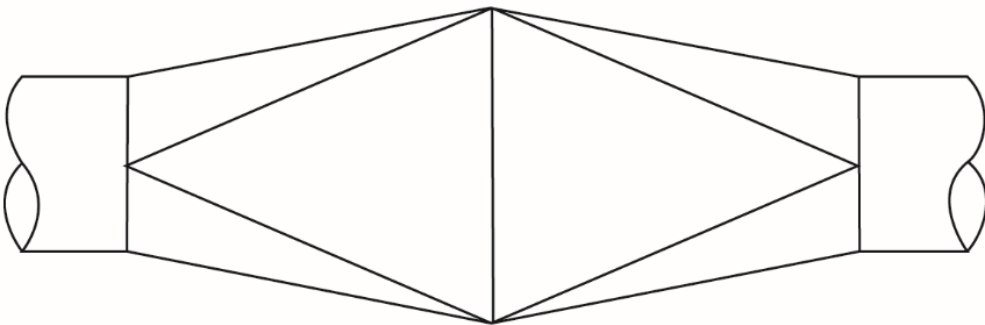


Figure 2.9. The cross section shape of the thin-walled tube structure in structural collapse phase and schematic representation of collapse mode.

When the general thin-walled tube structure exhibits collapse behavior, the central plastic hinge is formed and the plastic folding part is the structure in which the maximum deflection occurs. When viewed from the side, the collapse behavior is in the shape of a sagging curve, and when viewed from above, the central plastic hinge and oblique curved plastic hinge form a rectangle shape. Therefore, depending on the shape of the top view, the theoretical model of the collapse process of the thin-walled circular tube developed by many researchers is referred to as a star or diamond model.



(a) Star model



(b) Diamond model

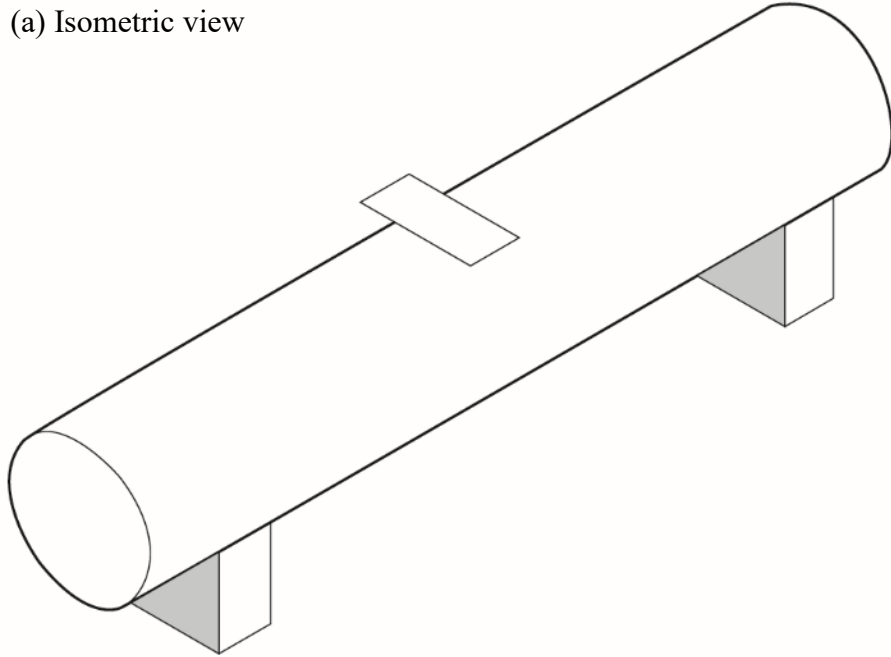
Figure 2.10. Theoretical model of collapse behavior of thin-walled tube structure subjected to 3-point bending load. (a) Star model. (b) Diamond model.

2.7 Expected collapse mechanism

In the previous section, we looked at the collapse process for thin-walled structure subjected to 3-point bending or pure bending. However, the problem to be solved in this research is the circular thin tube of a cowl cross bar, which has a 4-point bending form with two impact points, unlike the aforementioned 3-point bending with one impact point. Although the number of impact points is different for 4-point bending and 3-point bending cases, in the case of the thin-walled tube structure of cowl cross bar, it is similar to 3-point bending cases because the impact points of thin-walled tube structure of the problem are placed at $1/3$ point from the both ends. When dividing in half based on the tube's center, only one impact point is equal to one side. Assuming this state divided in half, it can be seen that the impact point in the 3-point bending state is slightly displaced rather than in the middle.

The collapse process of the thin-walled circular tube of the cowl cross bar under the given conditions can be predicted from the aforementioned theoretical model of 3-point bending. First, we approximated the expected deformation shape of thin-walled circular tube subjected to 3-point bending load. As studied through the theoretical model of 3-point bending, the sagging curve shape is predicted in the side view, and the deformation of the diamond shape is predicted in the top view at the impact point. Next, we approximated the expected deformation shape of thin-walled circular tube subjected to 4-point bending load. When predicting 4-point bending under a given condition, it is predicted that two concaves will occur depending on the impact point on the top line, although the sagging curve shape is on the bottom line of the tube from the side view. Also, in the top view, it is predicted that the deformation of two diamond shapes will occur depending on the impact point.

(a) Isometric view



(b) Side view



(c) Top view

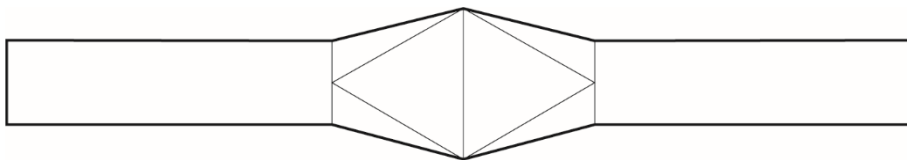
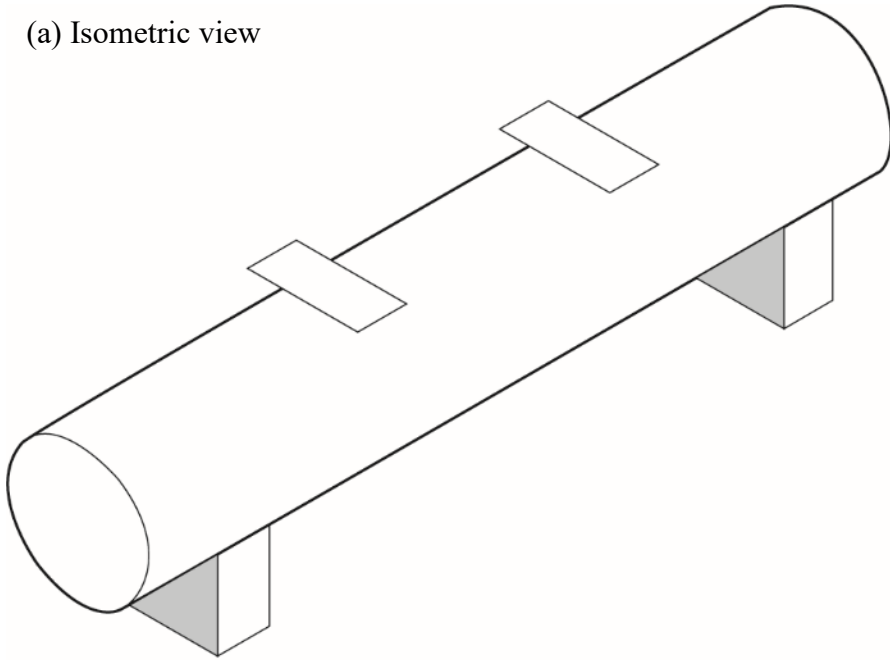


Figure 2.11. Schematic representation of expected deformation shape of thin-walled tube structure subjected to 3-point bending load. (a) Isometric view. (b) Side view. (c) Top view.

(a) Isometric view



(b) Side view



(c) Top view

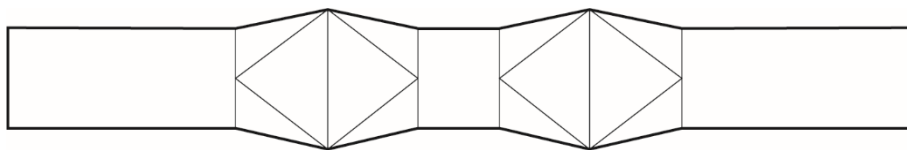


Figure 2.12. Schematic representation of expected deformation shape of thin-walled tube structure subjected to 4-point bending load. (a) Isometric view. (b) Side view. (c) Top view.

2.8 Plastic deformation

In the expected collapse mechanism of 4-point bending, the aforementioned star model or diamond model is expected to occur at two impact points. When predicting the collapse behavior of thin-walled circular tube, it is expected to have a sagging curve shape similar to 3-point bending. However, if we observe the predicted deformed shape of the thin-walled circular tube from the side, we can clearly find that it is different from the 3-point bending shape. The central portion of tube is the primary distinction between the two cases. In the collapse behavior of thin-walled tube structure subjected to 3-point bending case, the most deformed cross-section shape is the center of the tube and impact point. In the collapse characteristics of tube structure under 4-point bending case of cowl cross bar, the most deformed cross section shape is the impact point, not tube's center. Divide the tube's center in half to reveal this difference in detail.

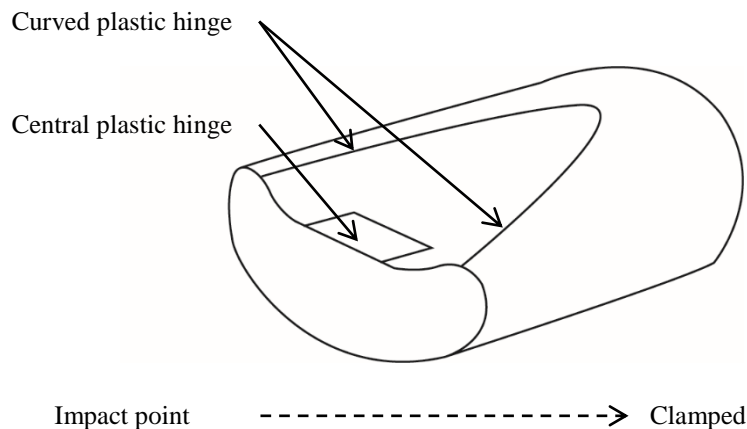


Figure 2.13. Expected deformation shape of thin-walled tube structure from impact point to clamped end and cross-section of the center of impact point.

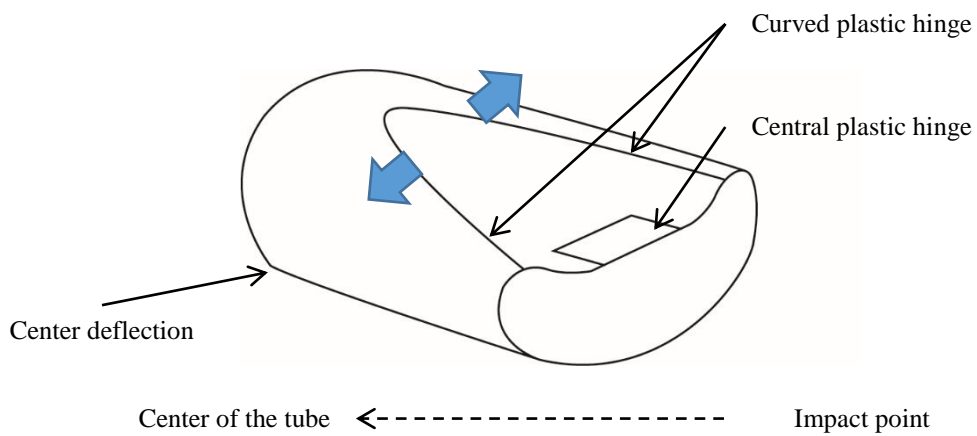


Figure 2.14. Expected deformation shape of thin-walled tube structure from the center of the tube structure to impact point and cross-section of the center of impact point.

In the case of 4-point bending, it is anticipated that it will go through three stages, which is similar to the collapse process of thin-walled circular tube under 3-point bending. Also, in two cases, the location of the impact is different, but the maximum collapse occurs in the cross-section of the impact point. Deformation at this impact point can be viewed as plastic folding, which in both cases results from the formation of plastic hinges.

In the deformed shape of structure under 3-point bending case, the deformed shape is sagging curve when we viewed from the side and maximum deflection of the tube is occurred at the tube's center. In the deformed shape of tube structure subjected to 4-point bending case, the deformed shape is sagging curve when we viewed from the side. Also, the maximum deflection occurs at the tube center. However, when the cross-section shape is compared along the tube's center line, the difference between the two cases is clearly revealed. In the case of 3-point bending, from the clamped end to the center of the tube, it gradually turns from a circular shape to an elliptical shape, and the cross section shape with the most deformation appears as soon as it reaches the center. However, in the case of 4-point bending,

from the clamped end to the center of the tube, the shape gradually changes from a circle to an oval shape, and then appears again as a circle shape as it passes through the impact point. In other words, the most deformed cross section shape appears at the impact point.

From the expected collapse characteristics of thin-walled circular tube under 4-point bending, it could be applied to the problem of cowl cross bar we have. The purpose of this study is to reduce the maximum deflection by engraving a slit pattern on the tube's surface in the case of thin-walled circular tube under 4-point bending. Therefore, based on the predicted collapse characteristics of the tube structure of cowl cross bar, a design concept is established to reduce maximum deflection. When viewed from the side of the cross section, the most deformation occurs at the impact point, and the deformation decreases toward the center of the tube. Therefore, the design concept to reduce the maximum deflection in this study is to extend the deformation range from the impact point to the center of the tube.

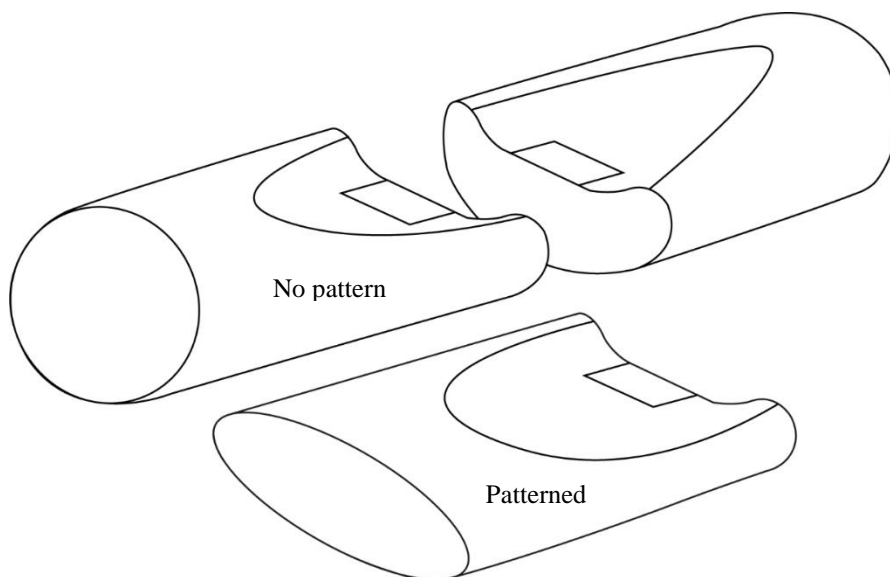


Figure 2.15. Expected deformation shape of thin-walled tube structure subjected to 4-point bending load with design concept. The design concept is to apply slit patterns to take more deformation of the tube structure and reduce the center deflection.

Chapter 3

Deformation of the tube without slit patterns

3.1 Introduction

In this chapter, we present the procedure for performing finite element analysis on thin-walled tube structure subjected to 4-point bending before confirming the aforementioned design concept. In particular, it is intended to confirm through finite element analysis whether the collapse characteristics of the tube structure of the cowl cross bar predicted under the given impact loading conditions occurs.

We introduce the process of modeling a thin tube structure under a given condition to a 4-point bending case with a finite element model by simplifying it. Then, for the efficiency of analysis time, we introduce the use of a half model to which symmetry is applied rather than the full model.

In order to apply the design concept of reducing the deflection of the structure by engraving the pattern mentioned in the previous chapter, the deformation shape of the structure without the slit pattern is analyzed. We present a method to analyze the collapse mechanism of the unpatterned tube and to select the position where the slit patterns will be engraved by comparing the predicted collapse mechanism.

3.2 Simulation set-up

We use a cowl cross bar of vehicles as the example thin-walled tube structure for this study. It is modeled as a thin tube fixed at all ends subjected to transverse impacts at two locations. Because it is crucial for the design of cowl cross bars for driver safety, the variable we aim to minimize is the deflection of the bottom-center point of the tube. Finite element analysis is used to determine the tube's deformation under these conditions for the half model with symmetrical conditions. The analysis's primary considerations are the tube's center displacement, and the bending rigidity.

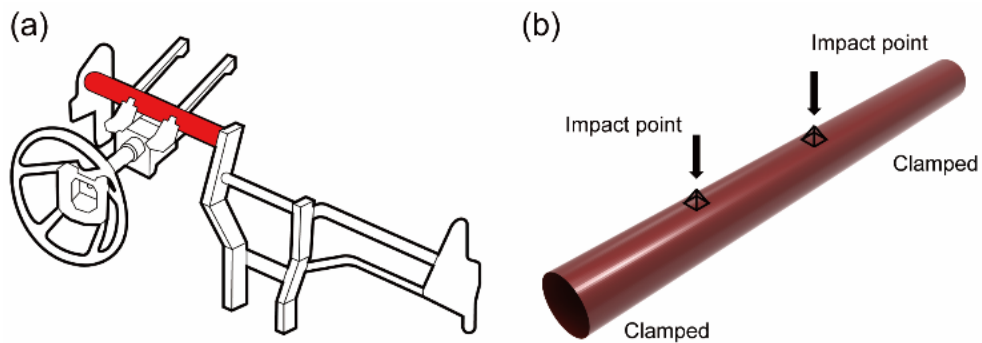


Figure 3.1. Problem definition of the thin-walled tube structure subjected to 4-point bending load. (a) Tube structure of cowl cross bar. (b) Idealized model.

The tube has an inner diameter of 68.6 mm and an outer diameter 71.4 mm, and it is 750 mm long. Its thickness is 1.4 mm. The half model was built to simulate transverse impact using a square steel plate with a mass and edge length of 100 kg and 30 mm. It is dropped with an initial speed of 5,000 mm/s from a height of 2 mm above the top surface of the tube, having an impact on one-third of the tube's center. A plastic-cyclic material model with a Young's modulus of 207 GPa, a Poisson's ratio of 0.3, a mass density of 7.85E-6 kg/mm³, and the yield stress (σ_y) of 255 MPa is used to simulate the material properties of the tube. The Armstrong-Fredrick nonlinear kinematic hardening rule uses the linear constant (**h**) of 280 GPa and the

nonlinear constant (ζ) of 1,300 with the relationship between stress (σ) and plastic strain (ϵ^P).

$$\sigma = \sigma_y + \frac{h}{\zeta} \{1 - \exp(-\zeta \epsilon^P)\} \quad (3.1)$$

The tube model is subjected to two contact conditions. Between the impactor and the tube, the single-sided contact condition is used, while the double-sided contact condition is used to consider the tube's self-contact. We use four node shell elements with roughly 240,000 nodes to build finite element half tube models while taking symmetry into account. Using the commercial analysis software ADINA, impact simulation is carried out. Dynamic-implicit analysis is carried out for 0.04 s with a 0.00005 s time increment.

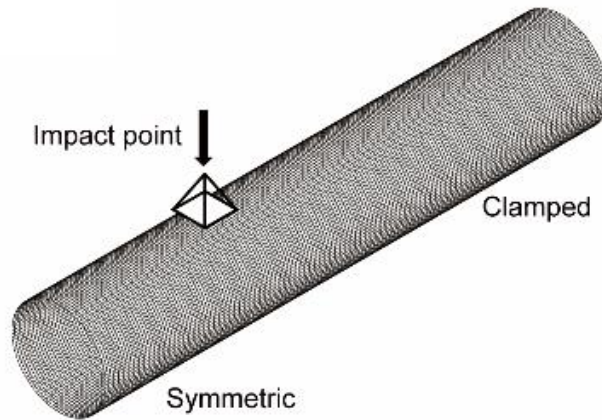


Figure 3.2. Finite element model of half thin-walled tube structure with symmetric condition.

3.3 Deformed shape of the tube from finite element analysis

3.3.1 Deformed shape of the half tube without slit patterns

For the unpatterned tube, we conducted the finite element analysis. The thin-walled tube's deformed shape is a u-shaped curve with the anticipated highest vertical deflection at the center. The stress is primarily concentrated on the fixed end, and the impact point shows the largest lateral deformation. The cross-section of the center, which has the highest deflection, has a mild oval shape and an ellipticity (e) of 0.2057 (e_{ref}).

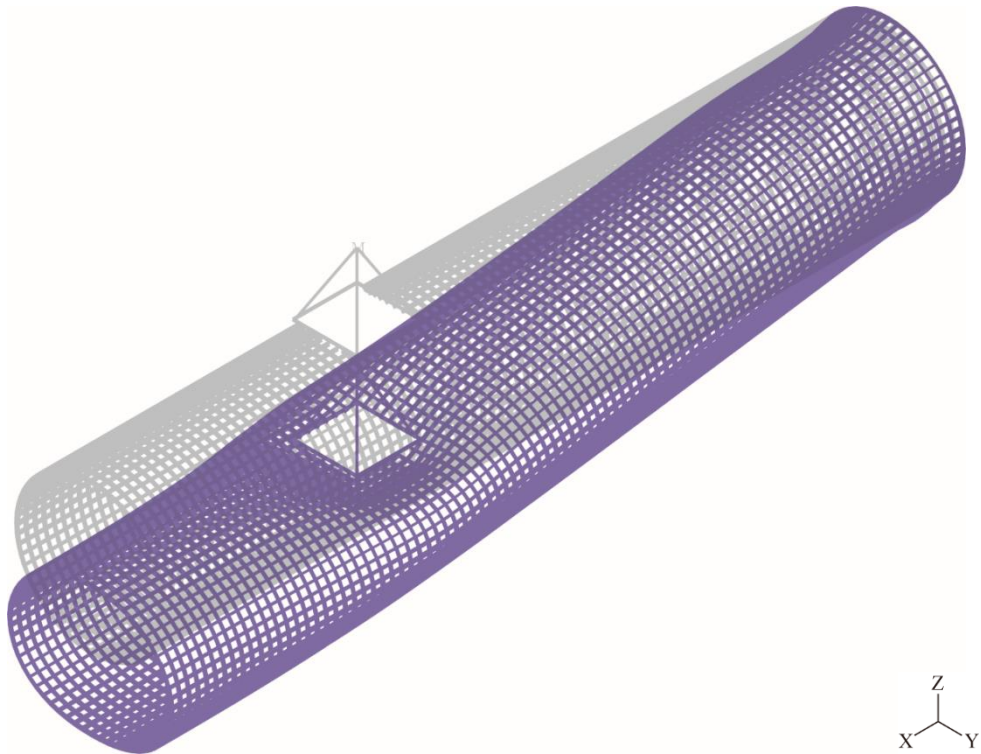


Figure 3.3. Isometric view of deformed shape and undeformed shape of thin-walled tube structure under impact loading from nonlinear dynamic finite element analysis.

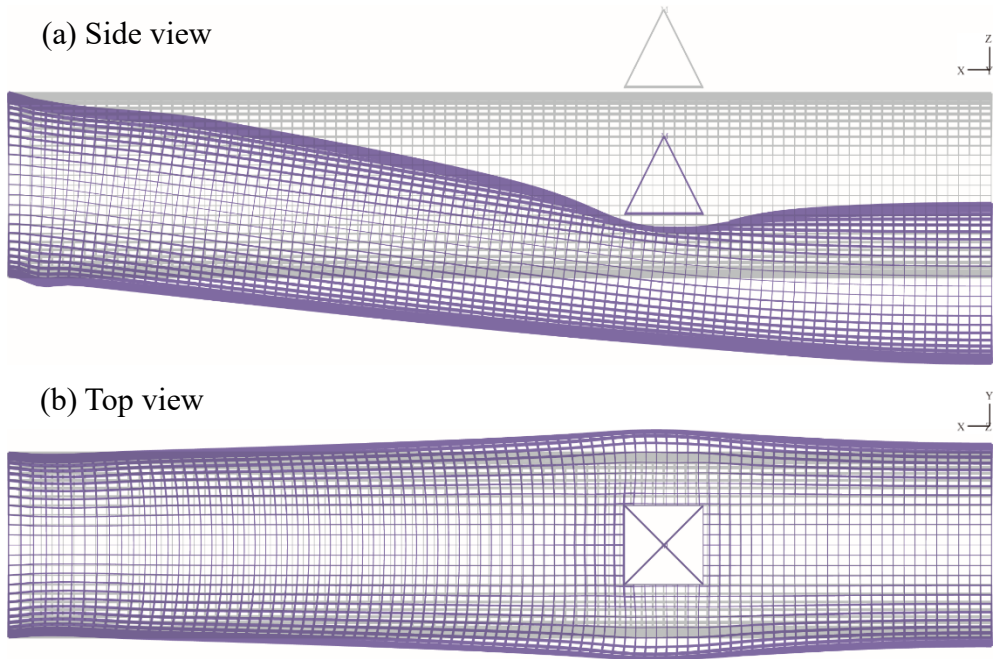


Figure 3.4. Deformed shape and undeformed shape of thin-walled tube structure under impact loading from nonlinear dynamic finite element analysis. (a) Side view. (b) Top view.

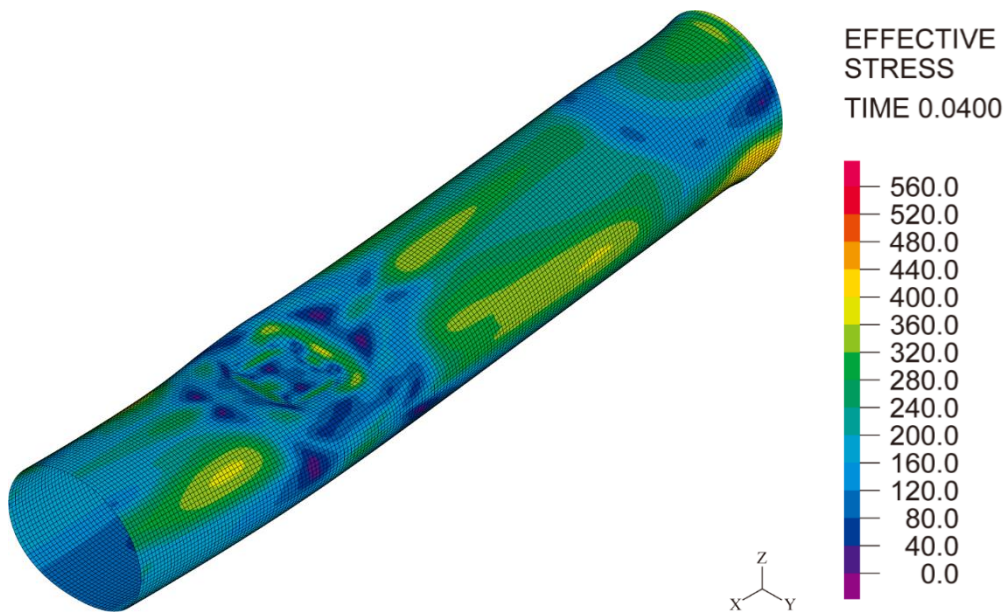
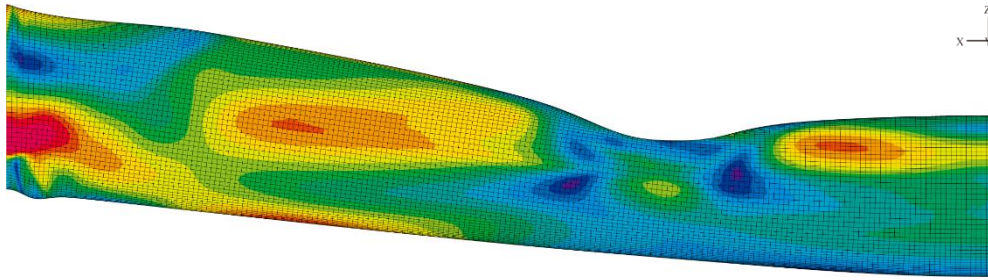


Figure 3.5. Isometric view of deformed shape with effective stress of thin-walled tube structure under impact loading from nonlinear dynamic finite element analysis.

(a) Side view



(b) Top view

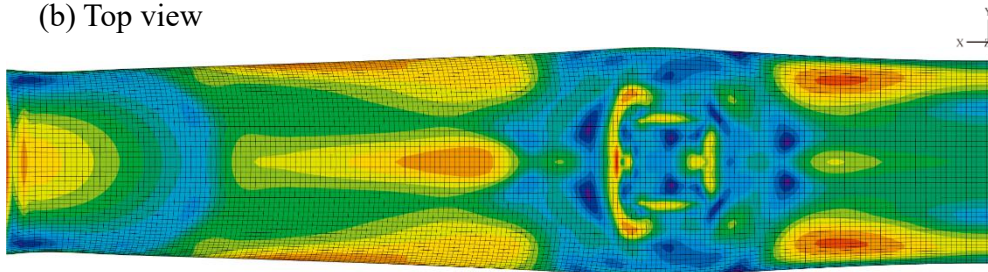


Figure 3.6. Deformed shape with effective stress of thin-walled tube structure under impact loading from nonlinear dynamic finite element analysis. (a) Side view. (b) Top view.

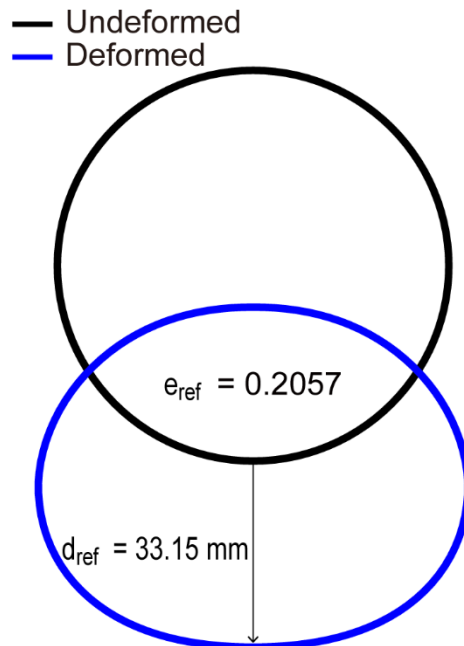
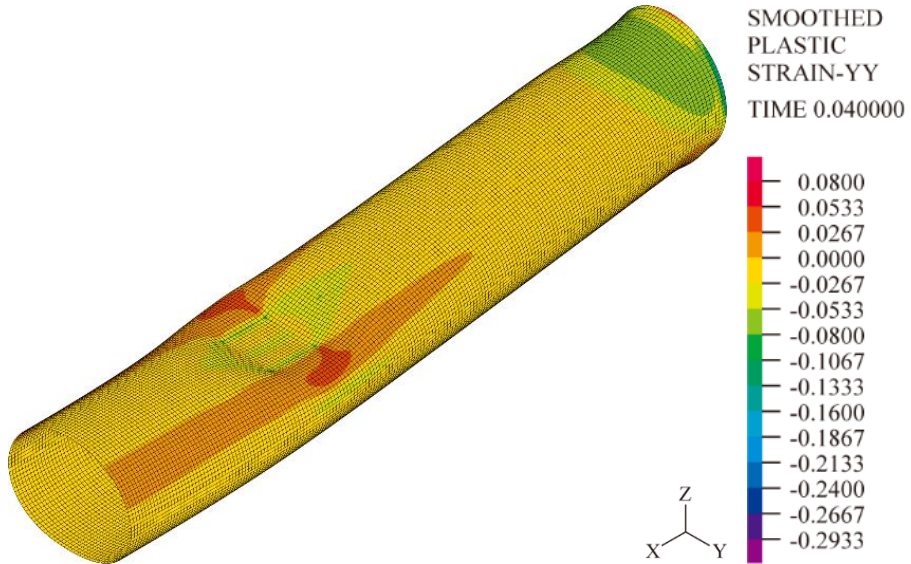


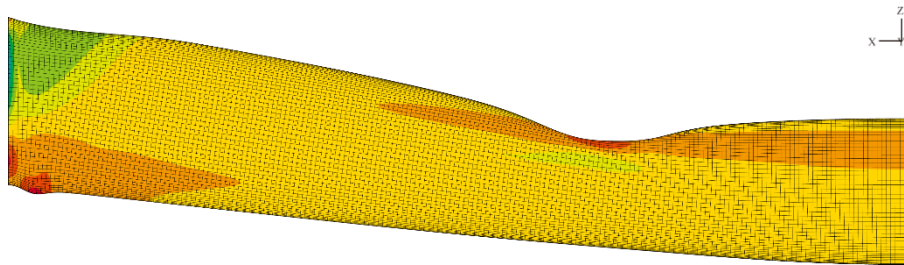
Figure 3.7. Deformed shape and undeformed shape of thin-walled tube structure under impact loading from nonlinear dynamic finite element analysis. Calculated the ellipticity and maximum center deflection.

The thin-walled tube subjected to 4-point bending's deformed shape was discovered through nonlinear dynamic finite element analysis, and it resembles the shape that the theoretical model for the thin tube under 3-point bending predicted. Through the side view of the deformed tube, the bottom line is deformed into a sagging curved shape, and the top line of the tube is deformed to deform into a single concave at the impact position. When the tube's deformed shape is viewed from top, at the impact point, the deformation similar to that expected with the diamond shape occurred. When examining the change of center cross-section, the existing circular shape when no loading is applied is slightly deformed into an elliptical shape after loading is applied. In particular, we focused on the tube center and impact position in the side view. The reason is that the impact point is vertically deformed by the impact loading, but the deformation is less at the center than the impact position. If the patterns are applied to these areas, it means that there is a possibility of causing more deformation between the impact point and the center. It is also related to the cross-section deformation shape, and there is a possibility of transforming slightly elliptical cross-section shape into an elliptical shape in which the minor axis is shorter in length while the major axis is longer. To reduce the maximum central deflection of the tube, more given impact energy must be consumed on plastic deformation, and it is necessary to change the plastic deformation geometry to a geometry that reduces the maximum central deflection. In other words, it is necessary to increase the plastic deformation region in that region by allowing more impact energy to be transferred from the impact position towards the tube center. By applying the patterns on the tube to generate more plastic deformation between the impact position and the tube center, the energy consumed for vertical displacement of the overall tube structure is reduced. This effect induces the reduction in the maximum center deflection of the tube.

(a) Isometric view



(b) Side view



(c) Top view

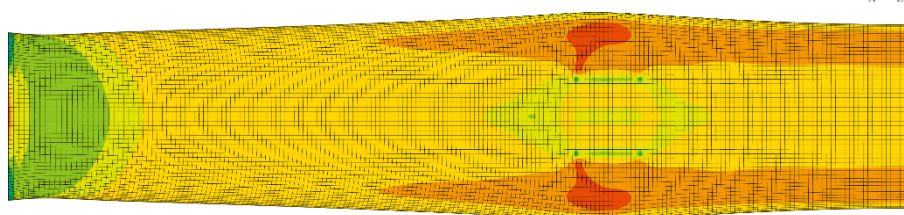
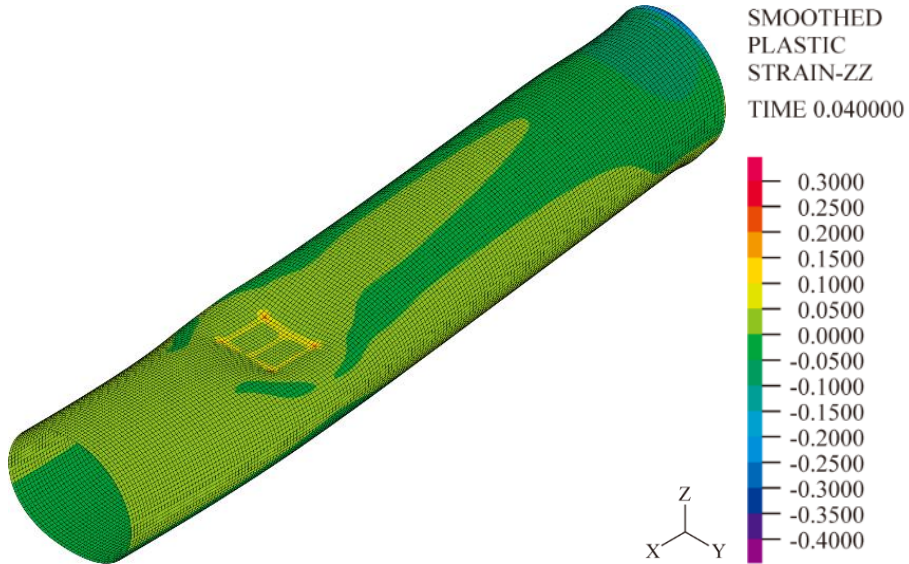
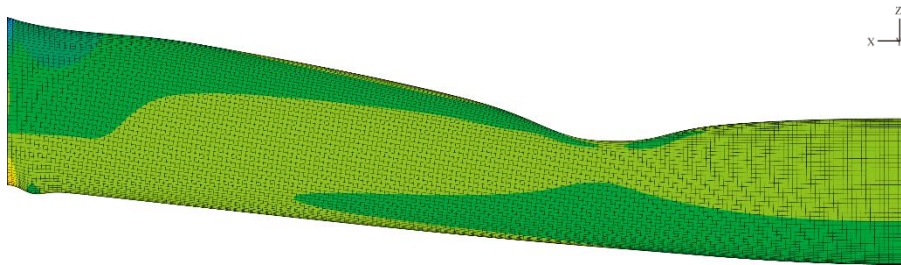


Figure 3.8. Deformed shape with plastic strain-yy of thin-walled tube. (a) Isometric view. (b) Side view. (c) Top view.

(a) Isometric view



(b) Side view



(c) Top view

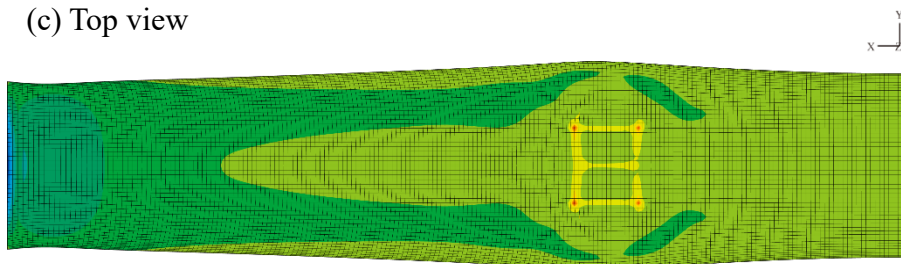


Figure 3.9. Deformed shape with plastic strain-xx of thin-walled tube. (a) Isometric view. (b) Side view. (c) Top view.

Next, to present the local deformation, we investigated the deformed tube shape with plastic strain using nonlinear dynamic analysis. In the tube deformed shape with plastic strain-yy, it means plastic strain in the y-axis direction, and color indicates whether it is stretched or contracted compared to the initial mesh. The isometric view of deformed shape of the tube with plastic strain-yy shows that the most stretched at the end of the square rigid plate at the impact point. The top view of the tube's deformed shape with plastic strain-yy shows that the sides of the tube are stretched from the impact plate to the center of the tube. However, except for the side of the tube, most of it is in a non-stretched state. In other words, there is a possibility that more plastic strain can be generated in the non-stretched part by applying patterns to the tube. In the deformed tube's shape with plastic strain-zz, it means plastic strain in the z-axis direction, and color indicates whether it is stretched or contracted compared to the initial mesh. The deformed tube with plastic strain-zz shows the diamond shape deformation of the theoretical model at the impact point.

Based on this discovery, we postulate that the tube's maximum displacement can be decreased if the center area can deform horizontally more. This would increase the ellipticity of the tube's cross-section. It would be preferable, in other words, if the impact energy could be used to further crush the central region rather than to move it. By conducting the simulation analysis for the tubes with different slits carved between the tube's center and impact plate as described in the following sections, we investigated this hypothesis.

3.3.2 Deformed shape of full tube without slit patterns

In general, only the half model of the tube is analyzed for efficiency of analysis time, but in this case, the full thin-walled tube model was also analyzed to confirm the entire tube's deformation. In isometric view of deformed shape of thin-walled tube structure without slit patterns, it looks similar to the shape predicted based on the theoretical model mentioned in the previous chapter. It can be confirmed that a star or diamond shape is formed and plastic folding occurs as in the theoretical model at two square-shaped impact points. Also, it is confirmed that plastic deformation of the tube is formed as oblique curved plastic hinges are formed to the right and left of impact point along the longitudinal direction of the tube.

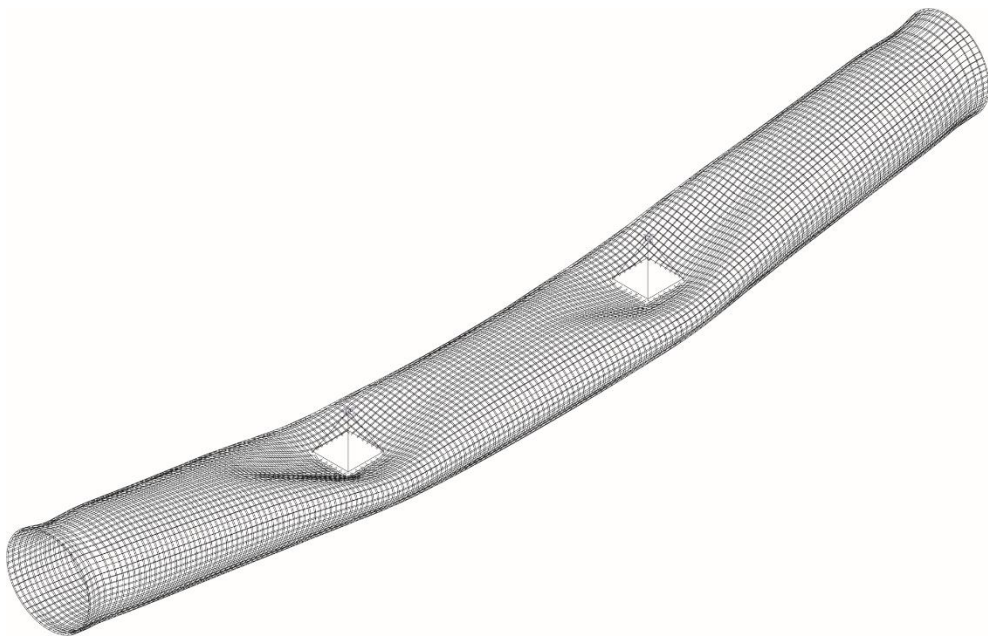


Figure 3.10. Deformed shape of thin-walled tube structure with meshes. Two white squares are rigid plate and impact point.

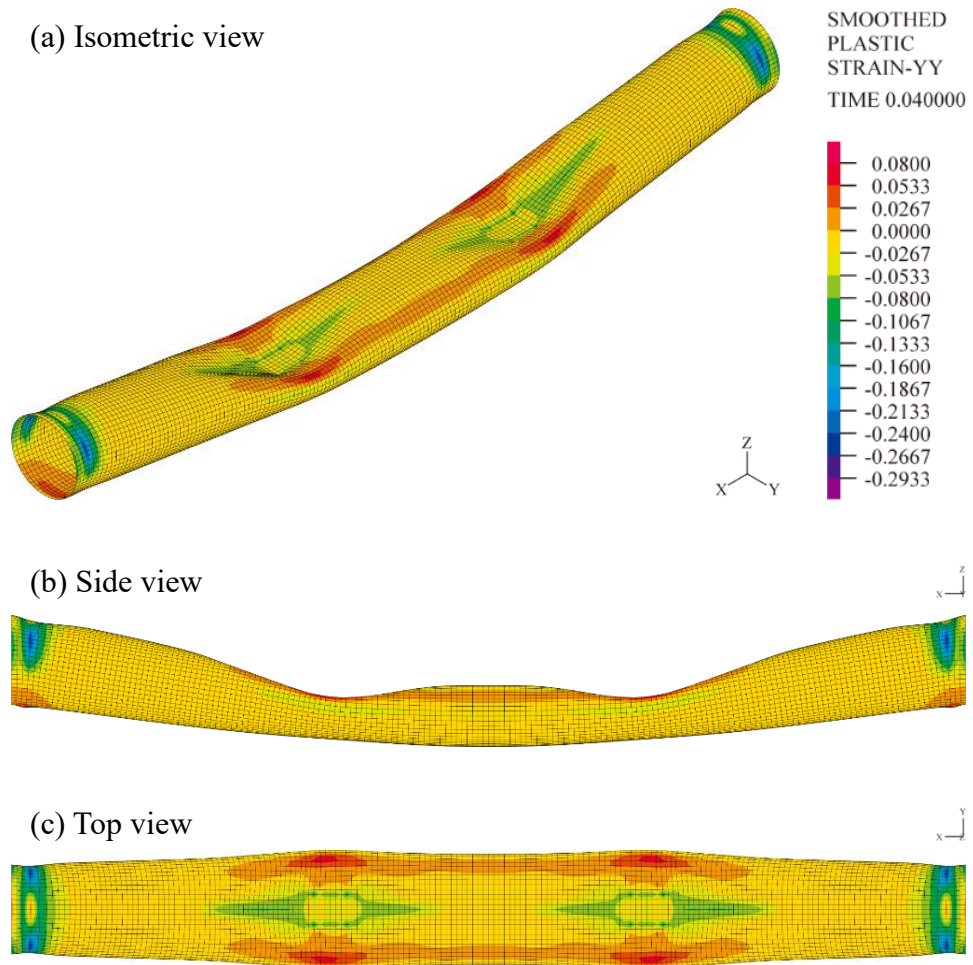


Figure 3.11. Deformed shape of thin-walled tube structure with smoothed plastic strain-yy. (a) Isometric view. (b) Side view. (c) Top view.

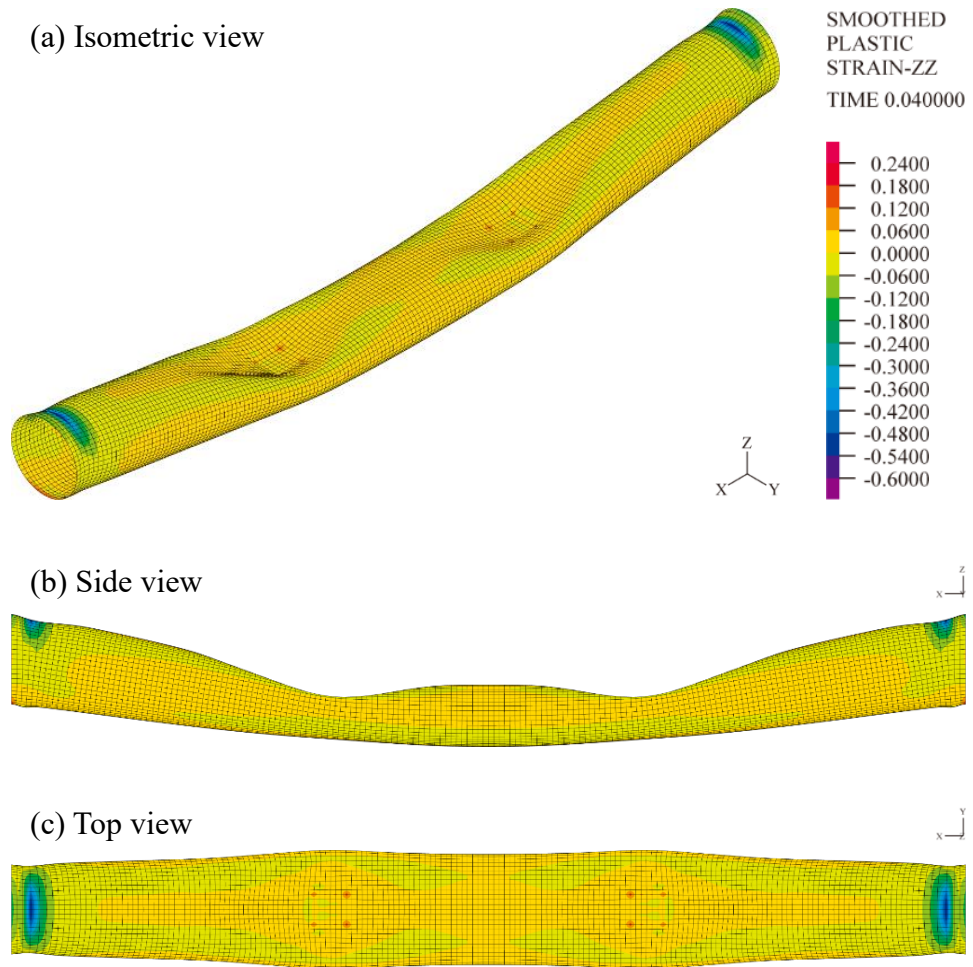


Figure 3.12. Deformed shape of thin-walled tube structure with smoothed plastic strain-zz. (a) Isometric view. (b) Side view. (c) Top view.

3.4 Selection of the part to be engraved with slit patterns

In side view of deformed shape of thin-walled tube structure without slit patterns, in the impact point part, plastic folding occurs and shows a concave shape, and it shows a shape that recovers closer to the original tube phase as it goes to the center of the tube. From the point of view of cross section, the cross-section at the impact plate shows the shape in which the most deformed plastic deformation occurs, and as it passes through the impact point and gets closer to the tube center, the cross-section shape recovers to a circular shape again. In the collapse process of the thin-walled circular tube, impact energy is transferred to impact point, and after plastic deformation occurs there, the energy is dissipated as it is transferred to the left and right. In other words, impact energy is consumed in plastic deformation, and there is a possibility that additional deformation can occur by examining the cross-section deformation state between the tube center and the impact point. Therefore, we selected the part where the slit pattern to be engraved to reduce maximum deflection in the thin-walled circular tube under transverse loading is between the tube center and the impact plate in the half model.

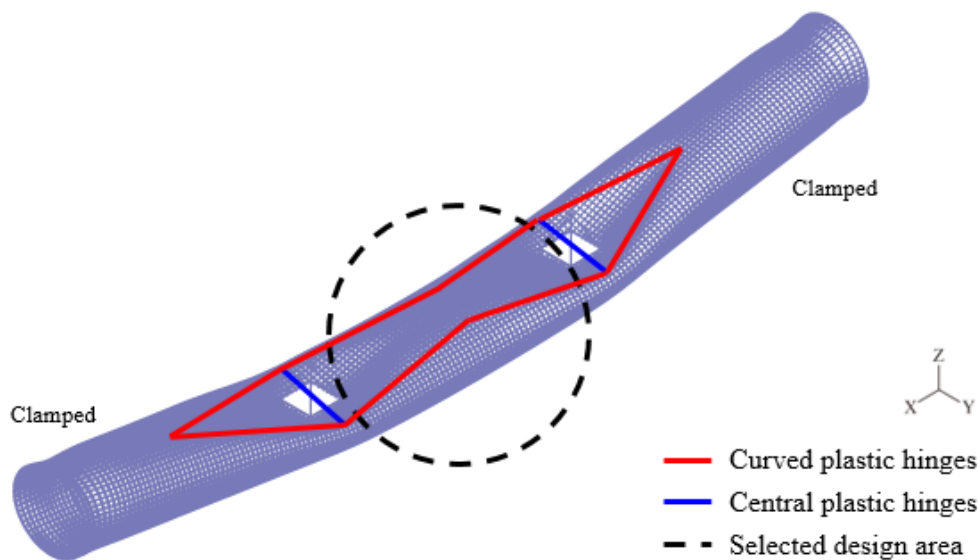


Figure 3.13. Selection of the part to be engraved with slit patterns. The blue line represents central plastic hinges, the red line represents, and the black dashed line represents the selected design area.

Chapter 4

Deformation of the tube with single slit

4.1 Introduction

In this chapter, we show how a thin-walled tube structure with slit patterns deformed in response to a transverse impact loading. The part to be engraved with the slit patterns is chosen based on the findings of the simulation analysis of the theoretical model and the half-tube model in the preceding chapter. Therefore, we introduce the refined simulation model of the tube for engraving slit patterns on it. In other words, the position where the pattern is to be engraved is selected among the entire tube, and various patterns are engraved on the corresponding area, and then finite element analysis is performed under the given impact loading conditions. To perform finite element analysis on tubes with different patterns under the same circumstances, the entire thin-walled tube structure is changed to consist of a sub-domain, sub-tube, and half tube. The maximum deflection (\mathbf{d}) at the center, the cross-section ellipticity, the bending (\mathbf{EI}) and torsional rigidities (\mathbf{GJ}) are the main variables for observing the change in tube's deformation according to the various slit pattern shapes.

4.2 Finite element modeling

4.2.1 Definition of the sub-domain

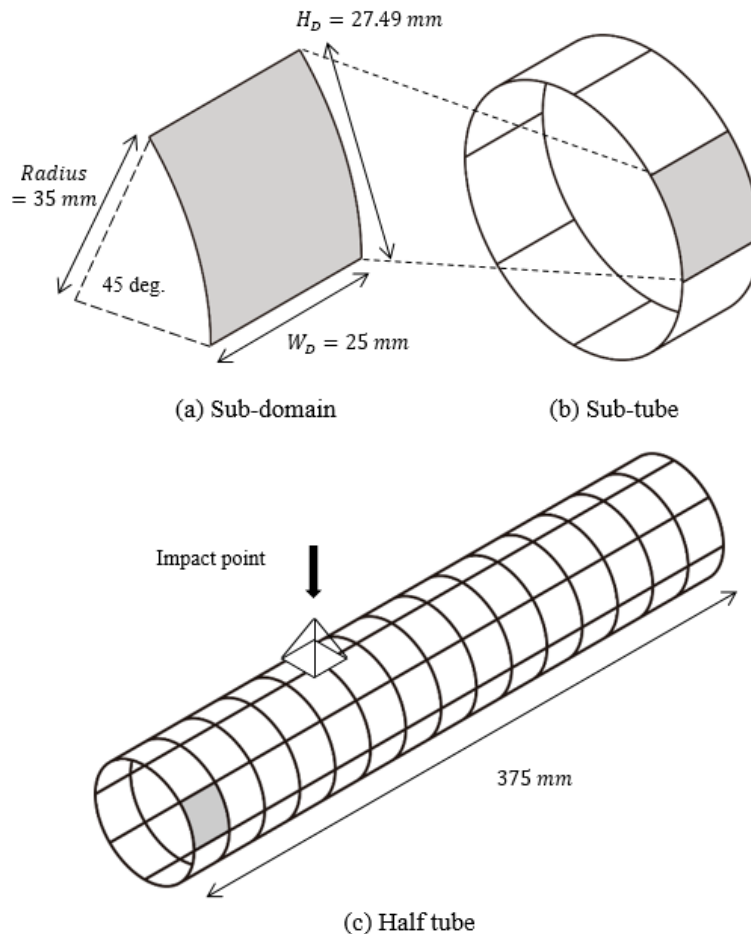


Figure 4.1. Finite element model with slit patterns and subdivision on the half tube model. (a) Sub-domain. (b) Sub-tube. (c) Half tube.

We split half tube into 15 sub-tubes along the horizontal axis, and then further split a sub-tube into 8 sub-domains to add slits to the tube. In other words, first, we constructed an almost square-shaped sub-domain, and formed one sub-tube by connecting 8 sub-domains. Then, 15 sub-tubes are connected to complete a half tube, and it is composed of a total of 120 sub-domains. The reason for dividing into square sub-domains is to repeatedly engrave slit patterns of various shapes in precise positions.

4.2.2 Definition of the slit pattern on a sub-domain

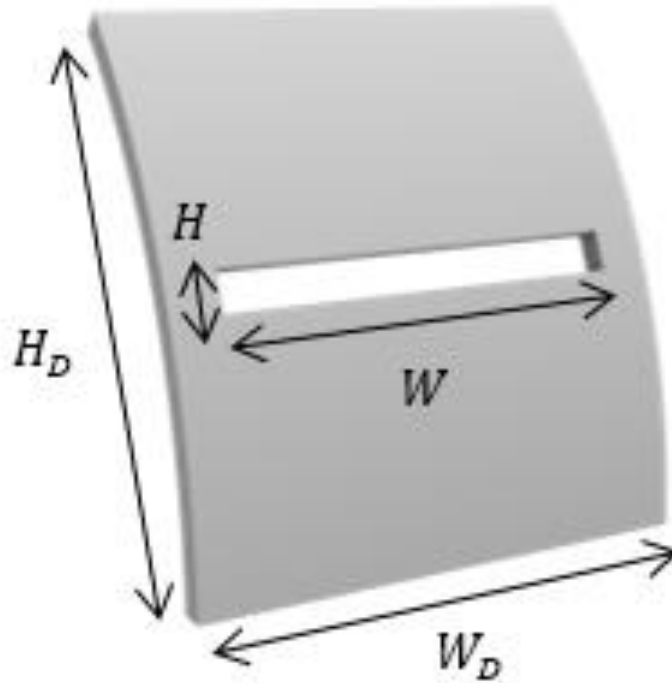


Figure 4.2. Definition of the slit pattern on a sub-domain.

The part selected to engrave the slits, certain sub-tubes are given rectangular slits with width (W) in the horizontal direction and height (H) in the vertical direction. Another design parameter to take into account is the total amount of patterns (P_N) in given sub-domain.

Here, using finite element analysis, we examine how slits affect the tube's deformation. For the tube with methodically widely varying slits, nonlinear dynamic-implicit analysis was used to determine the highest deflection under impact, and linear static analysis was used to determine the bending rigidity.

4.3 Deformed shape of the tube with different aspect ratio

4.3.1 Deformed shape of the tube

On each sub-domain, we first apply a single rectangular slit. In the finite element model, when a single rectangular slit is engraved in the sub-domain, the slit pattern is created in principle that the position is engraved in the center of each sub-domain. In other words, when the size of a single rectangular slit is determined, the slit pattern is engraved in the center in the longitudinal direction in the sub-domain and also in the 3D curved sub-domain. After a single rectangular slit pattern is engraved on a sub-domain, one sub-tube engraved with patterns consisting of 8 sub-domains is formed. Then, two consecutive sub-tubes are formed based on one sub-tube on which patterns are engraved. Two successive sub-tubes engraved with a pattern are placed in the thin tube's center. The half model has a total of 16 slits engraved as a result. In conclusion, as intended in the half tube finite element model consisting of 120 sub-domains, two consecutive sub-tubes from the center of the tube are patterned, and the remaining sub-tubes are created in the unpatterned form.

After that, the boundary and loading conditions are used to examine how a thin-walled tube structure with slit patterns collapse. For the boundary condition, one end of thin-walled circular tube is fixed and the other end is symmetric. The finite element analysis uses the half tube model, but as a result, the collapse mechanism of the full tube is implemented. For the loading condition, impact loading is applied in a drop weight method by creating a rigid plate at the 1/3 point of the full tube. Through nonlinear dynamic-implicit analysis of the thin-walled circular tube with a slit on a sub-domain, tube's deformation shape is calculated. The non-dimensional slit's width (W/W_D) and height (H/H_D) are respectively 0 to 0.8 and 0 to 0.6. We derive the center displacement (d/d_{ref}), cross-sectional ellipticity (e/e_{ref}), and bending rigidity (EI/EI_{ref}) from the finite element analysis, standardized with the reference value of the unpatterned tube.

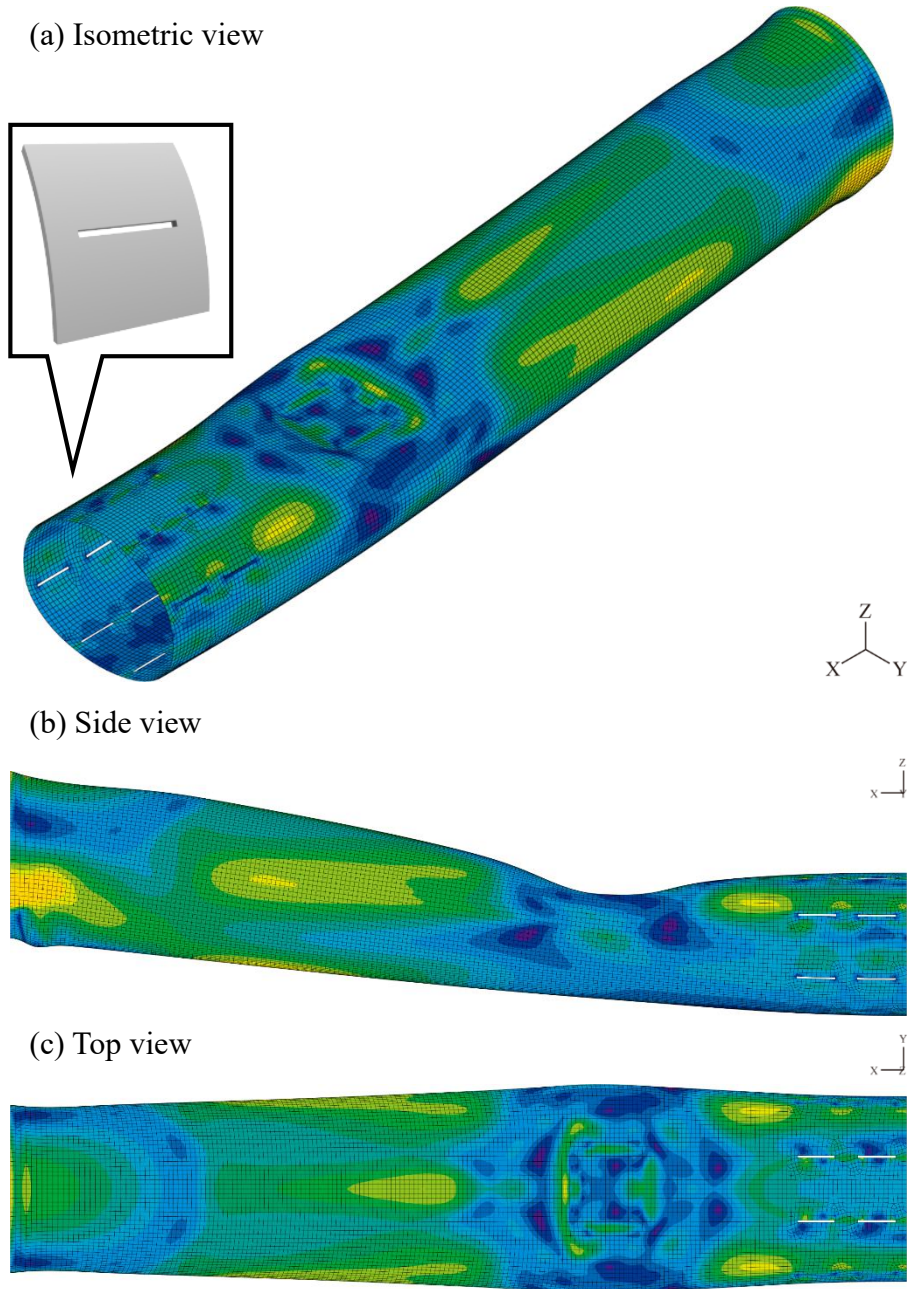


Figure 4.3. Deformed shape with effective stress of thin-walled tube with a longitudinal slit on each sub-domain. Longitudinal slit consists of A/A_D is 0.023, H/H_D is 0.036, W/W_D is 0.64, and aspect ratio is 0.0625. (a) Isometric view. (b) Side view. (c) Top view.

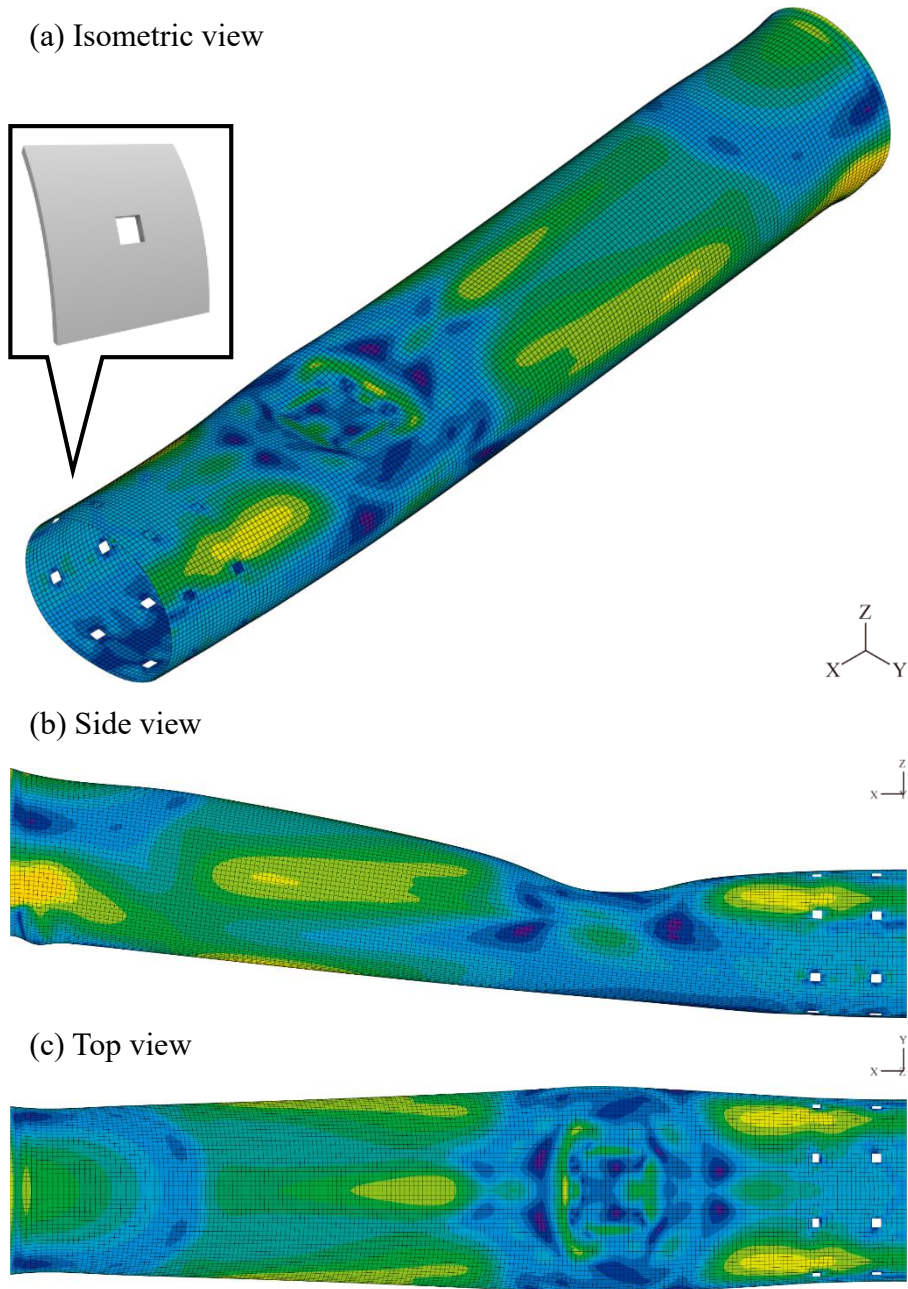


Figure 4.4. Deformed shape with effective stress of thin-walled tube with a square slit on each sub-domain. Square slit consists of A/AD is 0.023, H/HD is 0.146, W/WD is 0.16, and aspect ratio is 1. (a) Isometric view. (b) Side view. (c) Top view.

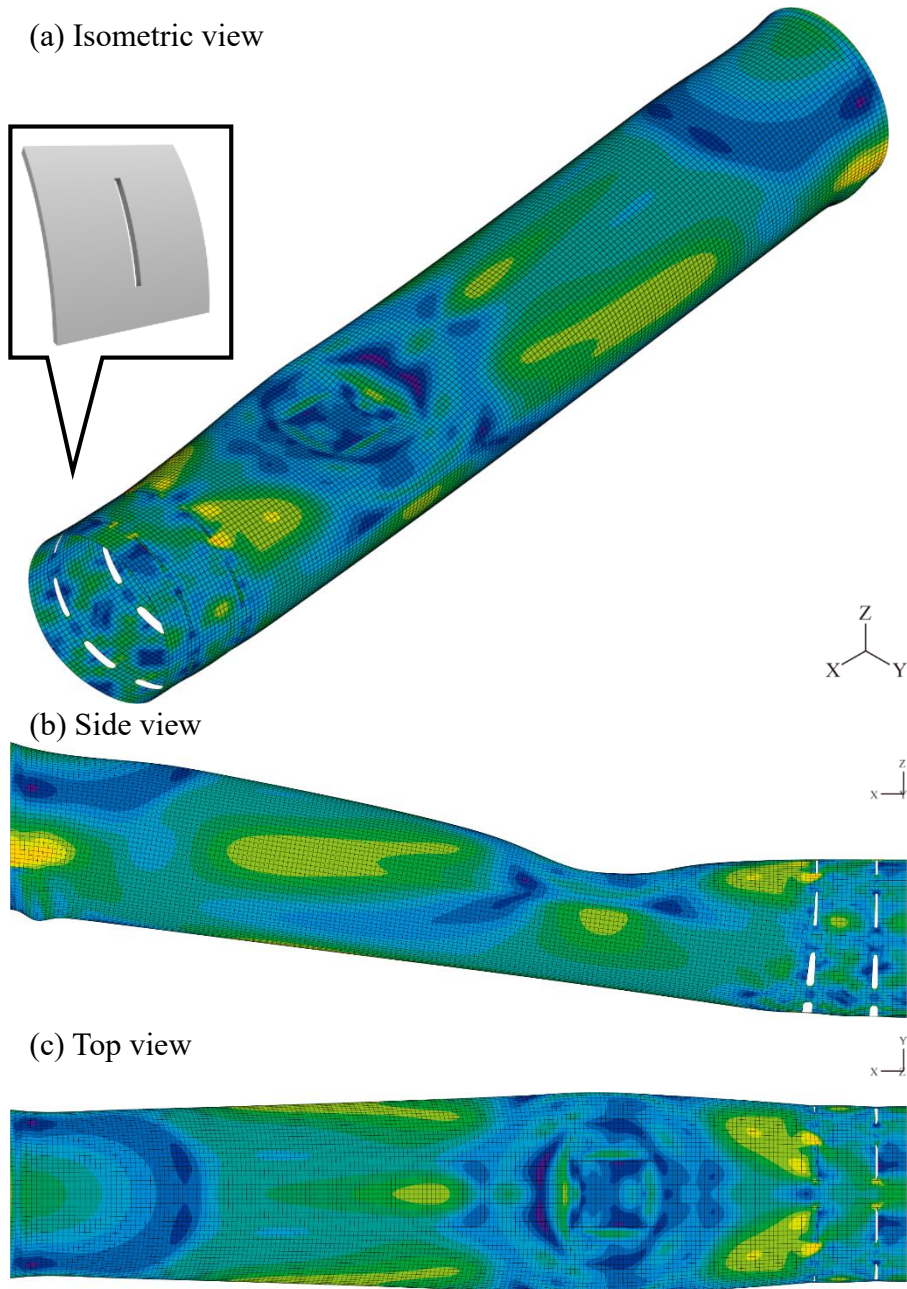


Figure 4.5. Deformed shape with effective stress of thin-walled tube with a circumferential slit on each sub-domain. Circumferential slit consists of A/AD is 0.023, H/HD is 0.582, W/WD is 0.04, and aspect ratio is 16. (a) Isometric view. (b) Side view. (c) Top view.

4.3.2 The effect of aspect ratio

In this chapter, a parameter study is conducted on the one slit pattern on each sub-domain. The range of single slit is applied from 0 to 0.6 for the non-dimensional height and 0 to 0.8 for width. Three representative types of slit, longitudinal, square, and circumferential slit, are chosen in order to accurately compare the effect a single slit's shape on the highest center displacement of the thin-walled circular tube under loading. The three representative slits have a fixed slit area and different aspect ratios. We obtain maximum center deflection and the ellipticity of cross-section from nonlinear dynamic finite element analysis, and bending and torsional rigidities from static finite element analysis.


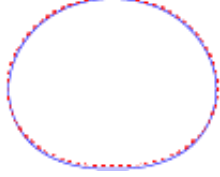
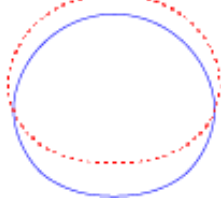
	Longitudinal	Square	Circumferential
Cross-section shape (Red dash: Reference Blue line: Patterned)			
Max. Deflection	- 2.13 %	+ 3.21 %	+ 36.24 %
Ellipticity	+ 9.07 %	- 10.81 %	- 53.49 %
Bending rigidity	- 0.36 %	- 0.83 %	- 8.67 %
Torsional rigidity	- 4.88 %	- 1.08 %	- 4.90 %

Table 4.1. Cross-section shape, maximum deflection, ellipticity of center cross-section, bending and torsional rigidity of the tube engraved with longitudinal, square, circumferential slit. All values are calculated as percent with reference to the value of the tube without patterns.

We fixed the area of the slit pattern to accurately compare the effect of the shape of the slit pattern on the greatest tube center displacement. Therefore, we study the effect of the pattern shape on the center deflection while comparing the deformation of tube to which longitudinal, square, and circumferential slits are applied with the same area but different shapes of the slit patterns. That is, the three representative slit patterns have different aspect ratios. The results of nonlinear dynamic finite element analysis on a tube with three representative slit patterns are contrasted with the deformation of the unpatterned tube as a baseline.

Comparing the maximum center deflection, when the longitudinal slit is applied, the tube's center deflection is minimized the most, and when the circumferential slit is applied, the center deflection of the tube is rather increased. Comparing the ellipticity of cross-section, when a longitudinal slit is applied, the ellipticity is increased, and when the remaining slits are applied, the ellipticity is rather decreased. Considering the relationship between the maximum center deflection and the ellipticity of cross-section, the assumption of reducing the center deflection is confirmed by deforming the central section into an oval shape, which is a key idea in the design concept stage. In other words, when transverse impact loading is applied to the thin-walled tube engraved with longitudinal slits, the central cross-section is deformed to an elliptical shape compared to the reference, and the maximum center deflection is reduced due to this effect. However, when transverse impact loading is applied to the thin-walled tube engraved with circumferential slits, the central tube's cross-section is deformed to a circular shape compared to the reference, and the maximum center deflection is increased due to this effect.

The reason for this phenomenon is the effective stress distribution on the thin-walled tube, which is shown through the deformed shape of the tube with effective stress determined through the nonlinear dynamic-implicit analysis. In the deformed shape with effective stress of the thin-walled tube without patterns, deformation occurred after transverse impact loading at the impact point, and the effective stress is concentrated around 45 degrees from the impact point to the center. The deformed tube shape with effective stress is indicated by the yellow clusters in the figure. The

meaning that the effective stress is concentrated in this part rather than being distributed in other parts of the tube can be interpreted as the potential to distribute the effective stress to other parts and cause further deformation in the transferred part. In the deformed shape with effective stress of the thin-walled tube engraved with longitudinal slits, the yellow area where the effective stress is concentrated in the deformed shape of the unpatterned tube is distributed to tube center by longitudinal slits, and the area of the yellow color is reduced. In the deformed shape with effective stress of the thin-walled tube engraved with square slit, the area where the effective stress is concentrated in yellow is not distributed to the center by the square slits, and the area in yellow is increased. In the deformed shape with effective stress of the thin-walled tube engraved with circumferential slits, the area where the effective stress is concentrated in yellow is not distributed to the center by the circumferential slits, but more concentrated in the circumferential direction, and the area in yellow is increased. In other words, the longitudinal slit effectively distributes the concentrated effective stress and makes the center part engraved with the patterns flexible, causing the cross-section to be deformed into an elliptical shape. Due to the effect of this longitudinal slit, the maximum center deflection is reduced. However, the circumferential slit prevents the concentrated effective stress to the center part, so cross-section is deformed into a circular shape.

Comparing the bending rigidity obtained by static finite element analysis, it decreases the most when the circumferential slit is engraved on the tube and the least decreases when the longitudinal slit is engraved. Comparing torsional rigidity, the decrease is the least when square slits are engraved on the tube. The reason for this phenomenon is that the shape of the center part of the tube remaining after cut-out of the slit makes the tube less soft than other patterns for in-plane shear under torsional loading.

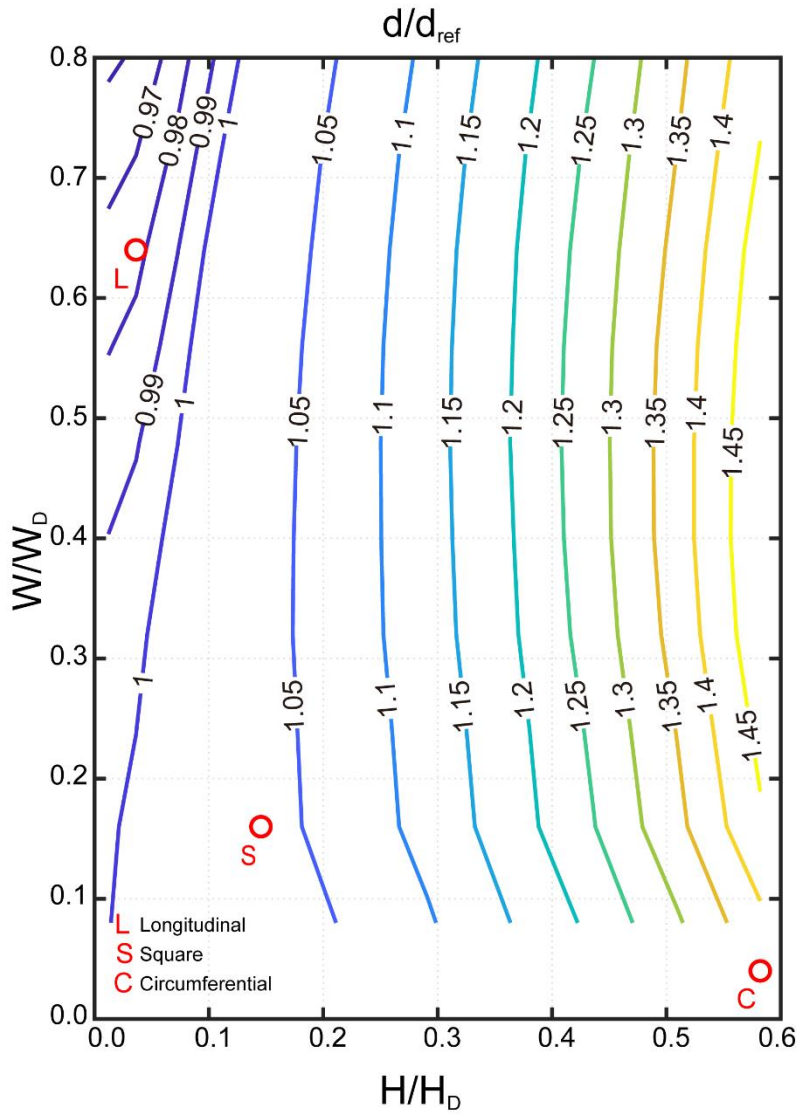


Figure 4.6. Contour map of the non-dimensional maximum center deflection.

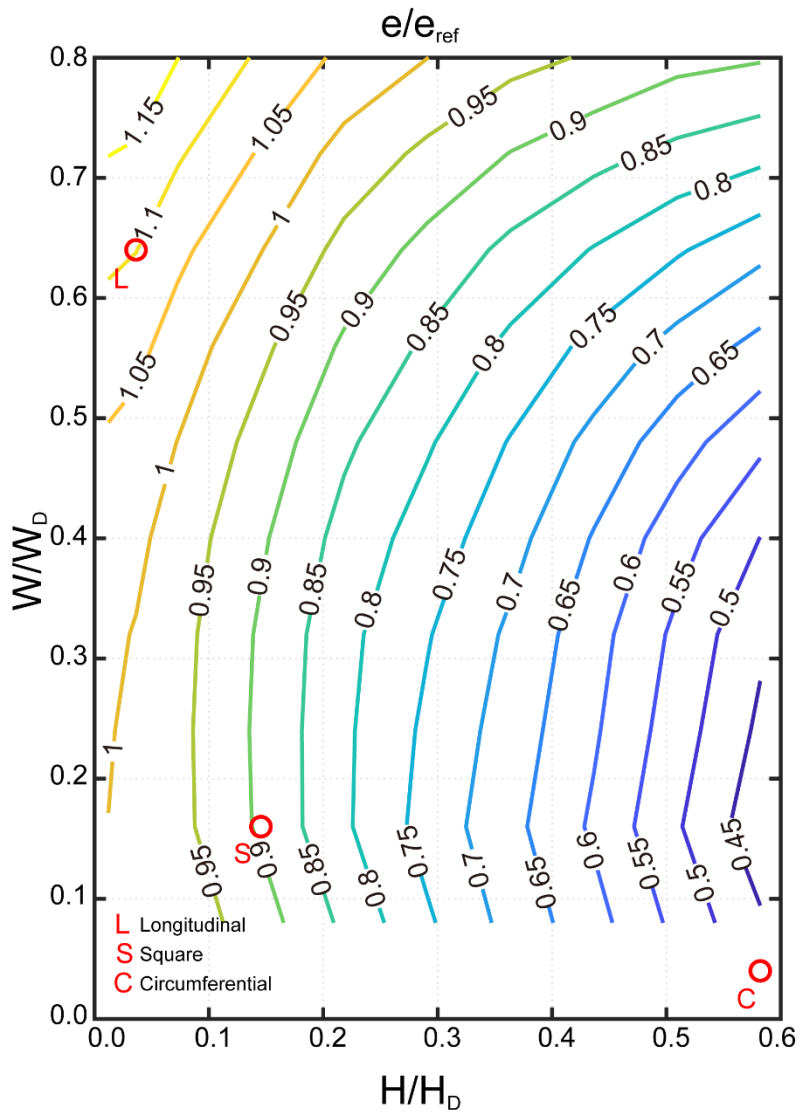


Figure 4.7. Contour map of the non-dimensional ellipticity of center cross-section.

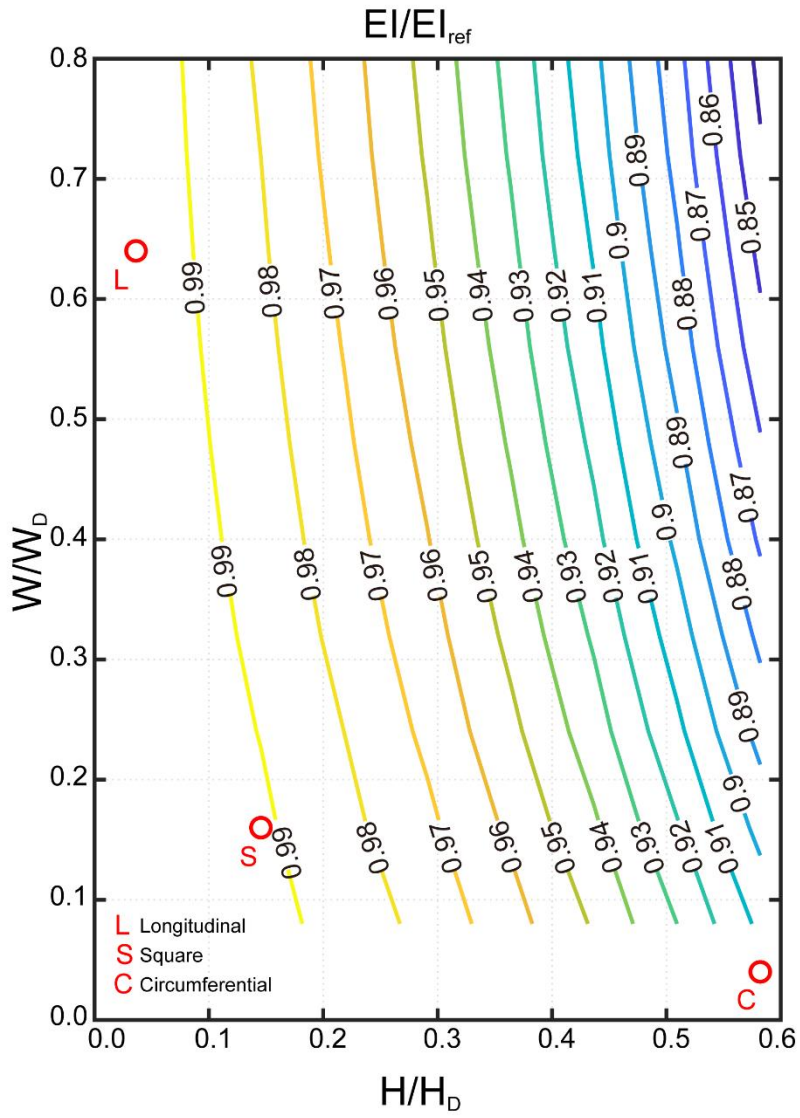


Figure 4.8. Contour map of the non-dimensional bending rigidity.

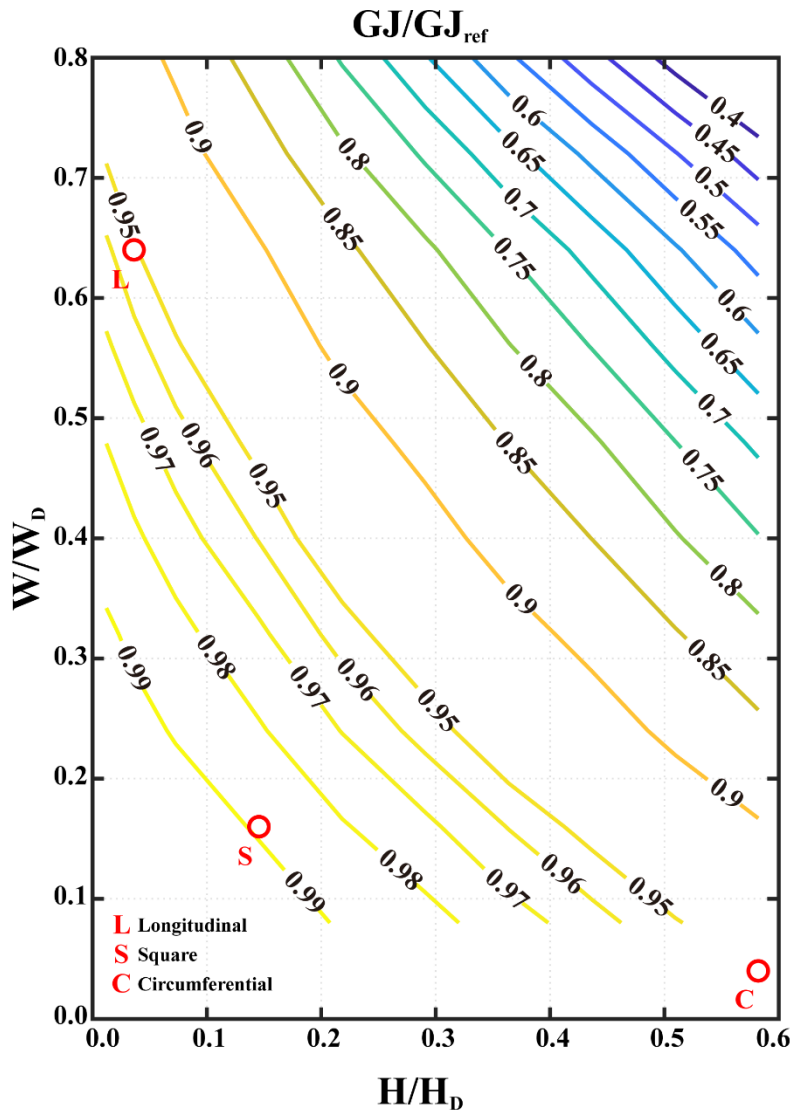


Figure 4.9. Contour map of the non-dimensional torsional rigidity.

4.3.3 Energy absorption of the tube

In this chapter, we calculate the energy that the thin-walled tube will absorb when it is hit transversely. In order to calculate the energy absorption (EA), force – displacement curve under the transverse loading was extracted as the reaction force and displacement at the impact point through the finite element analysis results previously performed. Calculating the area under force – displacement curves with slits of various aspect ratios will reveal the energy absorption of the tube.

Before obtaining energy absorption corresponding to each tube, as mentioned in Chapter 2, when the impact energy is applied to the tube, it should be considered that it is used as global bending deformation and plastic deformation. Therefore, it should be noticed that even if the energy absorption is the same, the global bending deformation and plastic deformation may appear differently depending on the shape of the slits engraved on the tube. To accurately compare these, the energy absorption of an un-patterned tube and a tube with longitudinal and circumferential slits having the same area of the slits but different aspect ratios were calculated.

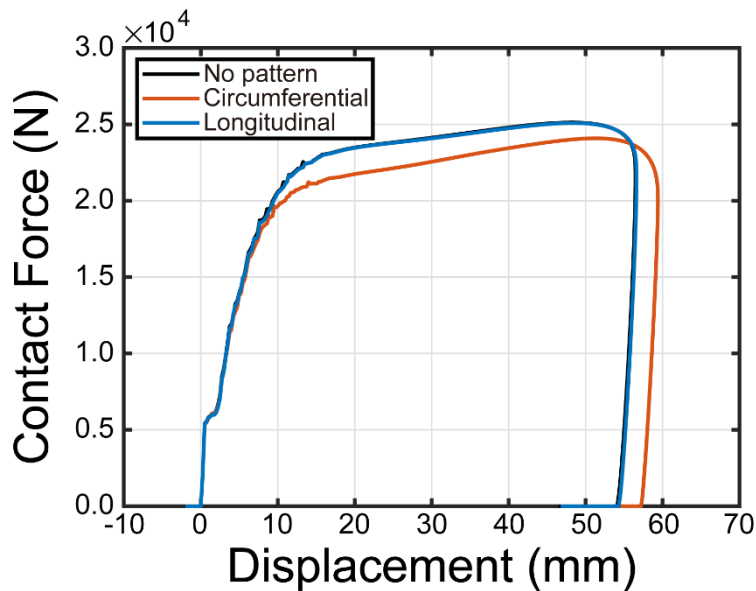


Figure 4.10. Force – displacement curve for un-patterned tube and tubes with longitudinal and circumferential slits under transverse impact loading.

	No pattern	Longitudinal	Circumferential
EA[kN * mm]	1229	1230	1232
Tube Volume [mm³]	1.155e+05	1.151e+05	1.151e+05
SEA [(kN * mm)/kg]	1357	1362	1363

Table 4.2. Energy absorption, tube volume, and specific energy absorption for un-patterned tube, longitudinal and circumferential slit patterned tubes.

First, the force – displacement corresponding to each tube was shown as the reaction force and displacement at the impact point extracted by conducting the nonlinear dynamic-implicit analysis. Next, the area under each curve was calculated using the trapezoidal method to calculate energy absorption. Additionally, the specific energy absorption (SEA), which was obtained by dividing the energy absorption by the tube’s mass density and volume product, was derived for accurate comparison. As a result of the tube’s reduced volume compared to the tube without patterns, the energy absorption is the greatest in a tube with circumferential slits, and the specific energy absorption is also highest. Comparing the energy absorption values of other tubes, there is, however, no appreciable difference.

The objective of this study is to minimize the permanent deflection that occurs when impact loading is applied as mentioned above. Therefore, when Table 4.1 and Table 4.2 are comprehensively compared, the tube with circumferential slits increases the displacement even though the value of energy absorption is high. However, the tube with longitudinal slits has no significant difference in energy absorption value from other tubes, but displacement can be reduced due to plastic deformation. That is, there is no significant difference in energy absorption, but there is a difference in the tube’s deflection due to plastic deformation according to the slit shape.

4.3.4 The local deformation effect of the slit

In this chapter, the time – dependent deformation shape of thin-walled tubes when applied to transverse impact was investigated. In the previous chapter, we analyzed the effect of slits with the same area but different aspect ratios on the tube’s deformation with slits. As a result, the tube with longitudinal slits increased the cross-section ellipticity and decreased displacement due to the slits. On the other hand, the tube with circumferential slit reduced the ellipticity and bending rigidity due to the slit patterns, and increased the displacement. It was predicted that one of the causes of this result could be the local deformation effect of the slits. Therefore, the local deformation of the slits was analyzed by comparing the tube’s deformation with the time. In addition, the reaction force generated at the point of impact was extracted over time to analyze how the deformation of the entire tube appeared over time. This is because it is possible to analyze in which section the tube’s plastic deformation occurs through the reaction force graph over time.

In general, when a load is applied to the tube, a moment occurs when the reaction force increases monotonically and then changes rapidly at some point. From

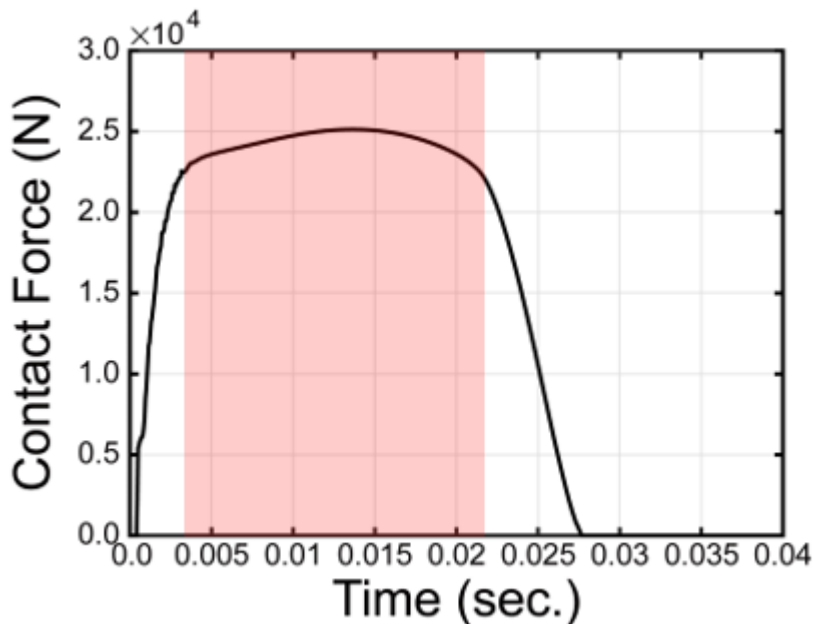


Figure 4.11. Reaction force graph as a function of time at the impact point of the tube without slit patterns. Plastic deformation of the tube occurs in the red region.

this moment on, the reaction force remains relatively gentle, and plastic deformation occurs in the tube. Figure 4.11 is a graph of the contact force as a function of time occurring at the impact position of the unpatterned tube. Here, approximately 0.004 sec. from 0.021 sec. It can be seen as the section where plastic deformation occurs, and it is also the section where the cross-sectional deformation occurs.

In particular, in this chapter, the local deformation of the slits was investigated by comparing the deformed shapes of tubes with slits having the same area but different aspect ratios. As a result, a graph of the contact force generated at the impact point of the tube analyzed in the previous section and engraved with longitudinal and circumferential slits is shown. As mentioned above, even for tubes with slits, the shape of the reaction force graph over time appeared similar to that of the tube without slit patterns. Through the change of reaction force, it is possible to roughly predict the section where plastic deformation occurs. In this section, deformation mainly occurs in tube's cross-section, and since it was predicted that it would appear differently depending on the slit shape, the tube's deformation over time was extracted. In particular, when extracting the tube's deformation to investigate the local deformation of the slits, which is expected to affect the cross-section, only the shape from the tube center to the impact position was extracted.

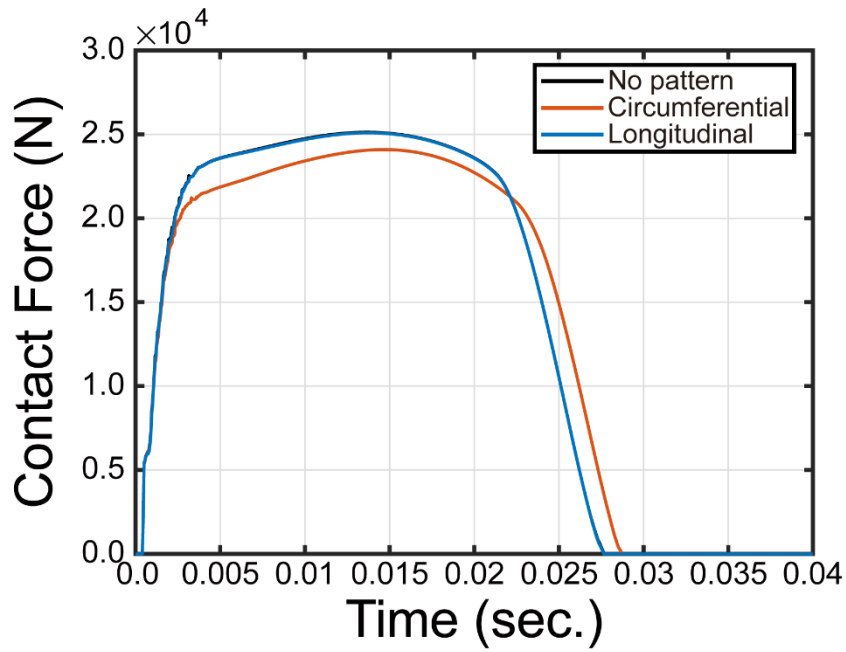


Figure 4.12. Reaction force graph as a function of time at the impact point of the tube without slit patterns and the tube with longitudinal and circumferential slits.

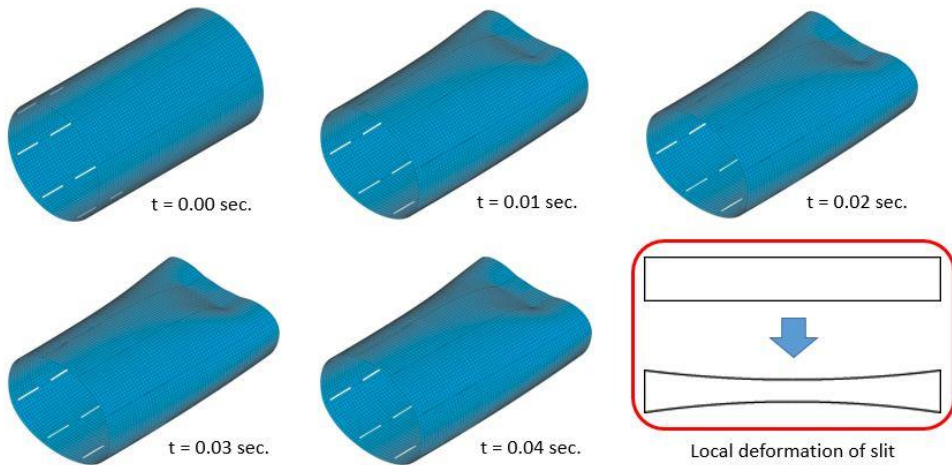


Figure 4.13. Deformation shape over time of tubes with longitudinal slits. The red box represents the local deformation shape of the longitudinal slit.

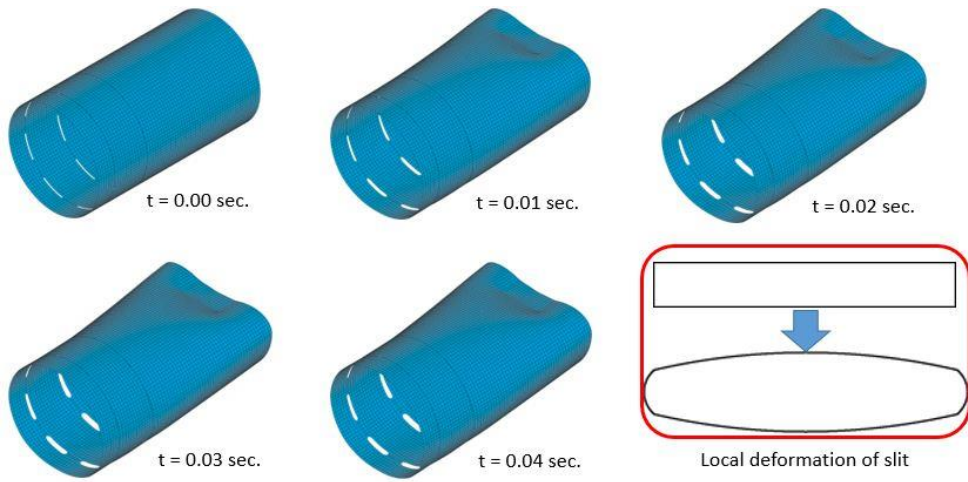


Figure 4.14. Deformation shape over time of tubes with circumferential slits. The red box represents the local deformation shape of the circumferential slit.

First, the deformation shape over time of the tube engraved with longitudinal slits is shown in Figure 4.13, and the local deformation shape of the longitudinal slit is the same as the red box, but the buckling effect is very insignificant. However, the longitudinal slits increased the ellipticity of the tube section and reduced the displacement. Next, the deformation shape over time of the tube engraved with circumferential slits is shown in Figure 4.14, and the local deformation shape of the circumferential slit is shown in the red box. However, unlike the deformation of the longitudinal slit, the local deformation effect of the circumferential slit had an effect on reducing the ellipticity of the tube section, thereby increasing the displacement. That is, in the case of a slit of the same area, the local deformation effect was greater in the case of the circumferential slit, and finally, the displacement of the tube increased by affecting bending rigidity and ellipticity.

4.4 Conclusion

We examined the deformation mechanisms of the thin-walled tube structure using two successive sub-tubes, each of which had a single rectangular slit on it. From nonlinear dynamic-implicit analysis, we calculated the greatest center displacement, the ellipticity of tube's cross-section, and bending and torsional rigidities. Next, all parameters are normalized using the value of the tube without patterns as the reference. We extracted deformation shape with effective stress and plastic strain of the tube under transverse impact loading.

Slits are typically added to a thin-walled tube to increase the maximum center displacement. Because the height of the slit affects the maximum center displacement, it is especially recommended to avoid slits that are long around the perimeter. The contour map has a small area of slit parameters where it is possible to reduce the tube's center displacement. It relates to longitudinally thin slits, which are successful in causing the cross-section to take on an elliptic shape under transverse impact loading. Though they are not significantly diminished, the bending rigidity exhibits a contour map that is similar to the maximum center displacement in that they change more noticeably with the slit height.

These findings imply that the decrease in the tube's bending stiffness, which is controlled by the slit height, is primarily responsible for the tube's increased maximum center displacement for the majority of the slit parameters. The maximum deflection of the tube decreases when longitudinally thin slits are present because more cross-sectional deformation is induced and less bending stiffness changes as a result. Indeed, depending on the relationship with the tube axis in terms of aspect ratio, simple slits of equal area can depict a noticeably different effect on the greatest center displacement. It should be noted that only when longitudinal slits are used does the cross-section's ellipticity increase. Use of square or circumferential slits reduces it to a smaller value than the reference tube's ellipticity.

Chapter 5

Deformation of the tube with multiple slits on each sub-domain

5.1 Introduction

In the previous chapter, nonlinear dynamic finite element analysis is performed on a tube with the rectangular slit on a sub-domain to investigate the effect of the pattern shape on the maximum center deflection. For a rectangular slit, finite element simulation is performed with non-dimensional height from 0 to 0.6 and width from 0 to 0.8. Based on the resulting tube's deformed shape with a single slit, maximum center deflection, ellipticity of cross-section, and bending and torsional rigidities are calculated. In particular, three representative patterns with a fixed area but various shapes are chosen in order to accurately compare the influence of the pattern shape on the tube's deformation shape. The three representative slits have different aspect ratios and are classified as longitudinal, square, and circumferential. For these three representative slits, only the one slit is engraved on each sub-domain, and slit patterns are engraved on two consecutive sub-tubes from the center of the tube. In other words, slits are engraved on only 16 sub-domains out of a total of 120 sub-domains, and the total number of engraved slits is 16. The deformed shapes of these representative three slit engraved tubes are compared, and when only one rectangular slit is engraved on each sub-domain, the longitudinal slit is effective in reducing the maximum center deflection of the tube. The reason for this phenomenon is that the longitudinal slit makes the central part flexible by distributing the concentrated effective stress of the tube and deforms the center cross-section into an elliptical

shape. Although the cutting of the material reduces the bending and torsional rigidities of static properties, the longitudinal slit reduces the maximum central deflection due to the aforementioned effect.

The effect of the quantity of patterns on center deflection of the tube is studied in this chapter using nonlinear dynamic finite element analysis on a thin-walled tube with multiple slits on a sub-domain by taking into consideration the influence of the pattern's shape. As in the previous chapter, maximum center deflection, ellipticity of center cross-section, bending and torsional rigidities are calculated through finite element analysis on thin-walled tube structure with slits subjected to transverse impact loading.

First, we looked into how the amount of slit patterns engraved in the sub-domain affected the tube's deformation. As a reference, we chose one slit from a rectangle slit on each of the sub-domains covered in the previous chapter. We take the method of dividing the reference into two directions in order to keep the area of the slit constant in each sub-domain and change the number of slits. The division method is selected as longitudinal division, which is the width direction of the slit pattern, and circumferential division, which is the height direction of the slit pattern. In a sub-domain, the position of the slit is located in the center of the sub-domain in the case of a single rectangular slit, but the divided slits are divided and arranged with the same interval in the direction of division. We divided a rectangle slit on a sub-domain from 1 to 6 in accordance with the division direction and defined the quantity of slits in the sub-domain as P_N .

Next, we search how the height of the slit pattern engraved in the sub-domain affects the tube deformation. We chose one rectangular slit from each of the sub-domains covered in the previous chapter to serve as a reference in this study as well. To compare the effect of the slit's height, we maintained the width of the reference slit and changed the height of the slit by controlling the height. Because the height of each slit varies in each sub-domain, the total area of the slits is different. We named the three representative slits as thin, medium, and thick slits according to their height. To compare the slit's number and the tube deformation with respect to the height,

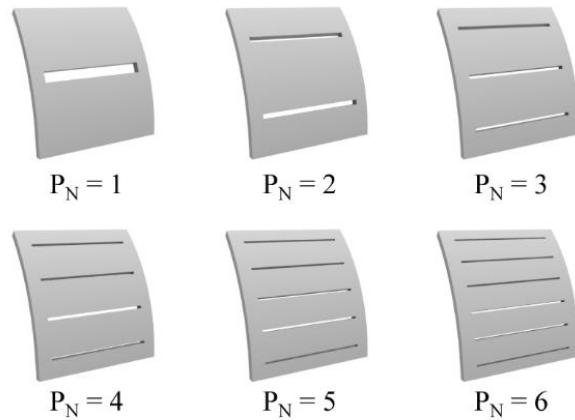
the size of each slit is fixed, and the number of thin, medium, and thick slits in each sub-domain is changed. Similar to circumferential division in the preceding section, the number of slits is changed from 1 to 6, and even though the amount of slits on a sub-domain increased, adjacent slits are arranged to have the same interval.

In addition, we searched into how different engraved slit patterns affected the deformation of the tube among all sub-domains. As a reference for this study, we chose a narrow slit from a single rectangular slit on each of the sub-domains covered in the previous chapter. We fixed the size of the reference slit and changed the range in which the slit patterns are engraved among all sub-domains to compare the effect of the slit pattern range. Basically, the range where the slit patterns are engraved is on two subsequent sub-tubes from the tube's center, and 16 sub-domains out of a total of 120 sub-domains are engraved. We named the slit pattern range as 2 sub-tubes, 3 sub-tubes, and 4 sub-tubes according to total amount of sub-tubes. The number of sub-domains occupied by the slit patterns is 16 sub-domains in 2 sub-tubes, 24 sub-domains in 3 sub-tubes, and 32 sub-domains in 4 sub-tubes. Since the size of the slits is the same, the area occupied by the slit patterns in each sub-domain is the same, but the total area of the slit patterns is different because the pattern ranges in which the slits are engraved is changed. The size of each slit is fixed, and the number of slits for 2 sub-tubes, 3 sub-tubes, and 4 sub-tubes in each sub-domain is changed to compare the quantity of slits and the tube's deformation with respect to the pattern range.

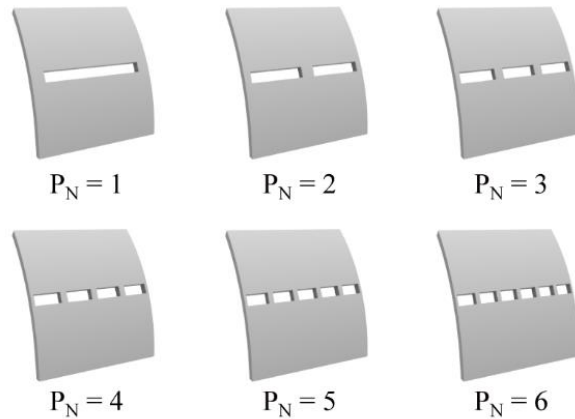
5.2 Deformed shape of the tube with different division direction

5.2.1 Deformed shape of the tube

We looked into how the amount of slit patterns within sub-domain affected the deformation of the thin-walled tube using the findings and insights from the previous chapter. In this section, we choose a single longitudinal slit of $H/H_D = 0.07$ and $W/W_D = 0.08$ as the reference to examine how the quantity of slit patterns within the sub-domain affects the tube deformation. We divided the reference pattern into two directions to change the number of slits and set the reference rectangular slit to change the amount of slit patterns in one sub-domain. In the previous chapter, when a single rectangular is engraved in the sub-domain, the slit rectangular slit pattern is created in principle that the position is engraved in the center of each sub-domain. First, the reference slit we selected in the finite element tube model is created within a sub-domain in the aforementioned manner. Then, the reference slit is divided into two directions selected by us so that total area of slit pattern is kept constant and the number of slits is changed. The pattern division along the two directions we selected is division in the circumferential direction, which is the height direction of the slit pattern, and division in the longitudinal direction, which is the width direction of the slit pattern. Basically, as mentioned in the previous chapter, slit patterns are generated on one sub-domain and engraved on two consecutive sub-tubes from the center of the tube. The slits divided from the reference rectangular slit are all arranged to have the same interval in the division direction. Each division's six P_N cases (1 to 6) are tested. H/H_D is defined as $0.07/P_N$ in the circumferential division, while W/W_D is set at 0.80. For the longitudinal division, W/W_D of $0.80/P_N$ and H/H_D of 0.07 are used. In conclusion, the 120 sub-domain half tube finite element model achieves the desired patterning of two sub-tubes in succession from the tube center while creating the remaining sub-tubes in the unpatterned form.



(a) Circumferential division



(b) Longitudinal division

Figure 5.1. Definition of slit pattern division from the reference rectangular slit. Six cases of P_N are created for each division. (a) Circumferential division. (b) Longitudinal division.

Next, simulation conditions are applied to analyzed collapse mechanism of thin-walled tube structure with slit patterns divided from the reference slit. Then, finite element analysis is performed using the tube model with each slit patterns, and the maximum center deflection, the center cross-section ellipticity, bending and torsional rigidities are calculated from the results. We investigate a reference single rectangular slit, circumferential division $P_N = 4$, and longitudinal division $P_N = 4$, to accurately compare the effect of the quantity of slits on the tube deformation.

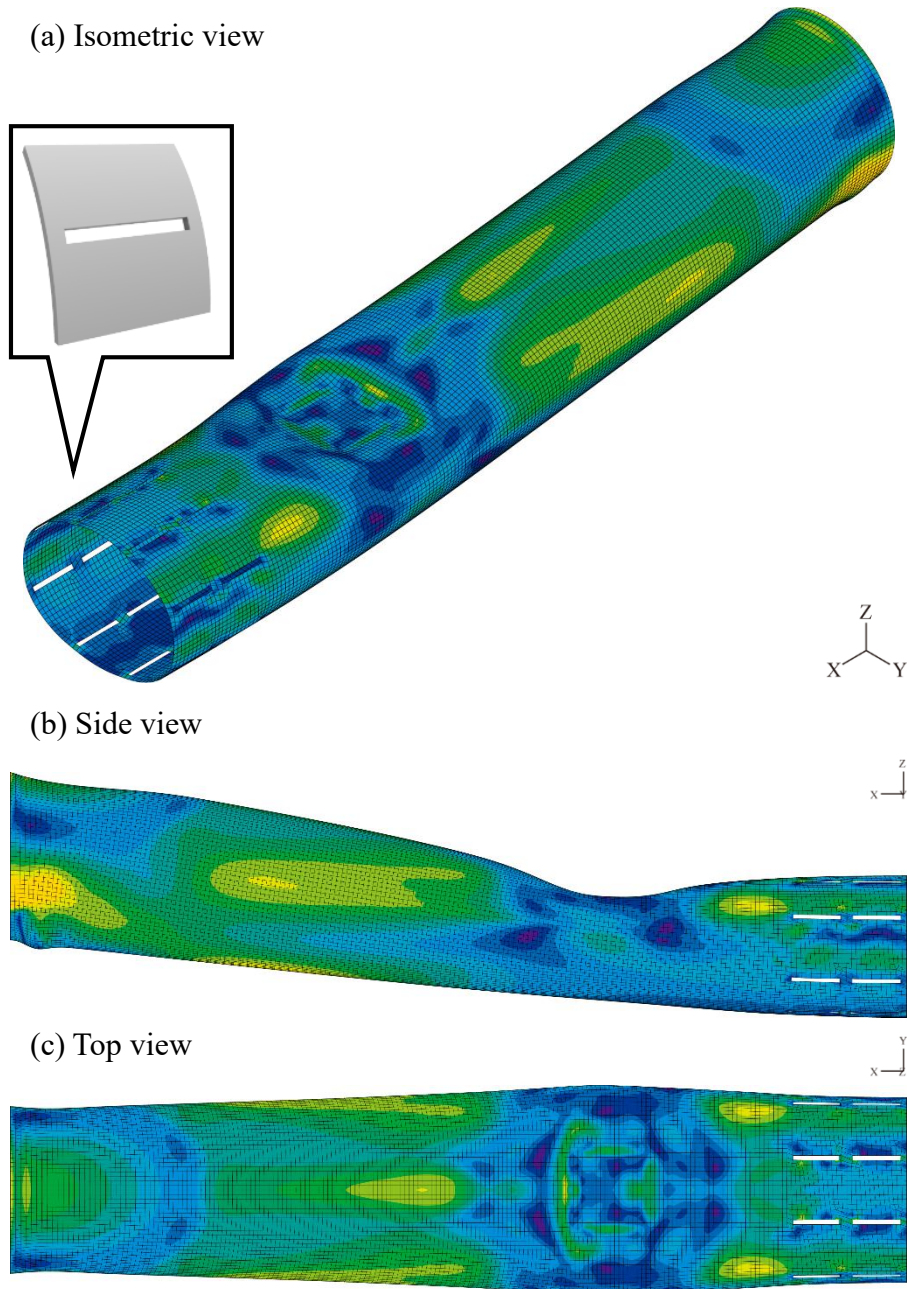


Figure 5.2. Deformed shape with effective stress of thin-walled tube with a reference slit on each sub-domain. The reference single rectangular slit consists of A/A_D is fixed at 0.058, H/H_D is 0.073, W/W_D is 0.800, and the number of slits on a sub-domain is 1. (a) Isometric view. (b) Side view. (c) Top view.

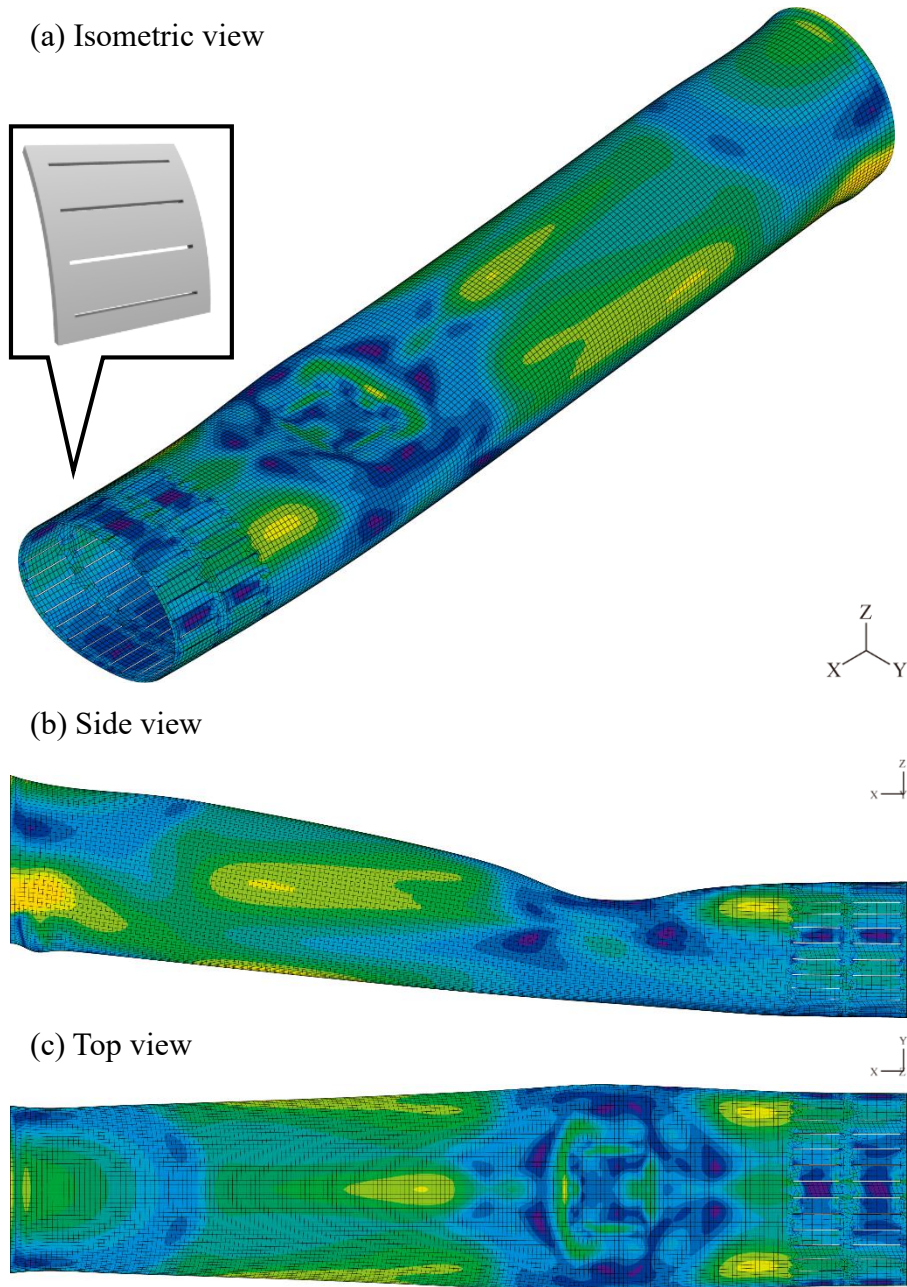


Figure 5.3. Deformed shape with effective stress of thin-walled tube with the circumferential division slit on each sub-domain. The circumferential division slit consists of A/A_D is fixed at 0.058, H/H_D is 0.018, W/W_D is 0.800, and the number of slits on a sub-domain is 4. (a) Isometric view. (b) Side view. (c) Top view.

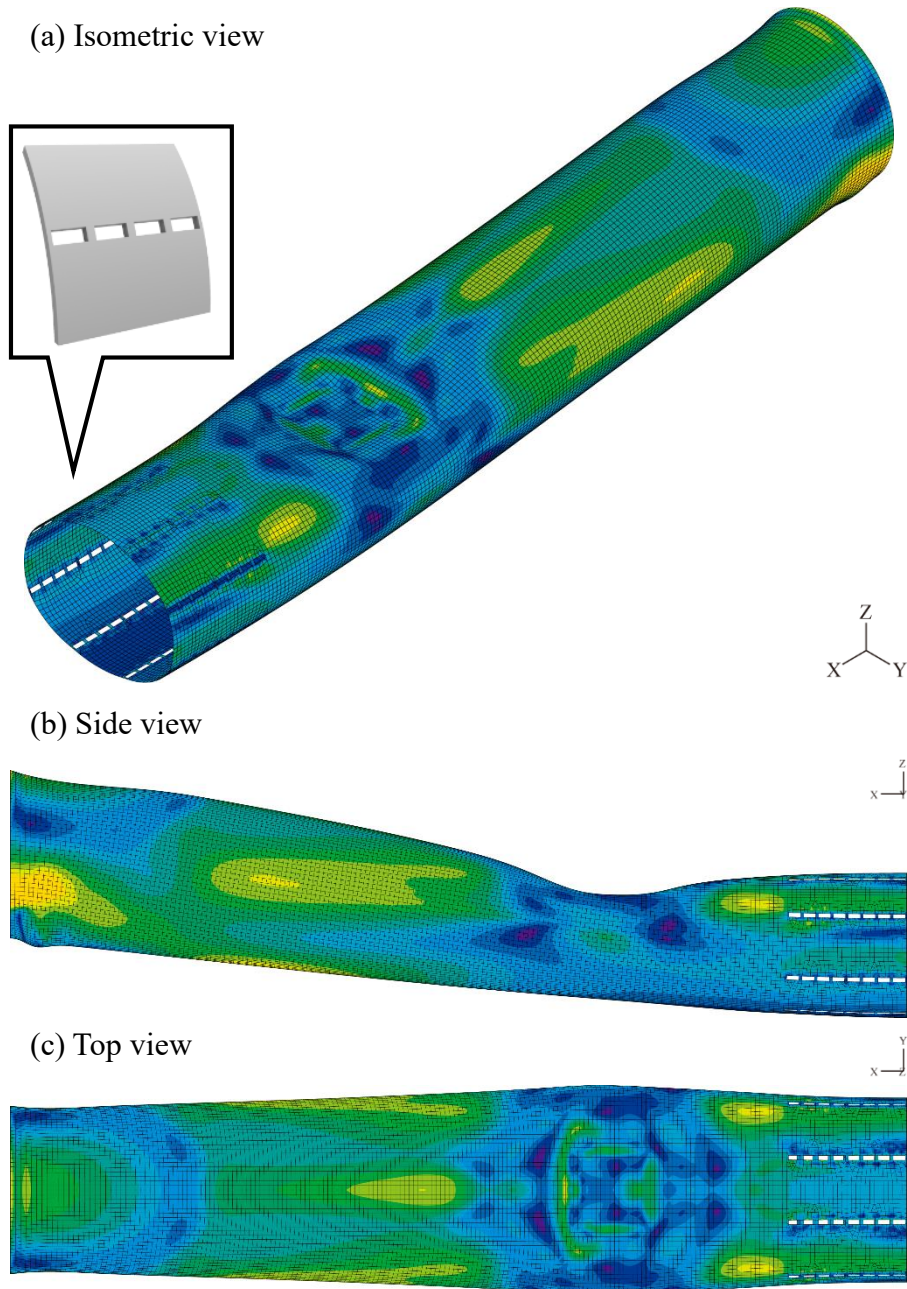


Figure 5.4. Deformed shape with effective stress of thin-walled tube with the longitudinal division slit on each sub-domain. The longitudinal division slit consists of A/A_D is fixed at 0.058, H/H_D is 0.073, W/W_D is 0.200, and the number of slits on a sub-domain is 4. (a) Isometric view. (b) Side view. (c) Top view.

5.2.2 The effect of different division direction

In this chapter, a parameter study is conducted on multiple slit patterns on each sub-domain. We choose a single longitudinal slit of $H/H_D = 0.07$ and $W/W_D = 0.08$ as the reference. A single rectangular slit is used as the reference, followed by circumferential division ($P_N = 4$) and longitudinal division ($P_N = 4$) to compare the effects of the amount of slits on sub-domain on the greatest center displacement of the thin-walled tube under loading. The three representative slits have a fixed the area of total slits and different division directions. We obtain maximum center deflection and the ellipticity of cross-section from nonlinear dynamic finite element analysis, and bending and torsional rigidities from static finite element analysis.

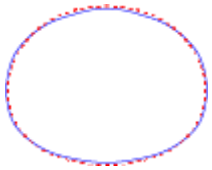
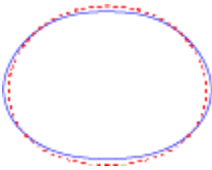
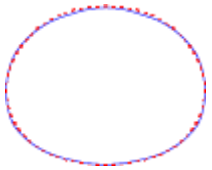
	Single	Circumferential division	Longitudinal division
Cross-section shape (Red dash: Reference Blue line: Patterned)			
Max. Deflection	- 2.46 %	- 6.83 %	- 0.28 %
Ellipticity	+ 16.12 %	+ 44.45 %	+ 5.56 %
Bending rigidity	- 0.94 %	- 0.85 %	- 1.01 %
Torsional rigidity	- 10.71 %	- 36.22 %	- 9.43 %

Table 5.1. Cross-section shape, maximum deflection, ellipticity of center cross-section, bending and torsional rigidity of the tube engraved with single, circumferential division, longitudinal division slits. All values are calculated as percent with reference to the value of the tube without patterns.

We fixed the area of the total slit patterns on a sub domain to accurately compare the effect of the number of the slit patterns on the maximum center. So, using a single rectangular slit as the reference, circumferential division slits, and longitudinal division slits that are applied with the same total area but different slit pattern division directions, we investigated the impact of the quantity of slit patterns on sub-domain on the center deflection of the tube. That is, the three representative slit patterns have different shapes and number. In particular, in this section, the number of patterns divided in two directions from a single rectangular slit as the reference is changed from 1 to 6. The results of nonlinear dynamic finite element analysis on a tube with three representative slit patterns are compared with the deformation of a comparable tube without slit patterns as a base point.

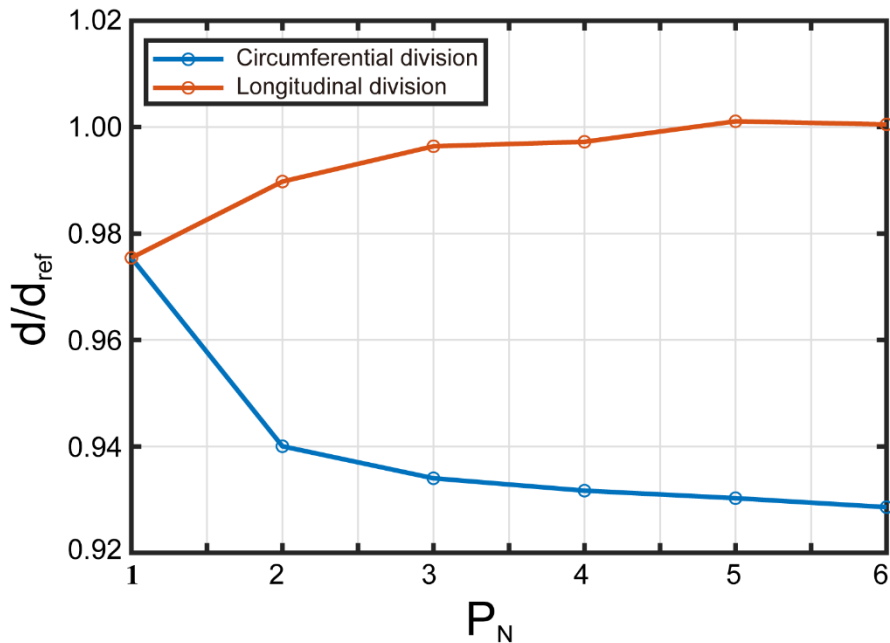


Figure 5.5. Non-dimensional maximum center deflection of the tube with respect to the division direction and P_N .

Comparing the quantity of patterns with slits on a sub-domain with the thin-walled tube's maximum center deflection, when the circumferential division slits with increasing the number of slit patterns are applied, the maximum center displacement is reduced, and when the longitudinal division slits with increasing the number of slit patterns are applied, the maximum center displacement is increased. In particular, as the quantity of slit patterns increases, the difference in the tendency of maximum center deflection according to the division direction of the slit becomes clear. In the case of circumferential division, the center deflection decreases and then converges, and in the case of longitudinal division, the center deflection increases and converges as the slit's number increases. In particular, a phenomenon close to the greatest unpatterned tube's center displacement is seen in the case of the longitudinal division slits.

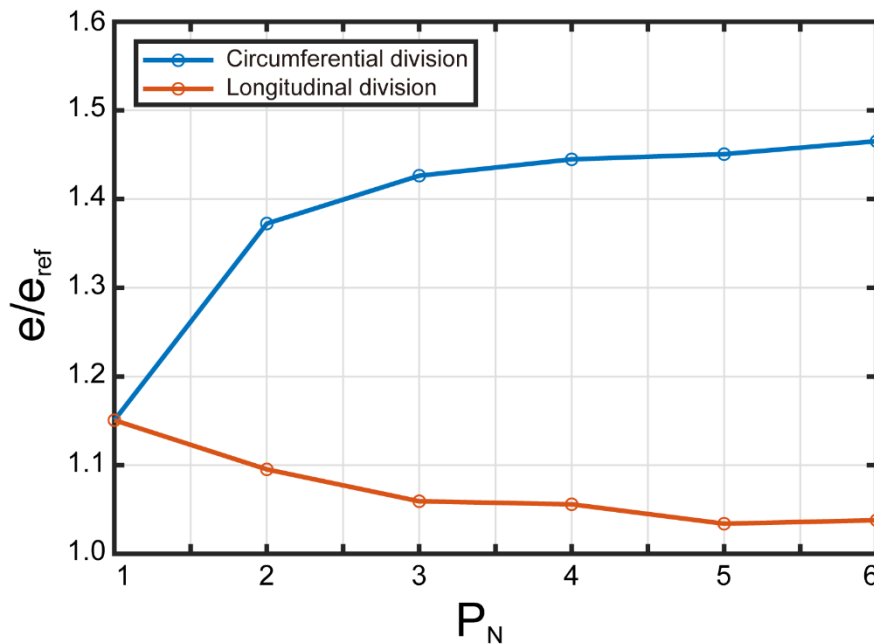


Figure 5.6. Non-dimensional ellipticity of the center cross-section of the tube with respect to the division direction and P_N .

Comparing the cross-section ellipticity with the quantity of slits on sub-domain, when the circumferential division slits with increasing the number of slit patterns are applied, the ellipticity is increased, and when the longitudinal division slits with increasing the number of slit patterns are applied, the ellipticity of center cross-section is decreased. In particular, as the number of slit patterns increases, it shows the difference in the tendency of ellipticity of center cross-section according to the division direction of the slits. In the case of circumferential division, the ellipticity increases and then converges, and in the case of longitudinal division, the ellipticity decreases and converges as the quantity of slit patterns increases. The ellipticity of the center cross-section of the circumferential and longitudinal divisions increased or decreased as the quantity of slit patterns increased, but showed a higher value compared to the ellipticity of the tube without slit patterns. Considering the relationship between the maximum center displacement and the ellipticity, the assumption of reducing the center deflection is confirmed by deforming the central section into an elliptical shape, which is a key idea in the design concept stage. In other words, when transverse impact loading is applied to the thin-walled circular tube engraved with circumferential and longitudinal division slits, the center cross section is deformed to an oval shape compared to the tube without slit patterns, and the greatest center deflection is reduced due to the effect. As the slit patterns engraved in s sub-domain are divided in the circumferential direction from a single rectangular slit as a reference, the center cross-section becomes more elliptical. However, as slit patterns are split longitudinally from a single rectangular slit as a reference, the center cross-section becomes more circular.

The reason for this phenomenon is the effective stress distribution on tube, which is shown through the tube's deformed shape with effective stress obtained through the nonlinear dynamic finite element analysis. First, we calculate the deformed shape with effective stress of the tube engraved with a single rectangular slit pattern, which is a reference, through nonlinear dynamic finite element analysis. Comparing the deformed shape with effective stress of the unpatterned tube and the tube with the reference rectangular slit engraved, the yellow area where the effective

stress is concentrated is reduced. This is the effect of a longitudinal slit pattern as explained in the previous chapter, because the effective stress that is concentrated due to the longitudinal slit is distributed and made the center part flexible in the circumferential direction. Also, the tube engraved with a single rectangular slit, which we use as a reference, has reduced maximum center deflection and increased the ellipticity of center cross-section compared to the tube without slit patterns due to the effect of the longitudinal pattern. In the deformed shape with effective stress of the thin-walled tube engraved with circumferential division 4 slit patterns on a sub-domain, the concentrated effective stress, indicated by the yellow area, is slightly wider, and the upper part of the tube changes to a dark blue area, indicating that the effective stress is more distributed. In the deformed shape with effective stress of the thin-walled tube engraved with longitudinal division 4 slit patterns on a sub-domain, the concentrated effective stress indicated by the yellow area is almost the same, and the dark blue area in the upper part of the tube is rather decreased, indicating that the effective stress is not distributed. In other words, the circumferential division slit effectively distributes the concentrated effective stress of the tube and makes the center part engraved with the slit patterns flexible, causing the cross-section to be deformed into an elliptical shape. Several longitudinal slits are created by circumferential division, and the longitudinal slit effect is slightly increased as several are arranged rather than one longitudinal slit. Due to the effect of the circumferential division from a longitudinal slit the maximum center deflection is reduced. However, the longitudinal division from a longitudinal slit prevents the concentrated effective stress to the center part, so cross-section is deformed into a circle than the cross section shape of the tube with circumferential division slits. In addition, the maximum center deflection and the ellipticity of center cross-section engraved with circumferential division slits show unusual trends depending on the number of patterns. As the quantity of divided slits on the one sub-domain increases, the maximum center deflection decreases and then converges, and the ellipticity of center cross-section increases and then converges. This tendency of maximum center deflection and ellipticity of center cross-section according to the

number of patterns needs to be explained by the movement of the cross-section. The most important principle here is that the cross-section of two successive sub-tubes engraved with the slit patterns of the tube changes from circular to elliptical. In addition, when a longitudinal slit pattern is engraved, it is deformed into an elliptical shape more under the influence of longitudinal slit than the unpatterned tube cross-section. First, the deformation of the unpatterned tube cross-section shows that the deformation occurs from a circle to an ellipse with one continuous line. Next, the tube cross-section deformation with the longitudinal slit pattern engraved on a sub-domain reveals that the longitudinal slit divides one continuous line into eight discontinuous curved lines. So, when there is only one pattern on each sub-domain, 8 discontinuous curves are gathered and deformation occurs from a circle to an ellipse. When there are two slit patterns on each sub-domain, one consecutive lines are divided into 16 discontinuous curves, and these curves are gathered to cause a transformation from a circle to an ellipse. In other words, the slit pattern could be thought of as a hinge connecting two discontinuous curves on either side in the tube cross-section. As the number of hinges increases, the discontinuous curves are more easily transformed from circular to elliptical. However, when the number of hinges reaches a certain level, the influence of discontinuous curves on deformation from circular to elliptical decreases. That is, as the quantity of slit patterns on a sub-domain increases, the number of discontinuous curves increases, and the effect on the transformation from circular to elliptical decreases. Therefore, as the number of patterns increases, there is a tendency to converge in the maximum center displacement and the ellipticity of center cross-section.

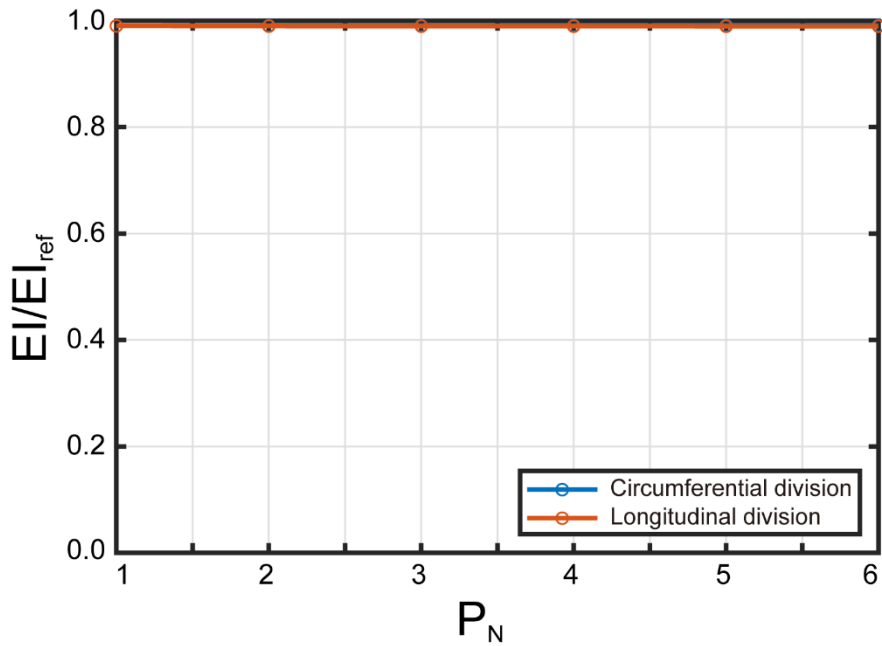


Figure 5.7. Non-dimensional bending rigidity of the tube with respect to the division direction and P_N .

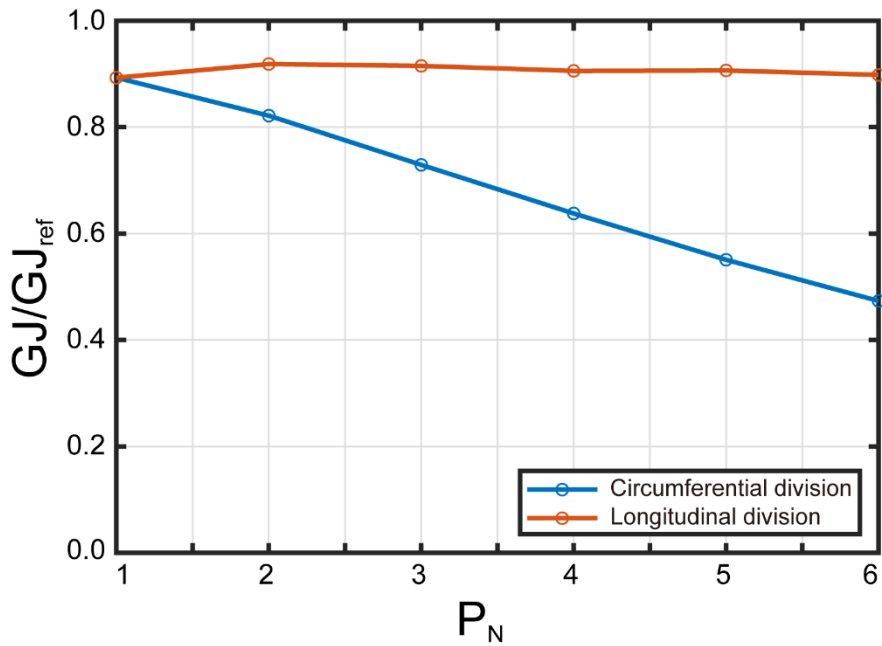


Figure 5.8. Non-dimensional torsional rigidity of the tube with respect to the division direction and P_N .

Comparing bending rigidity obtained by static finite element analysis, both circumferential and longitudinal division show little change as the number of patterns increases. In both cases, the reduction in bending rigidity compared to the tube without patterns is because the material was cut-out to engrave the pattern, and the fact that there is little change even if the number of patterns is increased is because the total area of the slit patterns is maintained.

Comparing the torsional rigidity according to circumferential and longitudinal division, it shows that the difference according to the division direction is remarkably displayed. As the number of divided patterns increases in longitudinal direction, the torsional rigidity of the tube hardly changes, but when the number of divided patterns increases in circumferential direction, it shows that the torsional rigidity of the tube decreases. This phenomenon occurs because of the shape of the area divided by the slits. Even if the number of divided patterns increases in the longitudinal direction, the torsional rigidity hardly changes because the shapes of the regions divided by the slits are almost the same. However, when the number of divided patterns increases in the circumferential direction, the torsional rigidity decreases because the shape of the region divided by the slit increases in shape weak to torsional loading.

It turns out the circumferential division is beneficial to reduce the maximum displacement under impact. The normalized displacement decreases monotonically with P_N while its effect is getting smaller. Due to the fact that the normalized displacement is actually increased, longitudinal division is completely useless. This phenomenon is primarily due to the circumferential division's tendency to deform the cross-section into an oval. The tube becomes more flexible in cross section deformation and the stresses become more distributed when there are multiple circumferentially divided slits. The cross-section deformation from impact position to central part, as indicated by less evenly distributed stresses, indicates that the energy is less efficiently used when slits are divided longitudinally. No matter the type of division, the number of slits has no effect on the tube's bending rigidity so long as the slit area is kept.

5.2.3 The effect of uniformly arranged slit patterns

In this chapter, we would like to explain why uniformly arranging the slit pattern is more effective in reducing center displacement than non-uniform arranging. First, for conceptual explanation, it is assumed that the place where the pattern is not engraved is a stiff element, and the part cut due to the pattern is assumed as the hinge element. The cross section of a tube with uniformly arranged slit patterns and a non-uniformly arranged tube is expressed as a stiff element and a hinge element. Basically, the cross section is deformed into a transversely flattened oval to reduce displacement due to impact loading. During this deformation process, in a tube in which the stiff element and the hinge element are uniformly arranged, the uniform spacing makes the stiff element easily deformed into an elliptical shape. However, non-uniform spacing in non-uniformly arranged tubes prevents the stiff element from deforming into an elliptical shape, so that it does not easily change to an elliptical shape. Therefore, the non-uniformly arranged tube is deformed in a circular shape than the uniformly arranged tube cross section, and the ellipticity value is also smaller. In conclusion, the more uniformly the slit patterns are arranged on the tube's surface, the easier the tube's cross-section is to be deformed into an elliptical shape, and the tube's center displacement can be reduced due to its effect.

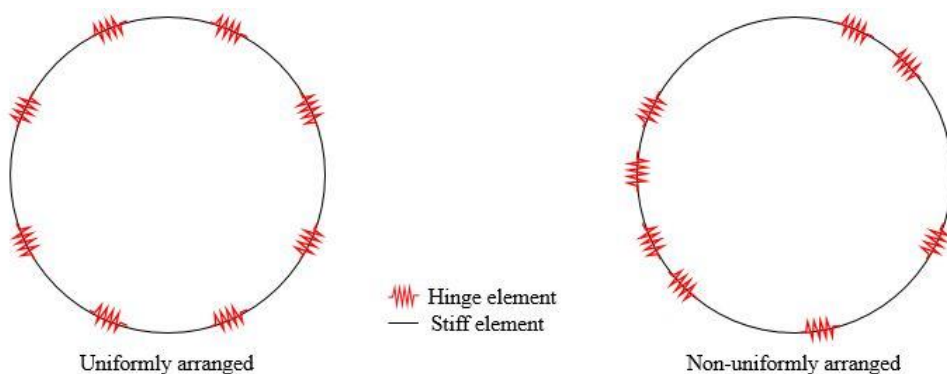


Figure 5.9. Conceptual explanation of tube sections drawn assuming stiff and hinge elements.

A parameter study was performed to verify that the aforementioned uniformly arranged slit patterns are more effective in reducing the center displacement of the tube than the non-uniformly arranged slit patterns. First, to control the arrangement of the slit pattern, the simulated case of the parametric study consisted of a half sub-tube consisting of parts 1, 2, 3, 4. We choose a single longitudinal slit of $H/H_D = 0.07$ and $W/W_D = 0.08$ as the reference. The reference model was chosen as a half sub-tube consisting of a total of 8 slits by uniformly applying 2 reference slits to 1 sub-domain. A total of 8 reference slit patterns consisted of cases from G1 to G6 with different arrangements. We obtain maximum center deflection and the ellipticity of cross-section from nonlinear dynamic finite element analysis. When comparing the maximum deflection for all cases, the uniformly placed reference case reduced the center deflection of the tube the most. Also, when comparing the ellipticity of the cross section, it is clear that the uniformly arranged reference case is the most elliptical. In conclusion, a uniform arrangement of the slits is advantageous for deforming the cross-section into an elliptical shape, which is beneficial in reducing the center deflection.

	Number of slits				Maximum Deflection (%)	Ellipticity (%)
	Part 1	Part 2	Part 3	Part 4		
Reference	2	2	2	2	- 7.63 %	+ 41.84 %
G 1	0	0	0	8	- 1.35 %	+ 3.41 %
G 2	0	0	8	0	- 4.21 %	+ 28.93 %
G 3	0	8	0	0	- 2.60 %	+ 27.10 %
G 4	8	0	0	0	- 1.57 %	+ 13.73 %
G 5	0	4	4	0	- 4.31 %	+ 27.84 %
G 6	4	0	0	4	- 4.41 %	+ 21.02 %

Table 5.2. Number of slits on part 1, 2, 3, 4, maximum deflection, and ellipticity of center cross-section of the tube engraved with slits. All values are calculated as percentage along with the tube without patterns.

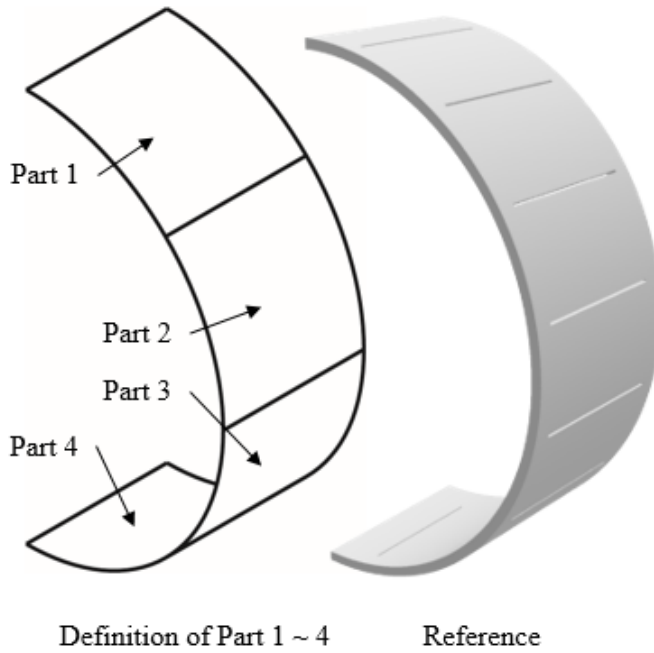


Figure 5.10. Definition of Part 1 ~ 4 on half sub-tube. Reference refers to a model in which two slits are uniformly arranged in one sub-domain.

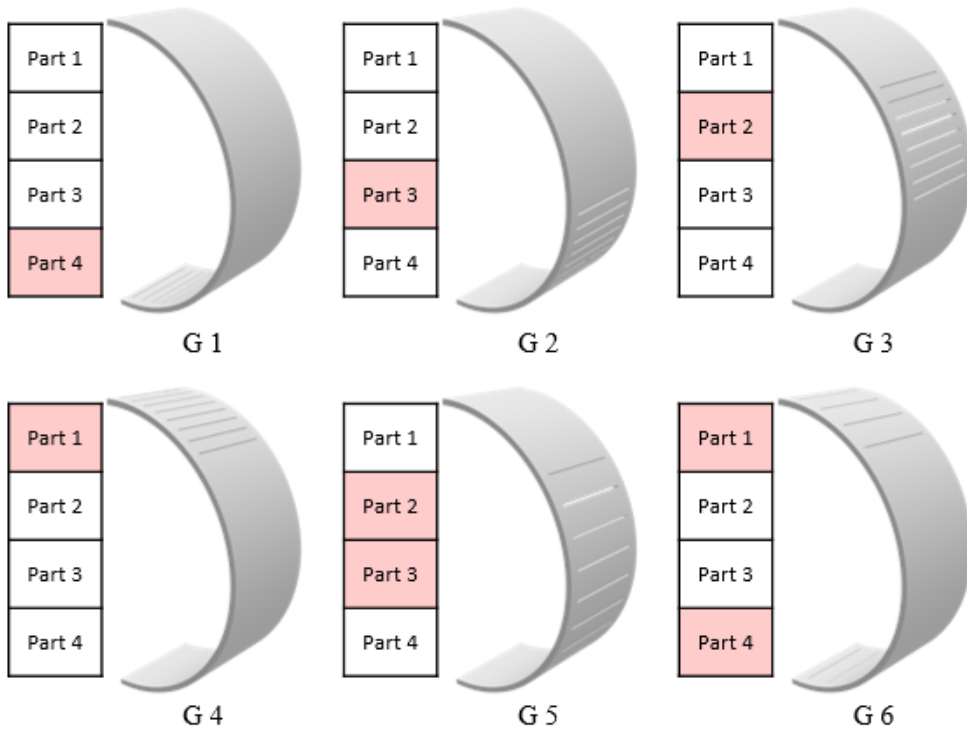


Figure 5.11. Definition of G1 ~ G6 models designed to have different slit pattern arrangements.

5.2.4 The effect of slit pattern under different loading conditions

In this chapter, the uniformly arranged slit pattern is effective in reducing the central deflection of the pipe, and it is investigated whether the effect is effective even when the loading condition is changed. The position where the slit patterns are engraved was designed to be engraved on two sub-tubes from the center of the tube, as in the previous chapters. We choose a single longitudinal slit of $H/H_D = 0.012$ and $W/W_D = 0.08$ as the reference to investigate the effect of the slit patterns within a sub-domain on the deformation of the tube under different loading conditions. The initial speed of the current drop weight technique was designed to be same, and the loading conditions were changed by adjusting the impact point to investigate the effect of the slit pattern according to the location of the impact point.

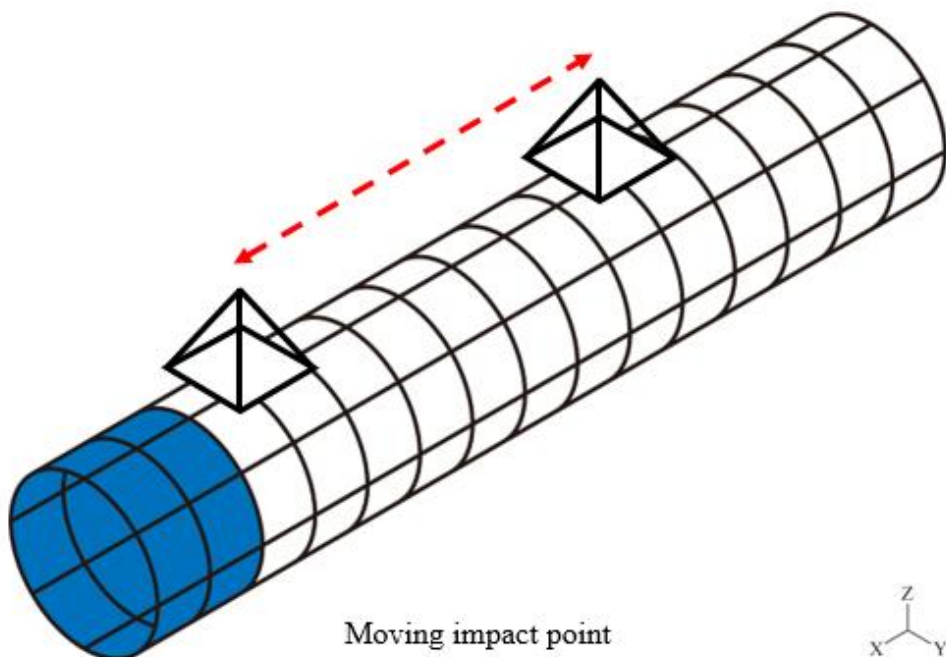


Figure 5.12. Definition of boundary condition change according to impact point movement.

The position of the conventional impact point is 1/3 of the entire tube, so it is located 125mm from the tube center in the half model. To change loading condition, the position of the impact point was adjusted from 75 mm from the center of the tube to 250 mm from the end of the tube. The interval to adjust the collision point was defined as the length of the sub-domain 25mm, and nonlinear finite element analysis were performed by applying 8 different impact point positions to one slit pattern case. Eight simulations were performed by applying 8 different impact points to the reference tube without slit patterns, and when there were slit patterns, a total of 48 simulations were performed by increasing the slit pattern from 1 to 6 in one sub-domain. In order to check whether the tube center deflection has the effect of reducing the tube center deflection by deforming the cross-section into an oval when different loading conditions are applied, the center deflection and the tube cross-section ellipticity were calculated through nonlinear finite element analysis.

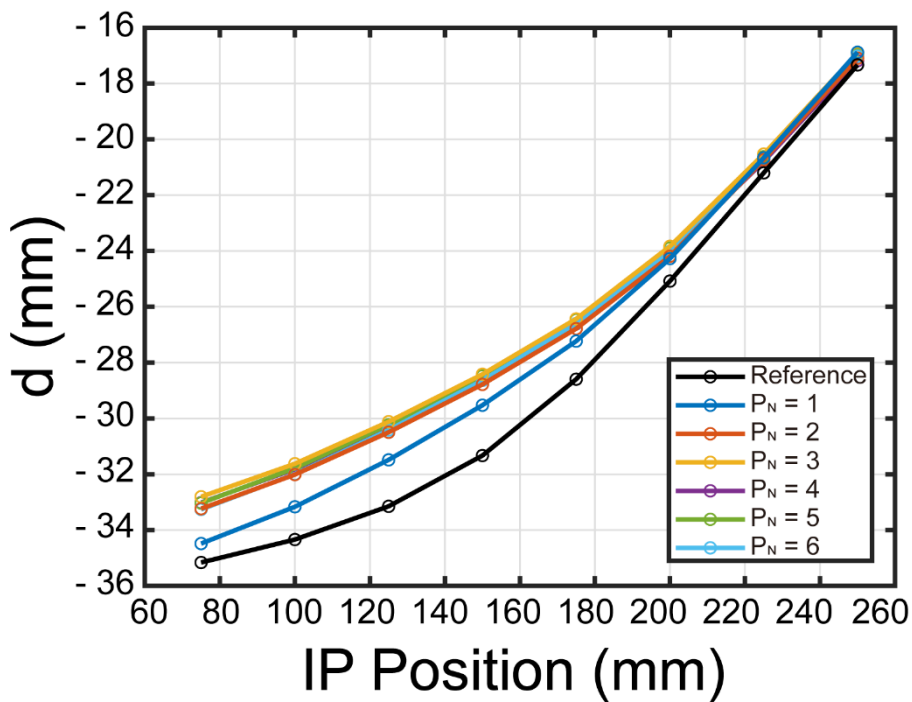


Figure 5.13. Center deflection of the tube with respect to the position of the impact point and the number of slit patterns (P_N).

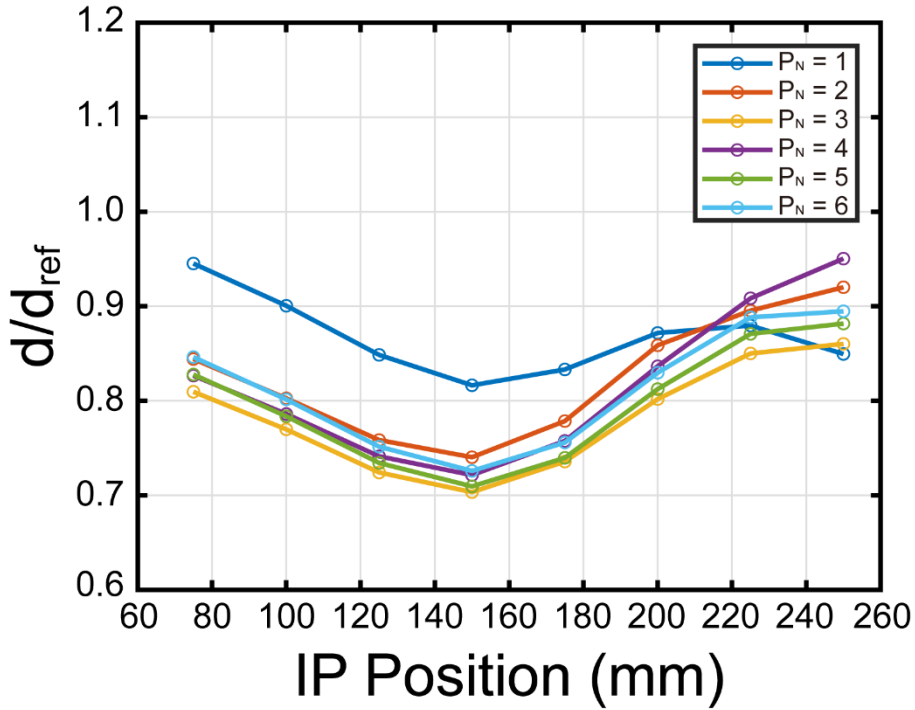


Figure 5.14. Non-dimensional center deflection of the tube with respect to the position of the impact point and the number of slit patterns (P_N).

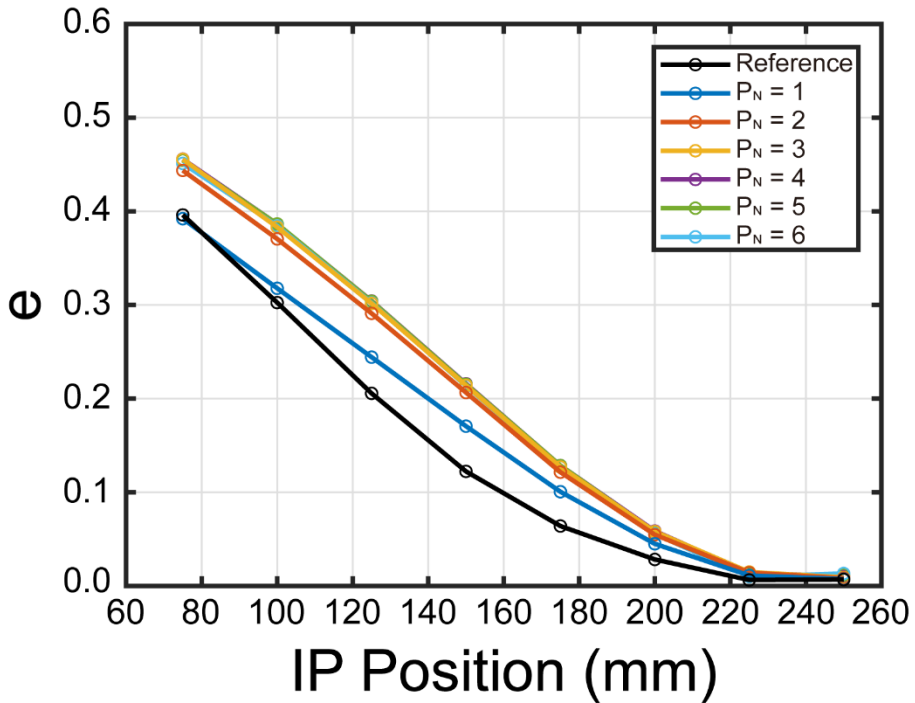


Figure 5.15. Ellipticity of the tube cross-section with respect to the position of the impact point and the number of slit patterns (P_N).

As mentioned in Chapter 2, when the loading is applied, tube plastic deformation mechanism will be most deformed at the impact point, and it is expected that the impact will gradually decrease from impact position to the center and the clamped end. In other words, it was predicted that the effect of slits on tube center deflection would be different due to 8 different loading conditions. In addition, since the loading condition was designed so that the impact point gradually moved away from the location where the slit patterns were engraved, it was expected that the influence of the slit patterns on the center deflection of the tube would gradually decrease. This was expected because the effect of plastic deformation from the impact point decreases as the distance between the impact position and the part where the slit patterns are engraved increases. Analyzing the center deflection graph of the tube according to the impact point, as expected, the effect of the slit patterns decreased as the distance between the impact point and the area where the slit patterns were engraved increased, and the effect of reducing the center deflection of the tube was confirmed. However, compared to tubes without slit patterns, it has been demonstrated that the reduction in center deflection due to slit patterns exists even when the impact point is changed. Next, when analyzing the non-dimensional center deflection graph according to the impact point, the effect and maximum value of the slit pattern appeared when the location of the impact point was about 150 mm, and it was found that the center deflection decreased the most. Also, as a result of analyzing the cross-section ellipticity graph according to the impact point, it was found that the effect of the slit pattern decreased as the distance between the impact point and the area where the slit pattern was engraved decreased as expected. In conclusion, even if the boundary condition is changed by adjusting the impact point, it has the effect of transforming the cross-section caused by the slit patterns into an elliptical shape, and this proves that the effect of reducing the center deflection still exists.

5.3 Deformed shape of the tube with different height

5.3.1 Deformed shape of the tube

In this section, we investigated how the height of slits within a sub-domain affects the tube deformation under transverse impact loading. For the purpose of examining the effect of the height slit patterns within a sub-domain on the deformation of the tube, we select a longitudinal slit with $H/H_D = 0.012$ and $W/W_D = 0.08$ as the reference. By setting the reference slit, the height of the slit pattern was changed and the number of slits was changed. The three single longitudinal slits we selected were named thin, medium, and thick slit patterns according to their height. The thin slit pattern is $H/H_D = 0.012$ and $W/W_D = 0.08$. The medium slit pattern is $H/H_D = 0.024$ and $W/W_D = 0.08$. The thick slit pattern is $H/H_D = 0.036$ and $W/W_D = 0.08$. To investigate the influence of the height of pattern on the tube deformation, W/W_D is fixed, and only the height of each reference rectangular slit pattern is different. Also, the deformation of the tube was investigated while changing the number of each reference rectangular slit pattern. In the previous chapter, when a single rectangular is engraved in the sub-domain, the slit rectangular slit pattern is created in principle that the position is engraved in the center of each sub-domain. First, reference slits of thin, medium, and thick selected from a finite element tube model are created within the sub-domains in the aforementioned manner. Then, the number of reference slits, thin, medium, and thick slits, is changed. The method of increasing the number of patterns is created by the circumferential division method of the previous section, and since the height of each reference slit is different, the total area of the slit is also different. As mentioned in the previous chapter, slit patterns are generated on one sub-domain and engraved on two consecutive sub-tubes from the center of the tube. When the number of reference rectangular slits increases, they are all arranged to have the same interval in the circumferential direction. Six cases of P_N (1 to 6) are tested for each reference slits of thin, medium, and thick.

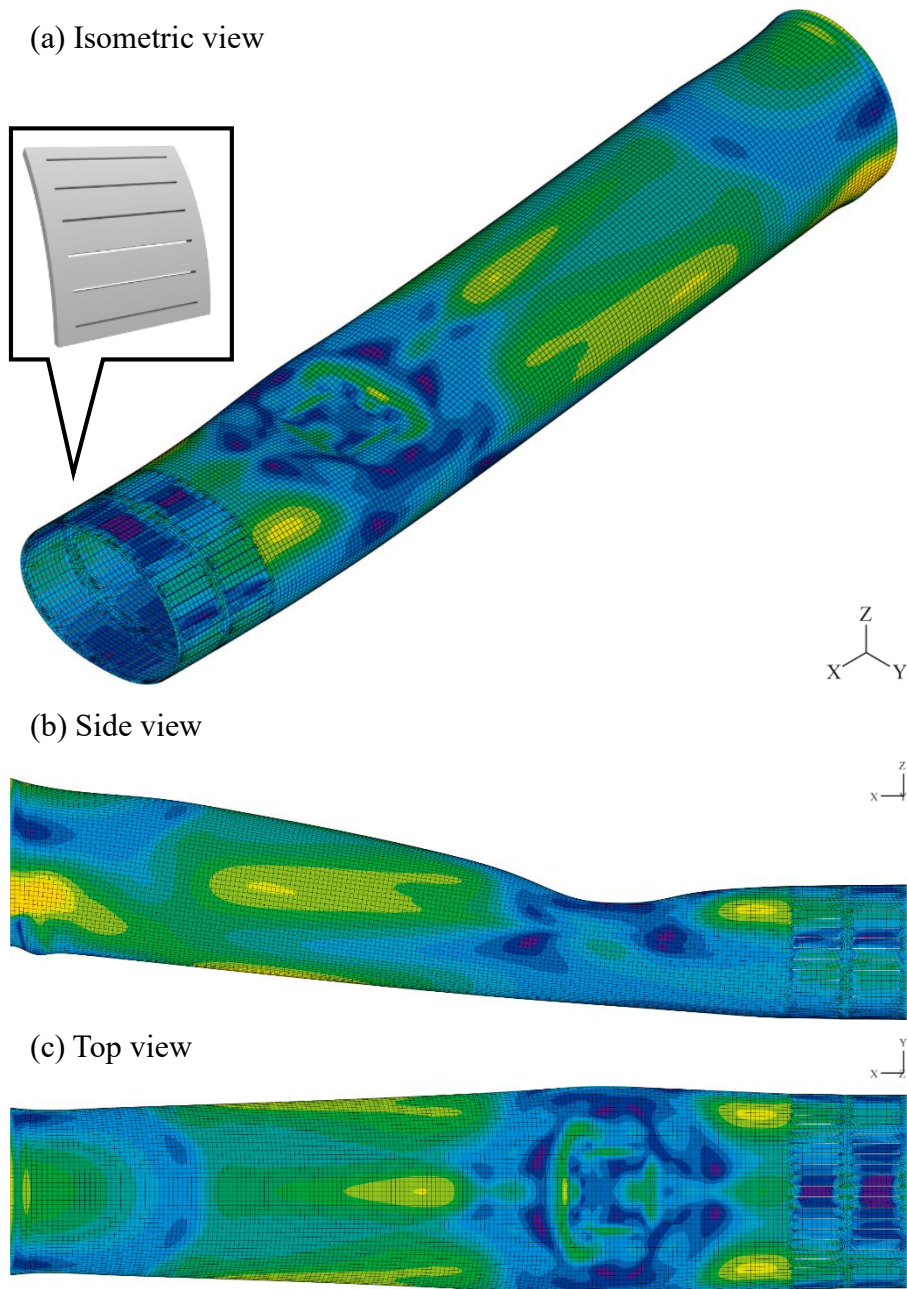


Figure 5.16. Deformed shape with effective stress of thin-walled tube with the thin slit on each sub-domain. The thin reference single rectangular slit has H/H_D of 0.012, W/W_D of 0.800, and the number of slit on a sub-domain is 6. (a) Isometric view. (b) Side view. (c) Top view.

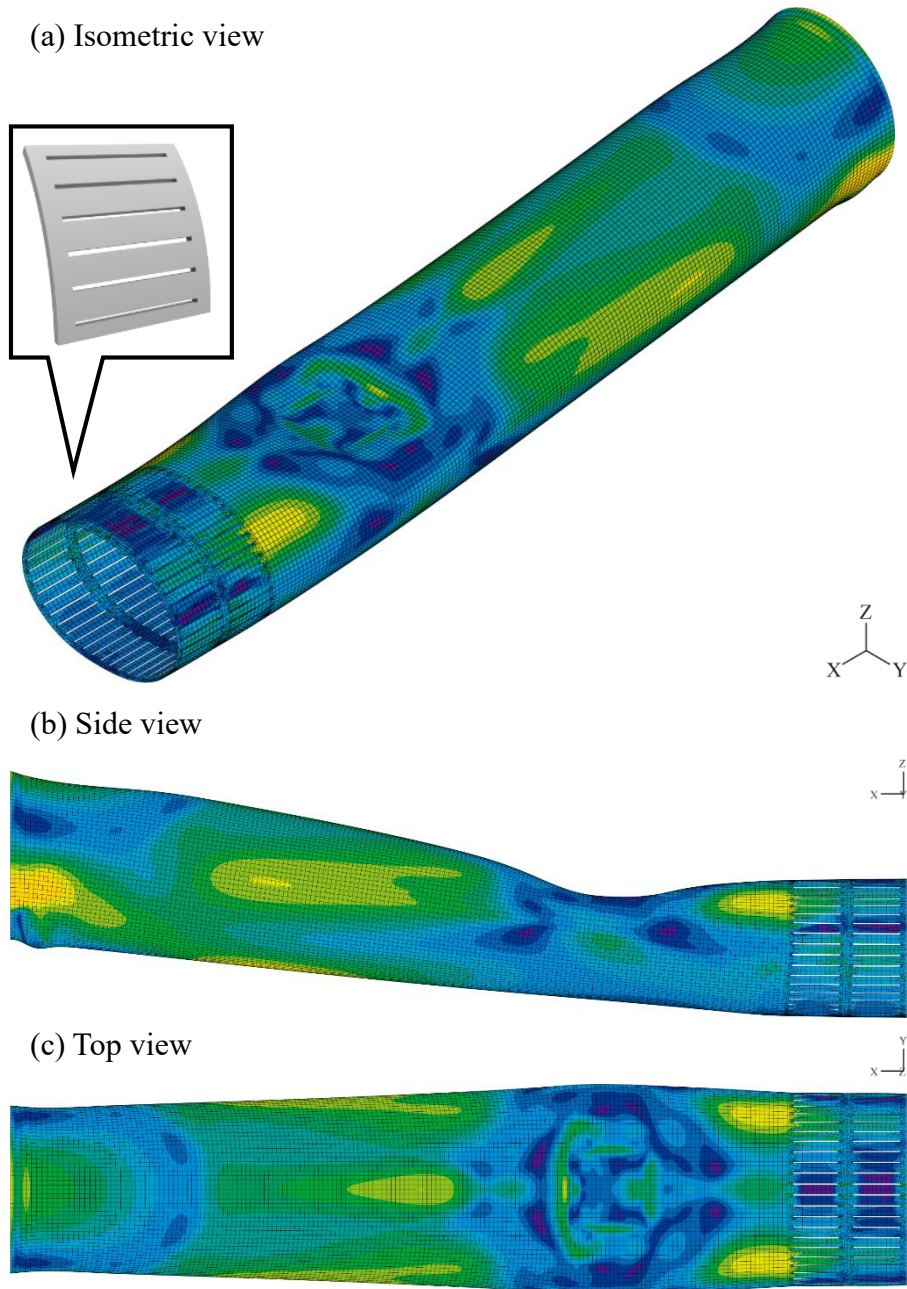


Figure 5.17. Deformed shape with effective stress of thin-walled tube with the medium slit on each sub-domain. The medium reference single rectangular slit has H/H_D of 0.024, W/W_D of 0.800, and the number of slit on a sub-domain is 6. (a) Isometric view. (b) Side view. (c) Top view.

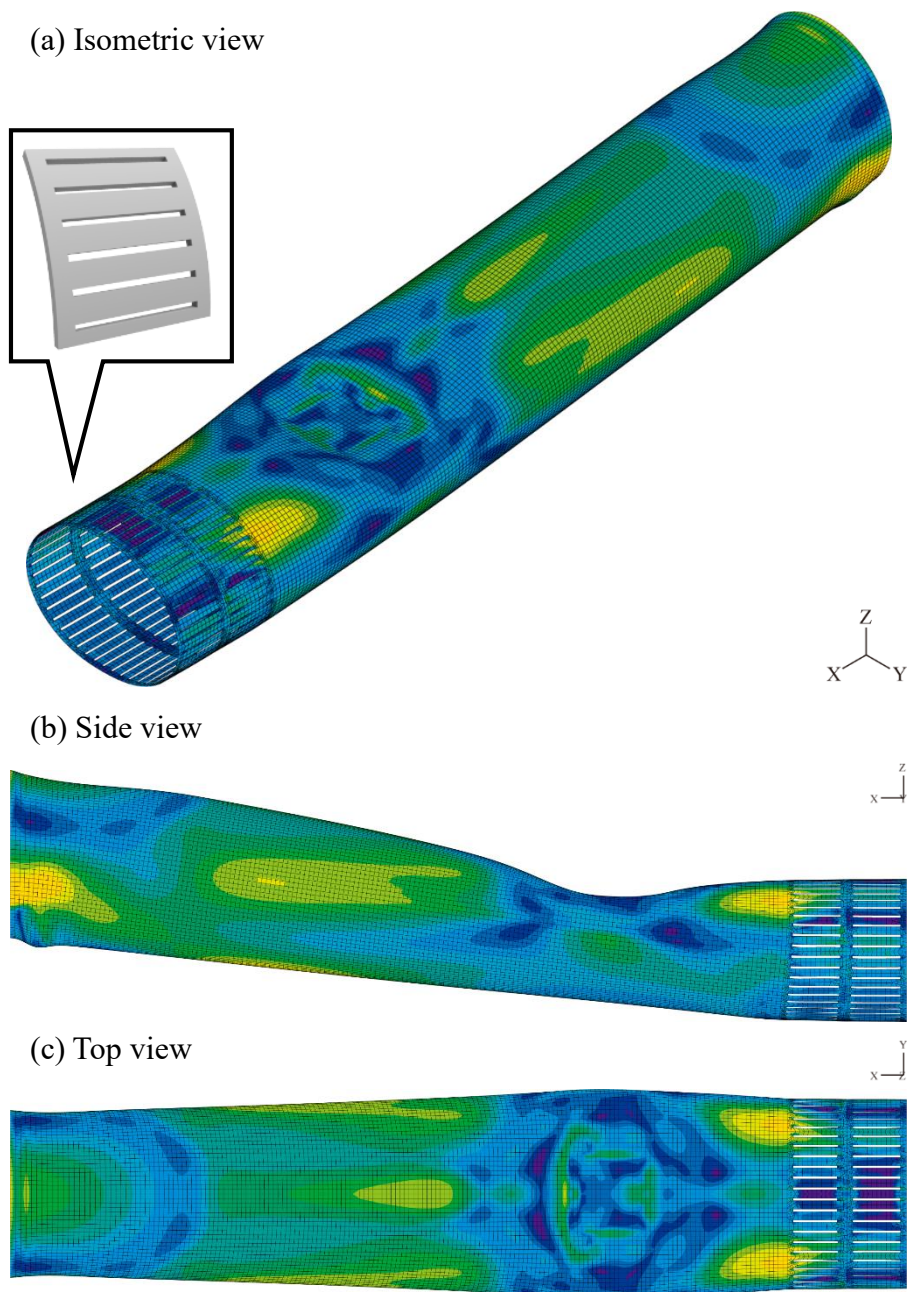


Figure 5.18. Deformed shape with effective stress of thin-walled tube with the thick slit on each sub-domain. The thick reference single rectangular slit has H/H_D of 0.036, W/W_D of 0.800, and the number of slit on a sub-domain is 6. (a) Isometric view. (b) Side view. (c) Top view.

5.3.2 The effect of different height

In this chapter, a parameter study is conducted on multiple slit patterns on each sub-domain. We choose a single longitudinal slit of $H/H_D = 0.012$ and $W/W_D = 0.08$ as the reference. In order to accurately compare the influence of the slit heights on a sub-domain on the maximum center displacement under impact loading, three representative types of slit, thin slit ($H/H_D = 0.012$ and $W/W_D = 0.08$), medium ($H/H_D = 0.024$ and $W/W_D = 0.08$), and thick ($H/H_D = 0.036$ and $W/W_D = 0.08$) are selected. Since the height of each of the three representative slits is different, the total area of slits also varies as the quantity of slit patterns on each sub-domain increases. We obtain maximum center deflection and the ellipticity of cross-section from nonlinear dynamic finite element analysis, and bending and torsional rigidities from static finite element analysis.

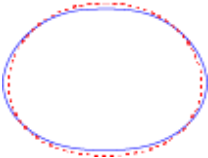
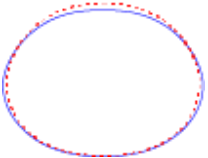
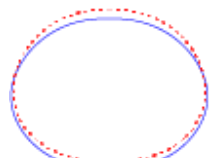
	Thin	Medium	Thick
Cross-section shape (Red dash: Reference Blue line: Patterned)			
Max. Deflection	- 7.28 %	- 1.62 %	+ 5.52 %
Ellipticity	+ 47.66 %	+ 35.64 %	- 20.48 %
Bending rigidity	- 0.85 %	- 1.84 %	- 3.01 %
Torsional rigidity	- 52.66 %	- 58.78 %	- 65.20 %

Table 5.3. Cross-section shape, maximum deflection, ellipticity of center cross-section, bending and torsional rigidity of the tube engraved with thin, medium, thick slits. All values are calculated as percent with reference to the value of the tube without patterns.

We selected three reference rectangular slit patterns with different heights, and performed nonlinear dynamic-implicit analysis with slits by changing the quantity of slits on one sub-domain in the circumferential direction. Therefore, we investigated the effect of the height of patterns on a sub-domain on the maximum center deflection while comparing the tube deformation to which thin, medium, and thick slits are applied with different total area of slits. That is, although the amount of slits engraved in one sub-domain is the same, the total area of slits is different because the height of each reference slit is different. In particular, in this section, to study the effect of the pattern height on the deformation of the tube, we focused on comparing the cases with different heights and the same number of slits on one sub-domain. The outcomes obtained by performing nonlinear dynamic-implicit analysis on the tube with three representative patterns of thin, medium, and thick slits are compared with the unpatterned tube's deformation as the reference.

First, the overall trend shows that as the number of slits increases, the maximum center deflection decreases and then increases in all cases for tubes with thin, medium, and thick slits engraved on the tube. In particular, when the number of slits is 2 rather than 1, the maximum center deflection tends to decrease. However, after the number of slits is two, the tendency for maximum center deflection to increase varies according to the height of the slits. When thick slits are applied to the tube, the maximum center deflection increases drastically, then when medium slits are applied to the tube, it increases monotonically when thin slits are applied to the tube. Also, when the number of slit patterns is 4 or more, the maximum displacement to which thick slits are applied is rather increased than the greatest center deflection of the unpatterned tube.

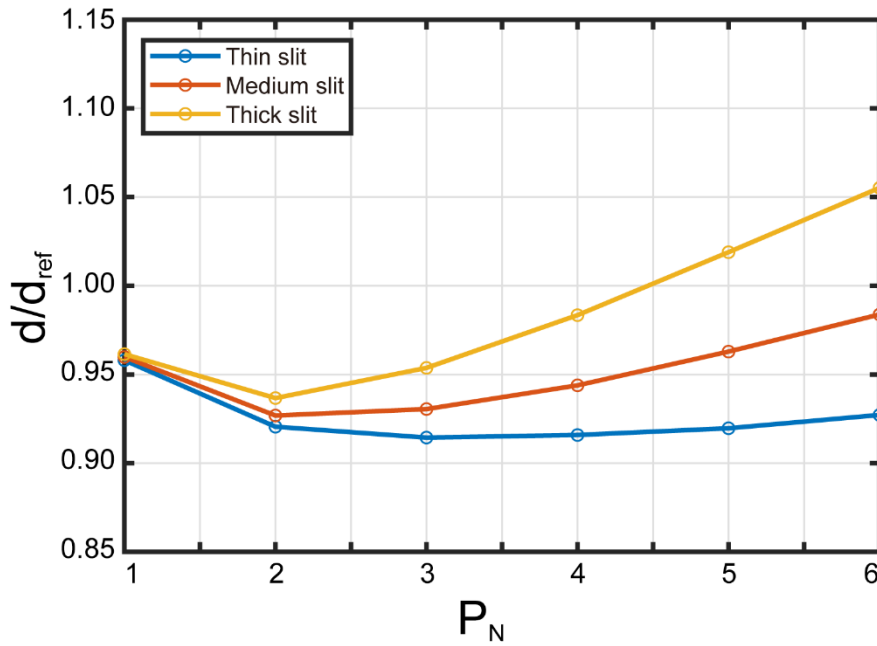


Figure 5.19. Non-dimensional maximum center deflection of the tube with respect to the thickness of the slits and P_N .

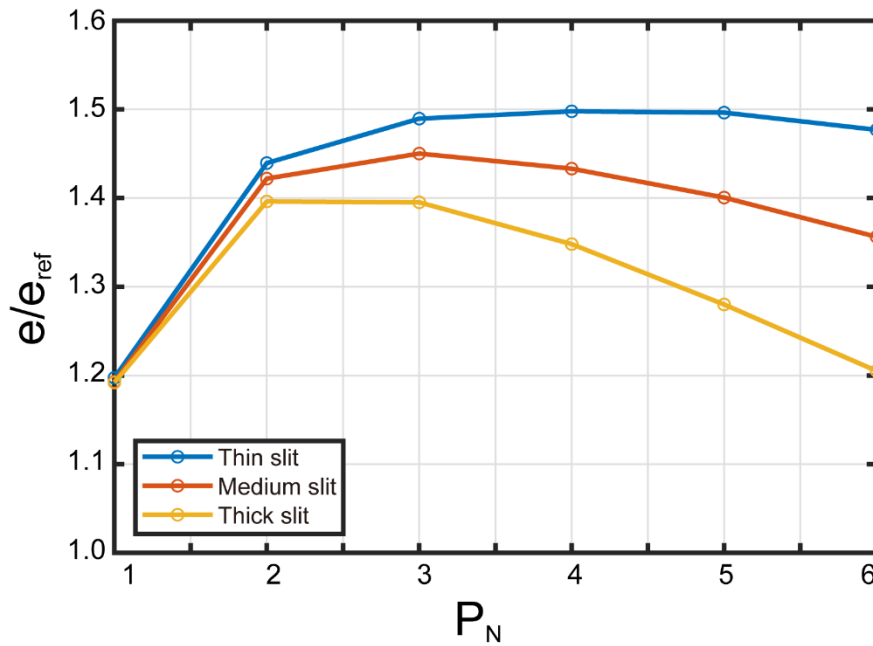


Figure 5.20. Non-dimensional ellipticity of the center cross-section of the tube with respect to the thickness of the slits and P_N .

Comparing the ellipticity of the thin-walled tube with thin, medium, and thick slits engraved on the surface and the number of patterns, the overall trend shows that the ellipticity increases and then decreases in all cases as the amount of slit patterns increases. When the quantity of slits is increased from 1 to 3, the ellipticity values of the tubes with thin, medium, and thick slits all increase. However, when the number of slits increases from 1 to 2, the ellipticity increase rate is larger than when the number of slits increases from 2 to 3. Also, when the number of slits is increased to 3 or more, the ellipticity of medium and thick slit tubes tends to decrease more than the ellipticity of the thin slit tube. When the ellipticity of the thin, medium, and thick slit tubes is compared when the number of patterns engraved in one sub-domain is the same, the ellipticity of the thin slit tube always shows the highest value regardless of the number of slits. all. On the other hand, the ellipticity value of the thick slit tube is the lowest. Considering the relationship between the maximum center deflection and the center cross-section ellipticity, as the number of patterns on each sub-domain increases, the trend of maximum center deflection and the trend of ellipticity show opposite trends.

The reason for this phenomenon is the effective stress distribution on the tube, which is shown through the deformed tube shape with effective stress obtained through the nonlinear dynamic finite element analysis. We calculate the deformed shape with effective stress of the tube engraved with three representative slits of thin, medium, and thick slits, through nonlinear dynamic finite element analysis. Similar trends can be seen in tubes engraved with thin, medium, and thick slits examined in this section and the tube engraved with circumferential division slits examined in the previous section. The most similar case in terms of maximum center deflection and ellipticity is when thin slits are engraved into the tube. The difference from the circumferential division slits in the previous section is that the total slit area is increased by increasing the number of slits in the reference, rather than maintaining the total slit area by dividing from the reference's slit. Although these differences exist, as the number of thin slits increases, the region engraved with slits becomes more flexible and the cross-section becomes elliptical shape by distributing the

concentrated effective stress on the tube without slit patterns. This is confirmed by the ellipticity value of the tube engraved with thin slits and the deformed shape of the tube with effective stress. That is, the principle of reducing the maximum center deflection by making the center part of the tube elliptical is the same. Also, when the number of patterns is 6, when comparing the deformed shape with effective stress of the thin, medium, and thick slit tube, the size of the region where the effective stress is concentrated is different. In the case of a tube engraved with thin slits, the area of concentrated effective stress indicated in yellow is the smallest, and in the case of a tube engraved with thick slits, it is the largest. This means that the thin slits distribute more concentrated effective stress to transform the cross-section into a more elliptical shape. However, differences that did not occur before appear in the maximum center displacement and the ellipticity of center cross-section of the tubes with medium and thick slits. The difference is that as the number of patterns increases, maximum center deflection and ellipticity decrease or increase, but convergence does not appear. As described in the circumferential dividing slits in the previous section, depending on the number of slits to be engraved, the tube cross-section is divided into several discrete curves with one continuous line divided by the slits. Divided multiple discrete curves have an effect on the ellipticity, and as the number of discrete curves increases, the effect on ellipticity decreases, resulting in the convergence of the ellipticity. This phenomenon is only seen in tubes with thin slits, but not in tubes with medium and thick slits. It is considered that the cause is not the effect of the number of slits, but the effect of the height of each reference slit. In particular, as the number of patterns increases in tubes with medium and thick slits, the phenomenon that the maximum center displacement decreases and then increases, and the ellipticity increases and then decreases are thought to be due to the difference in bending rigidity.

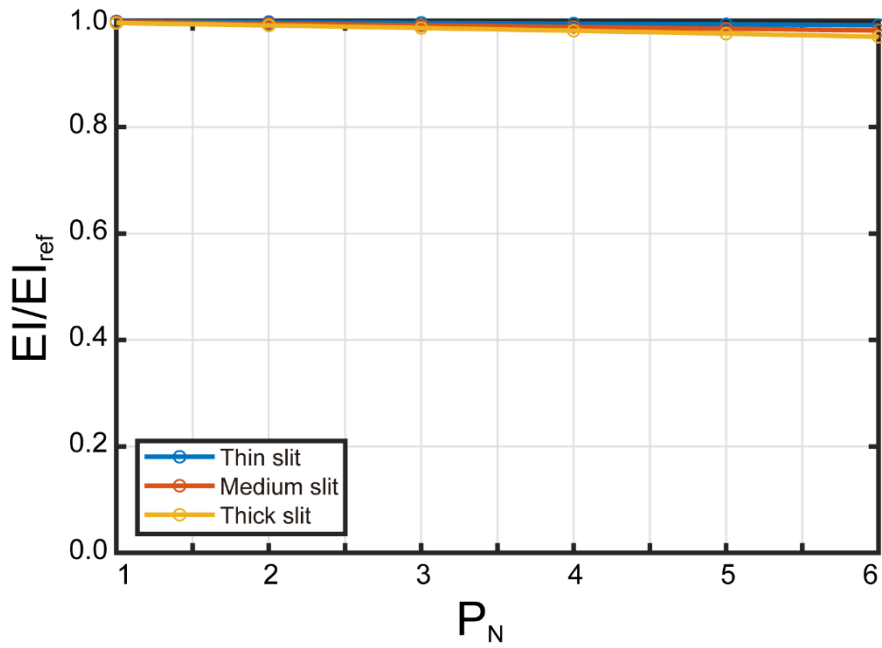


Figure 5.21. Non-dimensional bending rigidity of the tube with respect to the thickness of the slits and P_N .

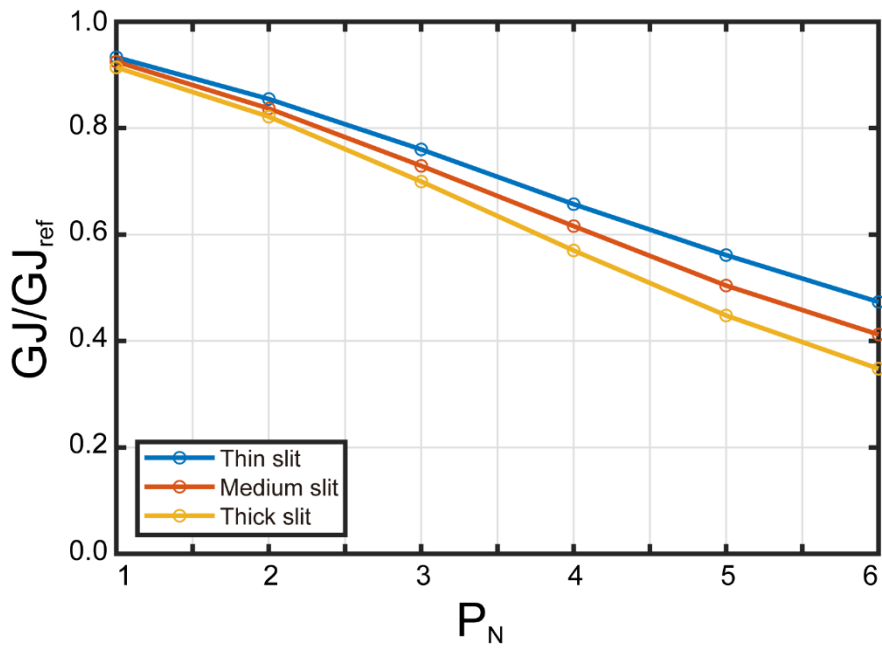


Figure 5.22. Non-dimensional torsional rigidity of the tube with respect to the thickness of the slits and P_N .

In this section, the remarkably different parts are revealed by comparing the maximum center deflection and the ellipticity of the tube without a reference pattern. As the number of patterns increases, the thick slit tube's maximum center deflection value exceeds 1.0 in the maximum center deflection graph of the thin, medium, and thick slit tubes. This means that when the number of thick slits exceeds 4, the greatest center displacement of thick slit tube rises rather than the maximum center displacement of the unpatterned tube. However, in the ellipticity graph of thin, medium, and thick slit tubes, there is no case where the ellipticity value of the tube is less than 1.0 as the quantity of patterns increases. This means that as the quantity of thin, medium, and thick slits increased, the ellipticity of the patterned tube in all cases was always higher than that of the tube without patterns, meaning that the cross-section became more elliptical. Considering these trends of maximum center deflection and ellipticity of center cross-section together, as mentioned above, as the number of slits increases, it should show a tendency to converge, but rather it tends to decrease or increase. This is considered as the effect of the pattern height on tube's deformation and is related to the bending rigidity of the different height slit tubes.

Static analysis is performed to determine the bending rigidity with thin, medium, and thick slit patterns depending on the quantity of slits. When calculating the bending stiffness, a full tube model is created and calculated by applying the bending loading. Comparing the bending rigidity of the different height slit tubes according to the change in the number of slit patterns, the overall trend of bending rigidity of the tube engraved with each pattern decreases as the number of patterns increases. The reason for this is that the area to cut-out the material increases as the number of slit patterns of different heights increases. Since the area occupied by the slit patterns of different heights selected by us is small in the entire tube, the amount of reduction in bending rigidity of the tubes engraved with slit patterns of different heights is not large. However, even if the number of slits is the same, the reduction in bending rigidity is also different because the height of each slit is different. That is, the bending rigidity of the thick slit decreases the most, and the bending rigidity of the thin slit tube decreases the least. Also, the location where thin, medium, and thick

slits are engraved affects the vertical stiffness of the tube as it is engraved locally on two successive sub-tubes from the center of the tube. Due to this effect, maximum center deflection with slits of different heights appears differently. In particular, in the tube with thick slits, the ellipticity increased compared to the unpatterned tube, but the maximum center deflection increased. Next, comparing the torsional rigidity of the thin, medium, and thick slit tubes, the torsional rigidity tends to decrease as the slit's number increases. In addition, as the pattern height increases and the quantity of slit patterns increases, torsion rigidity of the tube with slit patterns tends to decrease rapidly. This reason is the same as the tendency of circumferential division slits in the previous section, and it is because of the shape of the tube divided by the longitudinal shape slits. Regions excluding the longitudinal slits also creates longitudinal slit shapes, and since this shape is weak against torsional loading, as the number of patterns increases, the tube's torsional rigidity tends to decrease rapidly.

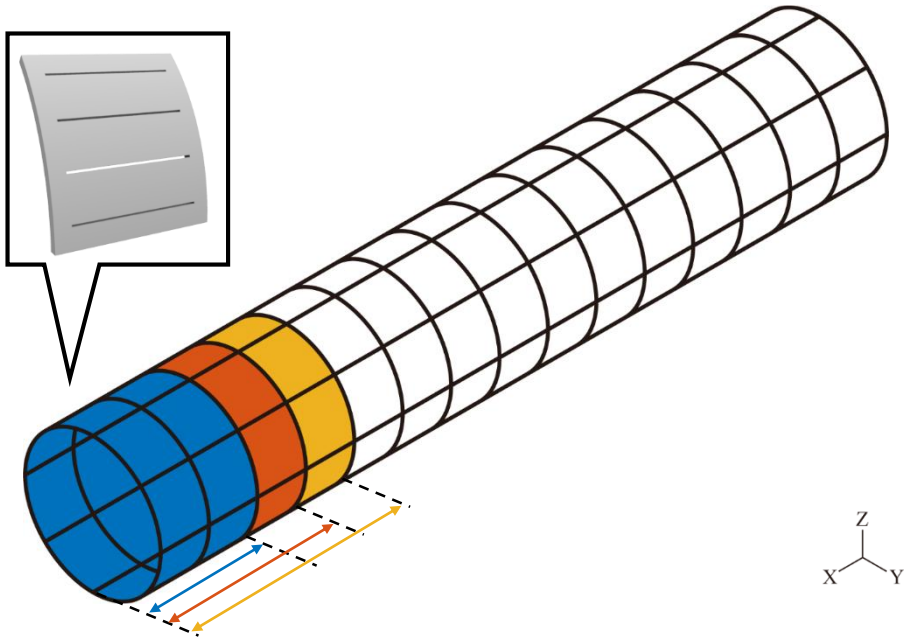
In conclusion, it is evident that thinner slits do a better job of reducing the center displacement during impact. For thinner slits, greater cross-section ellipticity and a smaller area of focused stresses are seen. The outcomes are similar for all P_N values. The tube displacement becomes more sensitive to pattern height as the amount of patterns per sub-domain increases, with the exception of small P_N values. This is likely because, in comparison to its effect on cross-sectional deformation, with increasing pattern size, slits have a greater impact on vertical stiffness in the engraved slits area. Therefore, when choosing the quantity and size of slits, we must take into account these conflicting effects.

5.4 Deformed shape of the tube with different pattern range

5.4.1 Deformed shape of the tube

In previous sections, we studied the influence of the shape, number, and pattern height on the deformation of the tube. With these results and the insights gained from the analysis of the results, in this section, we investigated how the patterned range affects the tube's deformation under transverse impact to further generate tube's plastic deformation. The expected result when the pattern engraved range is changed is that tube's plastic deformation occurs as the pattern engraved range becomes wider, and the tube center cross-section is deformed more elliptical according to the shape of the patterns. That is, we expect the effect of relatively reducing the energy consumed in the center deflection of the tube by controlling the range in which the pattern is engraved, so that the impact energy is more used in the tube's plastic deformation. We selected the slit pattern applied to one sub-domain to investigate how the pattern engraved range affects the deformation of the tube. We selected the single slit pattern in consideration of our previous results and insights, and the single slit pattern chosen is to arrange reference single longitudinal slit circumferentially in a sub-domain. We choose a single longitudinal slit of $H/H_D = 0.012$ and $W/W_D = 0.08$ as the reference to research the effect of the range on the deformation under transverse impact loading. When the reference single longitudinal slit pattern are increased and positioned in a circumferential sequence on each sub-domain, longitudinal slit patterns are always arranged to have the same interval as in the previous sections. The reason why the single longitudinal slit pattern is selected is because the four longitudinal slit pattern deforms the tube cross section more elliptical based on the results on the effect of the shape, number, and slit's height on the tube deformation under transverse loading.

(a) Isometric view



(b) Side view

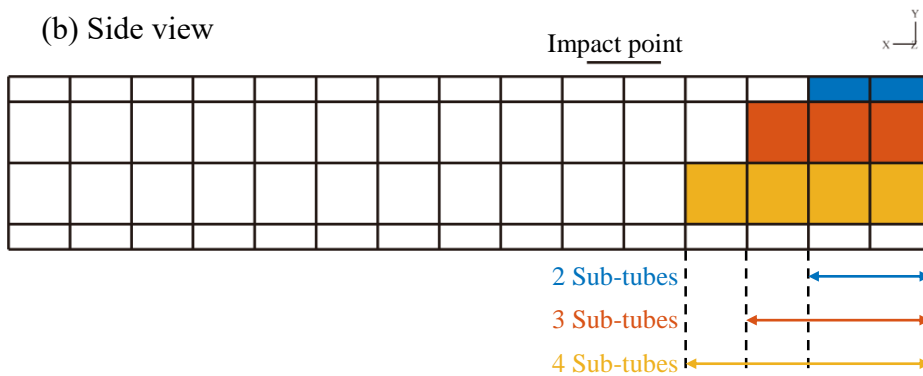


Figure 5.23. Definition of pattern range (2 sub-tubes, 3 sub-tubes, and 4 sub-tubes) on the finite element tube model with sub-domains. (a) Isometric view. (b) Side view.

Figure 5.16. shows the pattern range definition. In the initial stage of this study, we designed a sub-domain in the form of a square to define the slit pattern, and connected eight of them in the circumferential direction to create a sub-tube and a half-tube model consisting of a total of 120 sub-domains. The white rectangles shown in the isometric and side view of the tube model in Figure 5.16. represent sub-domains. In this section, it is necessary to define the pattern range to study the influence of the pattern range on the deformation. Also, the definition of the pattern range is defined as the number of sub-tubes engraved with slit patterns from the center of the tube. In all sections investigating the slit shape effect, number, and height on tube deformation, slit patterns are applied over two sub-tubes in succession from the tube center. In figure 5.16., it appears as the blue area, and the pattern range is defined as 2 sub-tubes and consists of 16 sub-domains. The pattern range is changed by increasing the number of sub-tubes, and an impact plate is located between the 5th and 6th sub-tube when viewed from the side of the tube. In this section, the pattern ranges are selected as 2 sub-tubes, 3 sub-tubs, and 4 sub-tubes in three cases considering the location of the impact point. 3 sub-tubes are shown as orange area in Figure 5.16. and consist of 24 sub-domains, and 4 sub-tubes are shown as yellow area and consist of 32 sub-domains. The slit patterns are engraved in each sub-domain, and the quantity of slit patterns on a sub-domain is changed from 1 to 6. In the case of the three representative 2 sub-tubes, 3 sub-tubes, and 4 sub-tubes, the area of the slit pattern occupied by one sub-domain is the same even if the quantity of patterns on a sub-domain is changed. However, because the pattern ranges are different, the number of sub-domains in which the slit patterns are engraved is different, and the total area of slit patterns is different. To research the influence of different pattern ranges on tube's deformation, nonlinear dynamic finite element analysis is performed by applying reference longitudinal slits to different pattern ranges on the tube and changing the number of them.

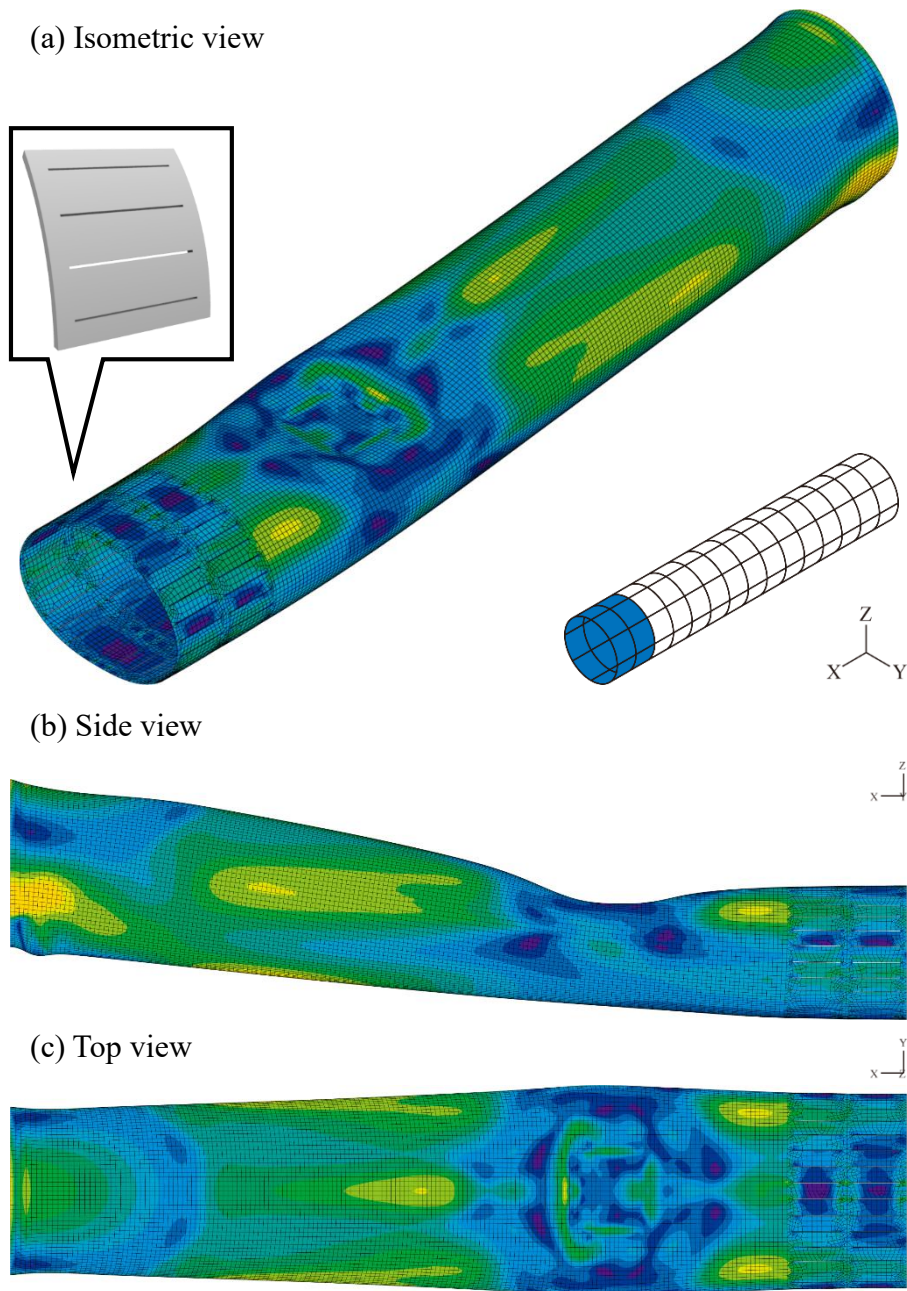


Figure 5.24. Deformed shape with effective stress of thin-walled tube with the reference slits on 2 sub-tubes. The pattern range is 2 sub-tubes, H/H_D of the reference slit is 0.012, W/W_D is 0.800, the number of slit on a sub-domain is 4, and the number of total slits is 64. (a) Isometric view. (b) Side view. (c) Top view.

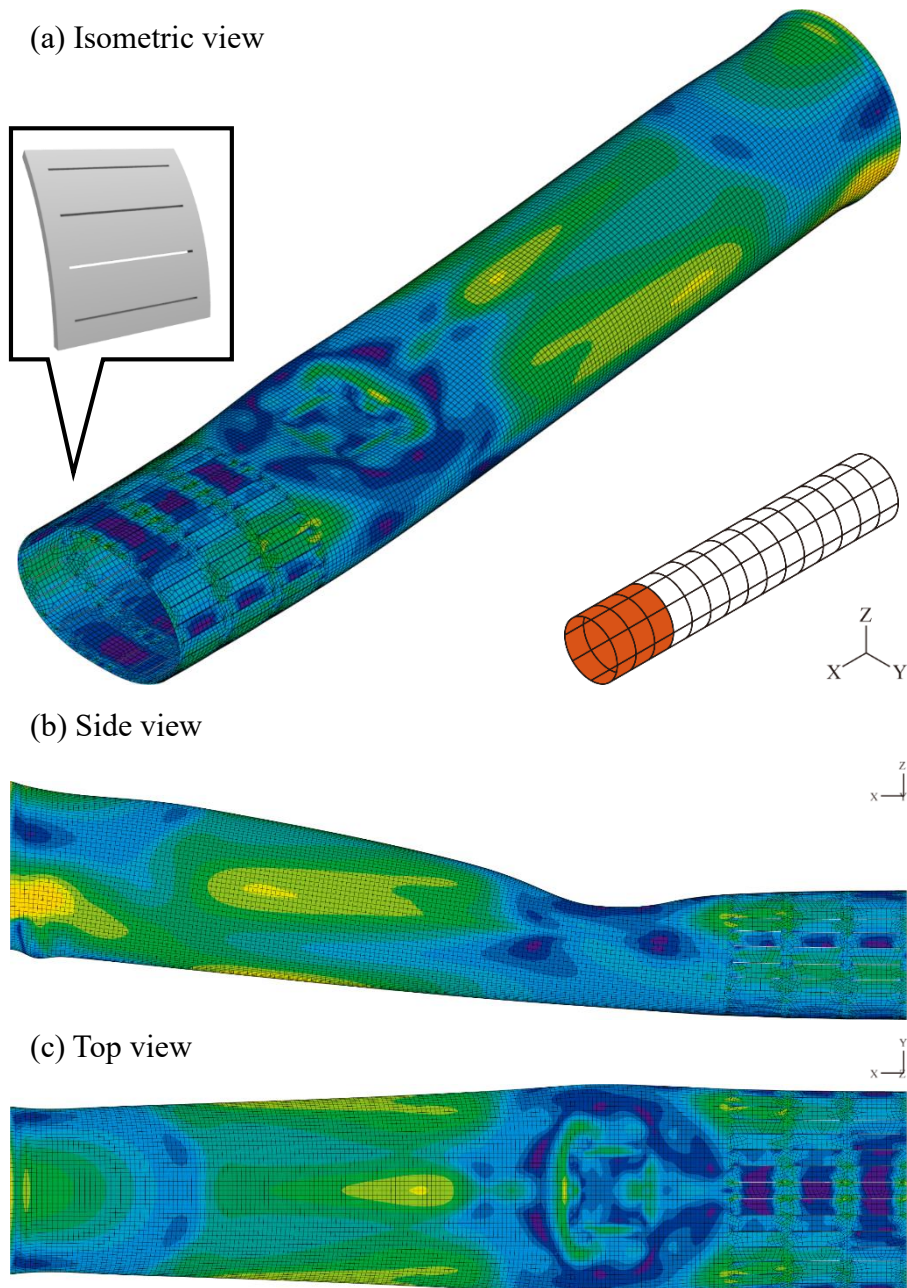


Figure 5.25. Deformed shape with effective stress of thin-walled tube with the reference slits on 3 sub-tubes. The pattern range is 3 sub-tubes, H/H_D of the reference slit is 0.012, W/W_D is 0.800, the number of slit on a sub-domain is 4, and the number of total slits is 96. (a) Isometric view. (b) Side view. (c) Top view.

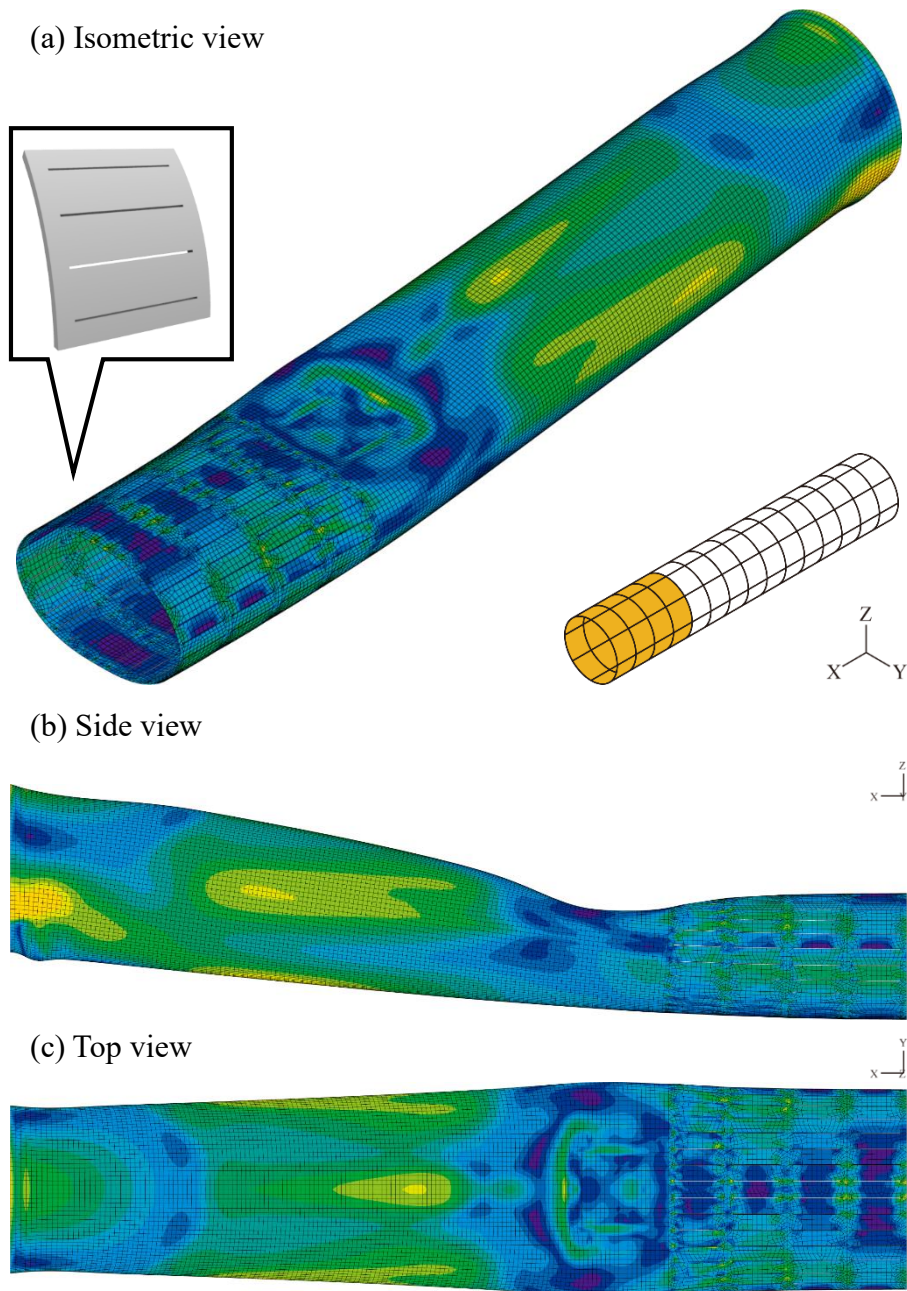


Figure 5.26. Deformed shape with effective stress of thin-walled tube with the reference slits on 4 sub-tubes. The pattern range is 4 sub-tubes, H/H_D of the reference slit is 0.012, W/W_D is 0.800, the number of slit on a sub-domain is 4, and the number of total slits is 128. (a) Isometric view. (b) Side view. (c) Top view.

5.4.2 The effect of different pattern range

In this section, we looked at how the pattern range of the tube with slits affects how the tube deforms under transverse loading. We choose a single longitudinal slit of $H/H_D = 0.012$ and $W/W_D = 0.08$ as the reference. The pattern range of the tube is changed to make the plastic deformation of the tube wider. The pattern range is defined as the number of sub-tubes in which slit patterns are engraved from the center of the tube, and the three representative pattern ranges are 2 sub-tubes, 3 sub-tubes, and 4 sub-tubes. The quantity of slit patterns engraved in one sub-domain is changed from 1 to 6, and the total slit area of the three representative pattern ranges differs depending on the pattern range. We obtain maximum center deflection and the ellipticity of cross-section from nonlinear dynamic finite element analysis, and bending and torsional rigidities from static finite element analysis.

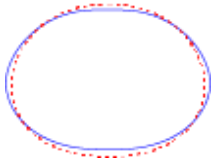
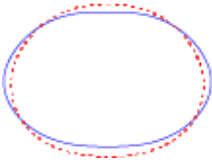
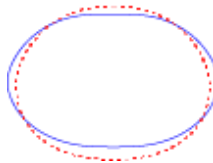
	2 Sub-tubes	3 Sub-tubes	4 Sub-tubes
Cross-section shape (Red dash: Reference Blue line: Patterned)			
Max. Deflection	- 8.41 %	- 12.07 %	- 15.14 %
Ellipticity	+ 49.79 %	+ 70.17 %	+ 79.18 %
Bending rigidity	- 0.55 %	- 0.83 %	- 1.01 %
Torsional rigidity	- 34.29 %	- 43.85 %	- 51.00 %

Table 5.4. Cross-section shape, maximum deflection, ellipticity of center cross-section, bending and torsional rigidity of the tube with pattern range of 2, 3, 4 sub-tubes. All values are calculated as percent with reference to the value of the tube without patterns.

In order to perform a nonlinear dynamic-implicit analysis of the pipe with slits, we chose three slit pattern ranges with the reference rectangular slit and varied the quantity of patterns on one sub-domain. When the quantity of patterns on one sub-domain, the slit patterns are arranged in circumferential direction and the interval between the slit patterns is the same. When the pattern range is 2 sub-tubes, slit patterns are generated in two consecutive sub-tubes from the center of the tube and occupy 16 sub-domains out of 120 sub-domains. When the pattern range is 3 sub-tubes, slit patterns are generated in three consecutive sub-tubes from the center of the tube and occupy 24 sub-domains out of 120 sub-domains. When the pattern range is 4 sub-tubes, slit patterns are generated in four consecutive sub-tubes from the tube center and occupy 32 sub-domains out of 120 sub-domains. Therefore, by applying reference rectangular slit patterns to various pattern ranges, we examine the influence of the pattern range on the maximum tube's center displacement. Although the quantity of patterns engraved in one sub-domain is the same, the total area of slit patterns is different because the pattern range of the tube is different. In particular, in this section, to study the influence of the pattern range on the tube deformation, we focused on comparing the cases with different pattern ranges and the same quantity of slit patterns on a sub-domain. The results are calculated through nonlinear dynamic analysis for tubes with different pattern ranges, and compared with the results of the unpatterned tube as a reference.

Comparing the maximum center displacement with pattern ranges of 2 sub-tubes, 3 sub-tubes, and 4 sub-tubes, the overall tendency of the highest center deflection according to the change in the quantity of slit patterns on a sub-domain is similar for the tubes with different pattern ranges. As the quantity of slit patterns increases, the maximum center deflection with three different pattern ranges decreases and then converges. In particular, when the number of slit patterns increases from 1 to 2, in three cases, the maximum center deflection decreases the most. Also, when the number of slit patterns is 3 or 4, the maximum center deflection of all tubes with different pattern ranges tends to converge.

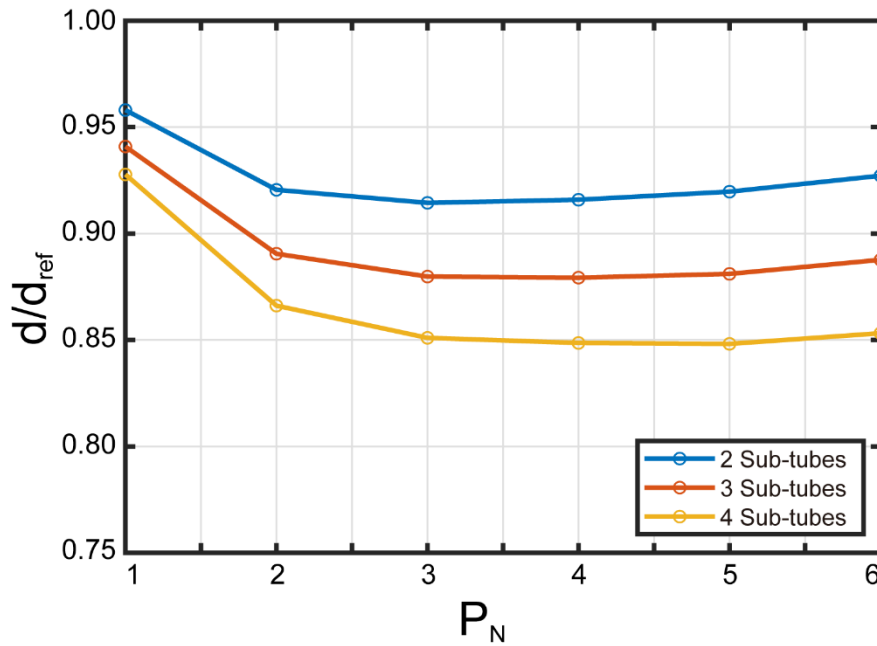


Figure 5.27. Non-dimensional maximum center deflection of the tube with respect to the different pattern ranges and P_N .

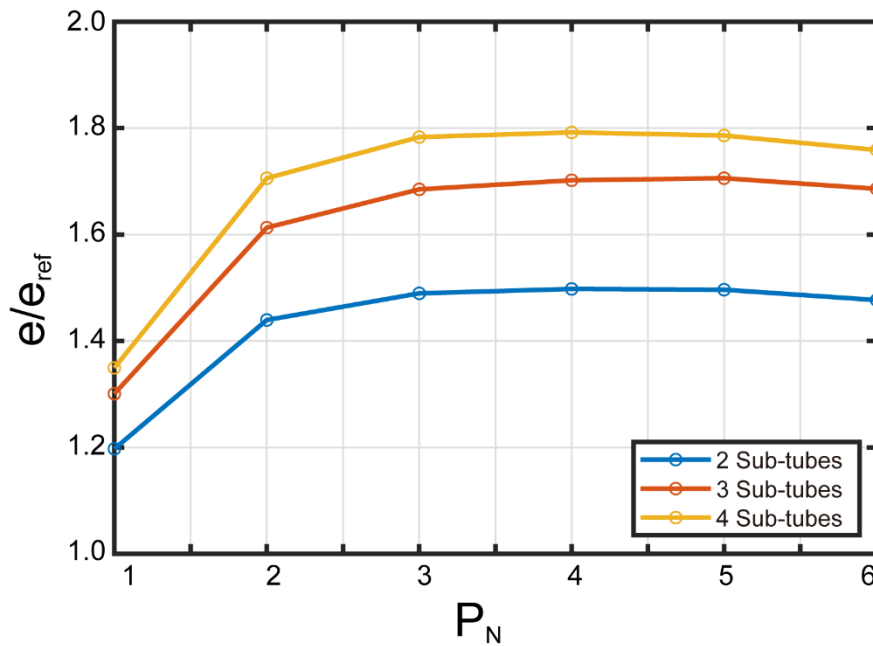


Figure 5.28. Non-dimensional ellipticity of the center cross-section of the tube with respect to the different pattern ranges and P_N .

The ellipticity change of tube center cross-section with different pattern ranges according to the number of slit patterns shows a similar tendency to the maximum center deflection. As the number of slit patterns increases, the ellipticity of center cross-section of the tubes with three different the pattern ranges of 2 sub-tubes, 3 sub-tubes, and 4 sub-tubes increases and then converges. In particular, when the number of slit patterns increases from 1 to 2, in three different pattern ranges, the ellipticity of center cross-section increases the most. Also, when the number of slit patterns is 3 or 4, the ellipticity of center cross-section of all tubes with different pattern ranges tends to converge.

As the quantity of slit patterns on a sub-domain increases, the trends in maximum center deflection and ellipticity of center cross-section of the tube show that the design concepts described in Chapter 2 are reflected. Our intended design concept is to reduce the maximum center deflection by making the center cross-section of the tube more elliptical by engraving slit patterns on a localized area of the tube. When the number of slit patterns is changed from 1 to 2, the maximum center deflection decreases the most and the ellipticity of center cross-section increases the most. The reason for this phenomenon is because of the principle that the discontinuous curve lines divided by the slit pattern are transformed from a circle to an ellipse from a cross-sectional perspective. The unpatterned tube's cross section changes from a circle made up of one continuous line to an ellipse. However, when a pattern is engraved on the tube, the cross-section is not one continuous line, and discontinuous lines divided by the slit patterns form a circle, and it changes to an oval shape by impact loading. That is, if one pattern is engraved on each sub-domain, the cross-section is divided into 8 discontinuous lines, and when two patterns are engraved on each sub-domain, the cross-section is divided into 16 discontinuous lines. Due to the quantity of discontinuous lines, the cross section is more effectively transformed from a circle to an ellipse when the number of pattern is two than when the number of pattern is one on each sub-domain.

Next, comparing the maximum center deflection and the cross-section ellipticity when the quantity of slits on a sub-domain is the same, the differences

according to different pattern ranges are shown in the highest center deflection and the cross-section ellipticity. The reason for this phenomenon is the effective stress distribution on the thin-walled tube, which is shown through the tube's deformed shape with effective stress from the nonlinear dynamic analysis. The finite element analysis on the tube deformation performed in this section is carried out by generating each finite element tube model with different pattern ranges. The way to engrave reference slits on a sub-domain is the arrangement in the circumferential direction referred to in the preceding section. The finite element model consists of different pattern ranges of 2 sub-tubes, 3 sub-tubes, and 4 sub-tubes from the sub-domain engraved with the reference pattern, and the remaining parts are composed of sub-tubes without patterns. Comparing the deformed shapes of tubes with different pattern ranges obtained by performing finite element analysis, the difference in effective stress distribution in the deformed shape is shown according to the different pattern ranges. The important difference in the deformed shape with effective stress in the three pattern ranges of 2 sub-tubes, 3 sub-tubes, and 4 sub-tubes is the concentrated effective stress region shown in yellow. When the pattern range is 2 sub-tubes, a yellow region exists, but when the pattern range is 4 sub-tubes, there is no concentrated effective stress region. In other words, the wider the pattern range, the more distribute the concentrated effective stress on the tube. Considering these deformed shape of the tubes, the maximum center deflection, and the ellipticity of center cross-section together, the wider the pattern range, the wider the flexible range of the tube due to the influence of patterns. In addition, the flexible part deforms the cross-section into an elliptical shape, and as a result, the maximum center deflection decreases. The expected effect of pattern range on the deformation of the tube is to widen the pattern range of the tube to expand the plastic deformation occurred in the tube. The deformed tube shape with different pattern ranges, as we intended, shows that when the pattern range is widened close to the impact point, more plastic deformation occurs and the center cross-section is more effectively elliptical.

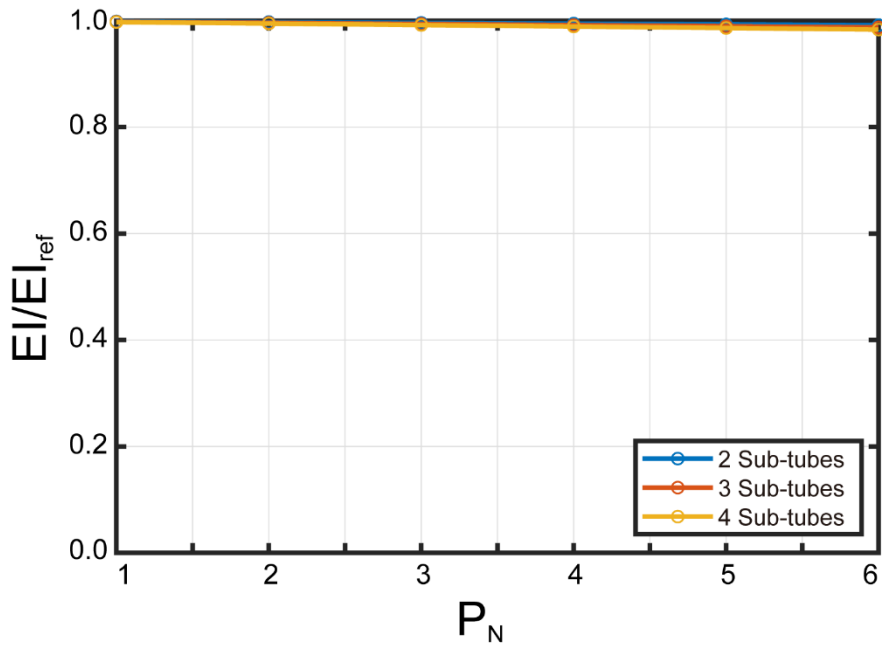


Figure 5.29. Non-dimensional bending rigidity of the tube with respect to the different pattern ranges and P_N .

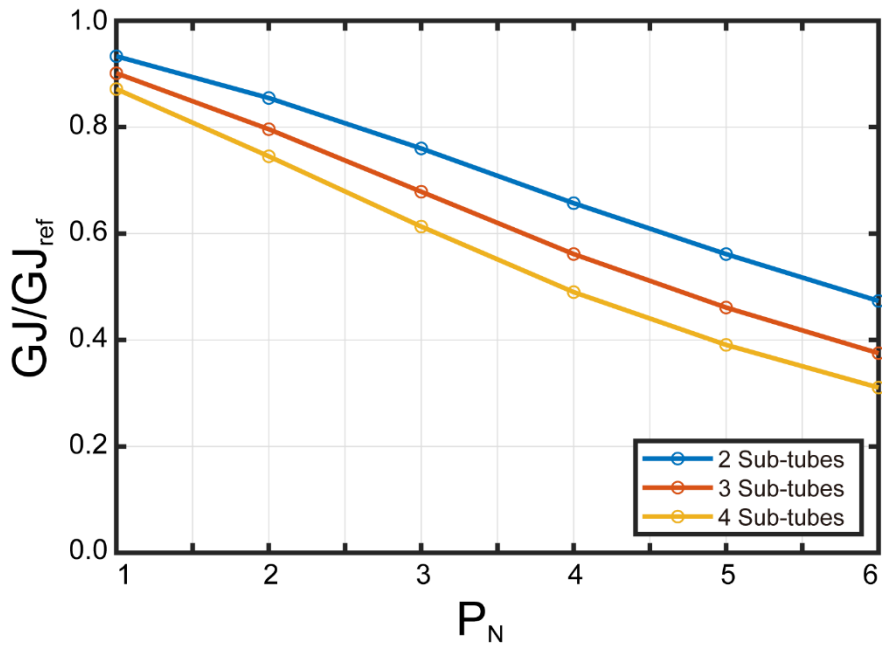


Figure 5.30. Non-dimensional torsional rigidity of the tube with respect to the different pattern ranges and P_N .

Static analysis is performed to determine the bending rigidity with three pattern ranges of 2 sub-tubes, 3 sub-tubes, and 4 sub-tubes based on the amount of slit patterns on a sub-domain. The overall tendency of bending rigidity of tubes with different pattern ranges decreases as the number of slit patterns increases. Also, even if the amount of slit patterns on a sub-domain is the same, the total number of slit patterns is different because the tubes have different pattern ranges. Therefore, the bending rigidity is further reduced when the pattern range is 4 sub tubes than when the pattern range is 2 sub-tubes. Since the reference slit pattern has a very small area, the bending rigidity of the tubes with different pattern ranges is almost the same as the bending rigidity of the tube without patterns. Next, comparing the torsional rigidity of the tube with three pattern ranges of 2 sub-tubes, 3 sub-tubes, and 4 sub-tubes, the torsional rigidity of tubes tends to decrease as the number of slit patterns increases. The reason for this is because of the shape of the tube divided by the slits of the longitudinal shape, and the tendency is the same as the torsional rigidity of the tube engraved with the circumferential division slits of the previous section. In other words, by cutting-out longitudinal slits from the tube, the tube shape is created in a form weak to torsional loading. Therefore, as the pattern range is widened, more longitudinal slits are generated and the parts weak to torsional loading are also increased, so the torsional rigidity is further reduced.

To sum up, as predicted, the center deflection decreases with the patterned range while increasing with the cross section ellipticity. The larger the more flexible area in cross section, the more evenly the stress is distributed along the tube. Consequently, the energy is more efficiently used as the cross section deforms due to the larger patterned area. However, when P_N reaches to 3~4, its effect becomes saturated. Related to prior parametric studies, the range of the patterned area has little effect on the bending rigidity.

5.5 Stress concentration in the deformed tube caused by the slit pattern

5.5.1 Stress concentration in the thin-walled tube with slit patterns

In previous sections, we studied the effect of the shape, amount, height of the slit pattern and the range of slit pattern on the deformation. Through the effect on the shape of the slit pattern, it was proved that the long slit shape in the axial direction of the tube was beneficial in producing an elliptical cross section and decreasing the center displacement. It was effective to reduce center deflection by arranging several longitudinal slits instead of one by changing the number in one sub-domain of the slit pattern, and it was more effective as the pattern height became thinner. In addition, it was demonstrated that the center deflection can be effectively reduced by making the slit pattern engraving range wider to enlarge the impact-induced plastic deformation area. In conclusion, by controlling the shape of this slit pattern, when transverse impact is applied to the tube, the center part is made flexible and energy is dissipated by plastic deformation. By controlling this plastic deformation, it was possible to deform the cross-section into an oval shape and reduce the center deflection as a result. The thin-walled circular tube used in the study is actually a part used as a cowl cross bar for a vehicle, so it is a structure that is deformed by instantaneous transverse impact. Since the tube structure dented by impact is not recycled, stress concentration was not considered under the condition of instantaneous impact load. However, the cowl cross bar experiences a situation in which vibrations or very minute bending loads are repeatedly generated while the vehicle is being driven, unless a momentary impact occurs. In general, it is known that when a slit pattern is engraved on a tube structure, stress concentration occurs around the slit pattern, causing problems such as cracks and fatigue. Therefore, even in the thin-walled tube structure of this study, stress concentration will occur around the slit pattern due to the engraving of the slit pattern. In order to recognize the stress concentration problem due to the slit pattern of the cowl crossbar, the boundary condition was changed to a general displacement load condition rather than an

instantaneous impact condition. The existing boundary conditions were all kept the same, and the loading condition applied to the rigid plate at the impact point was changed from the drop weight method to the displacement method. Displacement load is a method of pressing the tube and rigid plate down by 20mm from the moment when the tube and rigid plate contact the gap of 2mm. Finite element analysis was performed by applying the changed loading condition, and the deformation shape of the tube without a slit pattern and the tube with a slit pattern was compared. The deformed tube shape was expressed as stress distribution. Through the analysis results, the tube's center deflection and the stress distribution were derived, and the place where the highest effective stress occurs is indicated by a red triangle. Comparing the unpatterned tube's deformed shape and the tube with the slit pattern, it is evident that center cross section is deformed into an oval shape due to the slit pattern, reducing center deflection. In addition, when the stress distribution and the position of the maximum effective stress were compared, the maximum effective stress occurred near the impact point when there was no slit pattern. However, when the slit pattern is engraved, it can be confirmed that it occurs around the slit pattern, not around the impact point. Comparing the maximum effective stress values, it can be seen that the slit pattern has a higher value than the case without the slit pattern. This proves that the slit pattern caused stress concentration around the slit pattern.

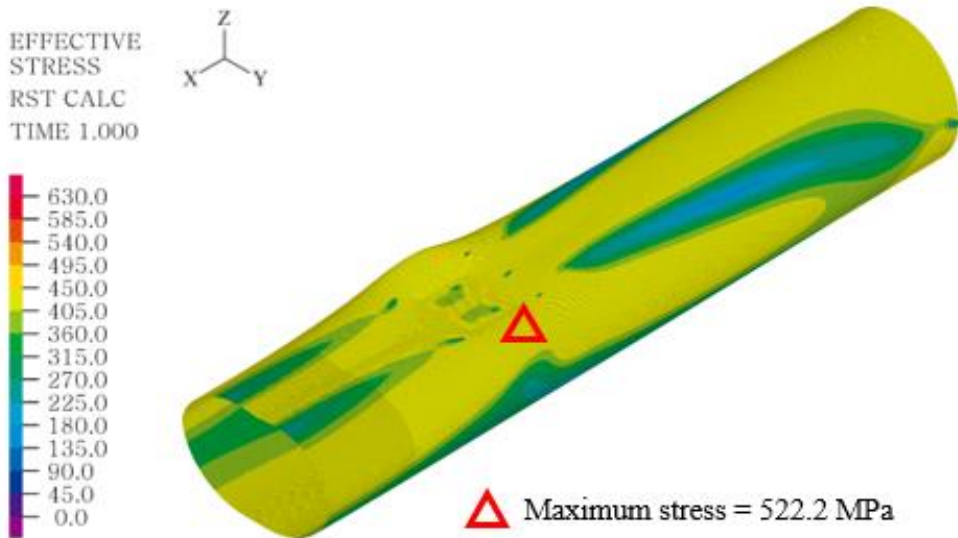


Figure 5.31. The stress distribution of the deformed shape of the tube without slit patterns. A red triangle indicates where the maximum effective stress occurs.

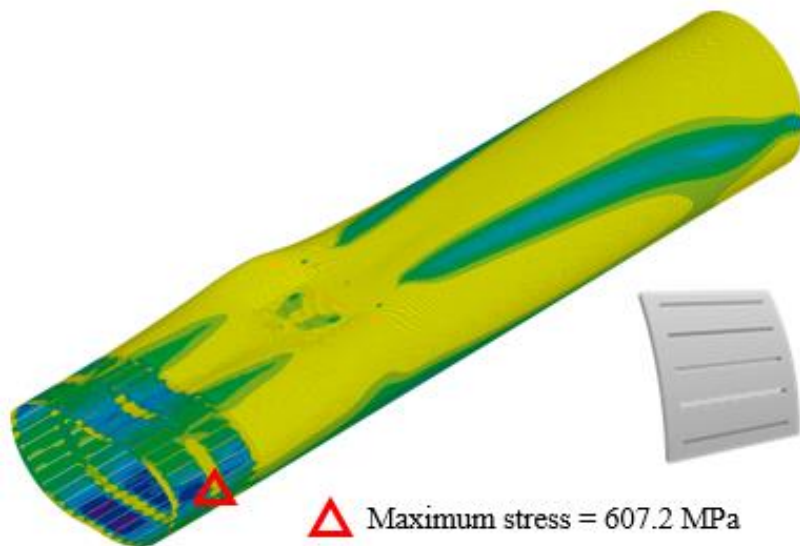


Figure 5.32. The stress distribution of the deformed shape of the tube with slit patterns. A red triangle indicates where the maximum effective stress occurs.

5.5.2 Slit pattern design to reduce stress concentration

Through the previous section, the maximum effective stress value of the unpatterned tube and the tube with slit patterns were compared. As a result, it was confirmed that the maximum effective stress value increased by about 16% due to the slit patterns. As described above, when stress concentration occurs, the possibility of problems such as cracks and fatigue generally increases in the slit pattern region. In order to reduce the possibility of these problems, it is essential to adjust the position where stress is concentrate or to modify the shape of the slit pattern that can reduce the maximum effective stress value. Therefore, this section introduces the modified slit pattern shape to reduce the stress concentration while maintaining the center deflection reduction effect caused by the existing slit patterns. For the shape of the modified slit pattern, the height and length of the slit were fixed to maintain the effect of the existing slit pattern, and a method of engraving holes at both ends of the slit was applied to reduce the stress concentration occurring around the slit pattern. The modified slit pattern was applied to the tube to perform finite element analysis under the given simulation conditions, and as a result, center deflection, deformed shape with stress distribution, and maximum effective stress were calculated. For the modified slit patterns, the number of patterns was applied from 1 to 6 in 1 sub-domain.

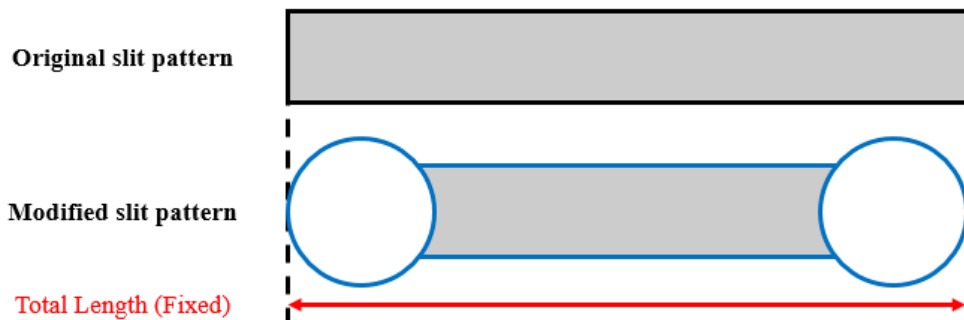


Figure 5.33. Original slit pattern means a rectangle slit pattern. Modified slit pattern is a form in which holes are drilled at both ends of the slit pattern, and the blue border line means the final shape of the modified slit pattern.

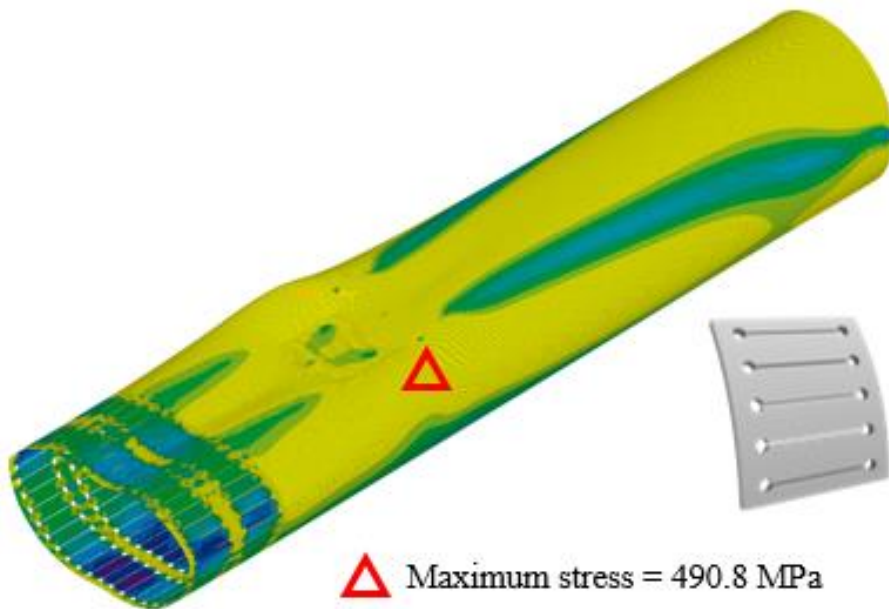


Figure 5.34. The stress distribution of the deformed shape of the tube with modified slit patterns. A red triangle indicates where the maximum effective stress occurs.

First, comparing the non-dimensional deflection according to the quantity of patterns in 1 sub-domain, it can be confirmed that the reduction effect of the center deflection due to the slit pattern to be maintained is maintained. This is because, when designing the modified slit pattern, the height and total length of the pattern were kept the same to maintain the center deflection reduction effect due to the slit pattern. The overall shape of the modified slit pattern was designed to be similar to the previous rectangular slit pattern, so that center cross section was easily deformed into an oval shape due to slit pattern. However, in the modified slit pattern, holes were formed at both ends, and the overall pattern area was larger than the previous rectangular slit, so the center deflection decreased slightly less.

Next, comparing the relationship between non-dimensional center deflection and non-dimensional maximum effective stress, it is clear that the maximum effective stress is reduced by about 15% on average due to the modified slit pattern. The effect of reducing the maximum effective stress is due to the holes formed at both ends of the modified slit pattern. In general, the cause of stress concentration is at the sharp edge of the existing rectangular slit, and to solve the stress concentration problem, a hole is drilled here to dissipate the effective stress a little more effectively. In conclusion, the maximum effective stress values were reduced by applying the modified slit pattern, and the center deflection reduction effect due to the slit pattern was maintained, thereby reducing the possibility of occurrence of problems such as cracks and fatigue due to stress concentration.

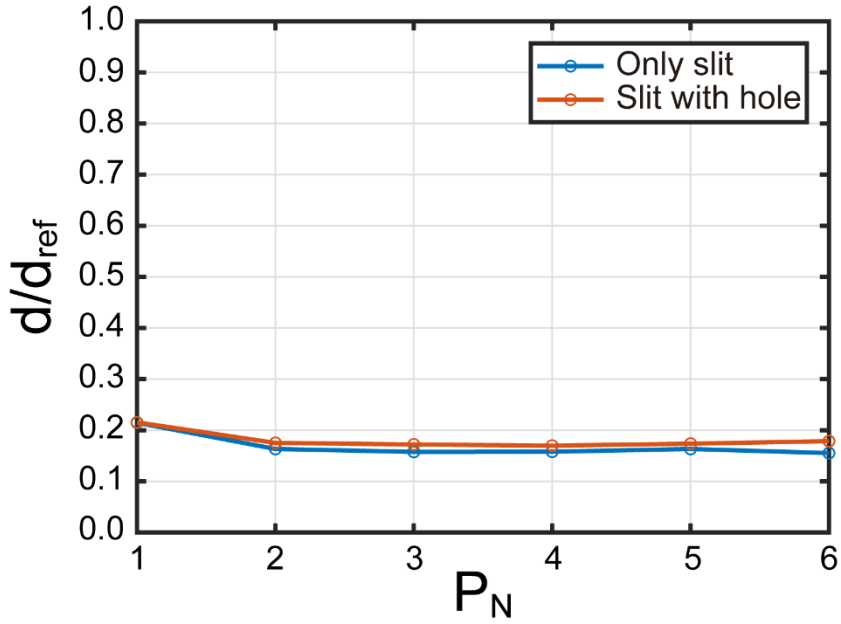


Figure 5.35. Non-dimensional center deflection of the tube with respect to the different slit pattern and P_N .

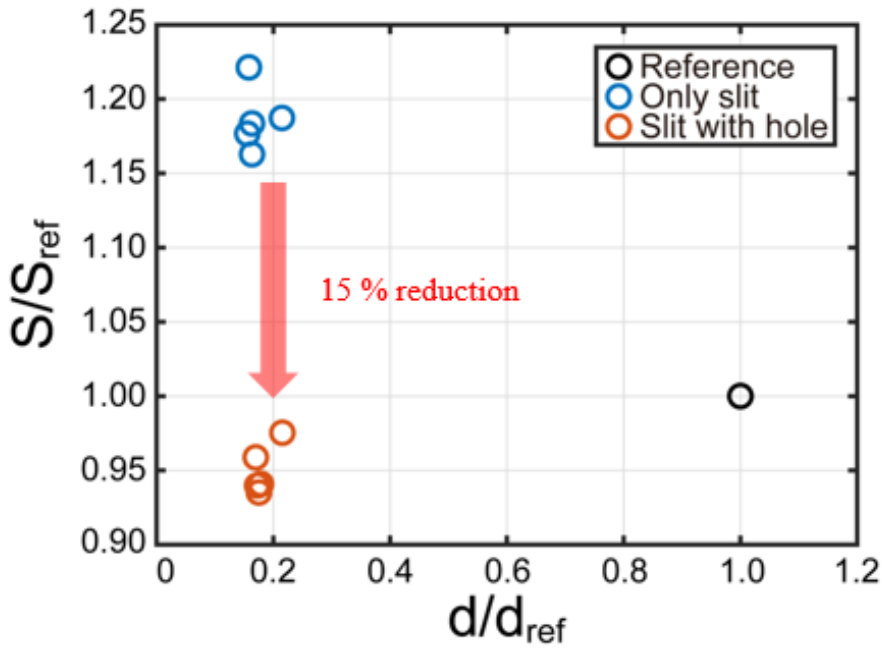


Figure 5.36. Non-dimensional maximum effective stress of the tube with respect to non-dimensional center deflection and different slit pattern.

5.6. The effect of slit pattern on thin-walled tubes of different shapes

In this chapter, we study whether the effect of the pattern also affects thin-walled tubes of other shapes. In the previous chapters, only circular tubes were considered. Considering the plastic deformation of circular thin-walled tube under transverse loading, the position where the slit will be engraved was defined. To engrave the slit, the finite element model was reconstructed from sub-domain to sub-tube and half tube. Slit patterns were engraved in the sub-domain, and the effect of the shape, number, height, and range of patterns engraved on plastic deformation of circular thin-walled structure was analyzed. The effect of this slit pattern was used to reduce permanent deflection of circular thin tubes due to transverse impact. Therefore, to confirm whether the effect of the slit pattern can be applied to thin tubes of different shapes, finite element models of thin-walled tubes having different shapes were constructed and nonlinear finite element analysis was performed. Longitudinal slit patterns were engraved and the pattern range was applied to a section of 100 mm from the center of each tube. All values are % values compared to tubes without patterns, and maximum center deflection, width and height of cross-section were calculated. In conclusion, it was confirmed that the center deflection due to the transverse impact can be reduced by applying the slit patterns even if the shapes of the tubes are different.

	Circle	Rectangle	Hexagon
Max. Deflection	- 14.90 %	- 0.57 %	- 13.07 %
Cross-section Width	+ 8.44 %	+ 2.57 %	+ 2.81 %
Cross-section Height	- 13.55 %	- 0.81 %	- 6.74 %

Table 5.5. Maximum deflection, cross-section width and height for circle, rectangle and hexagon shaped thin-walled tube. All values were calculated as % based on each tubes without patterns.

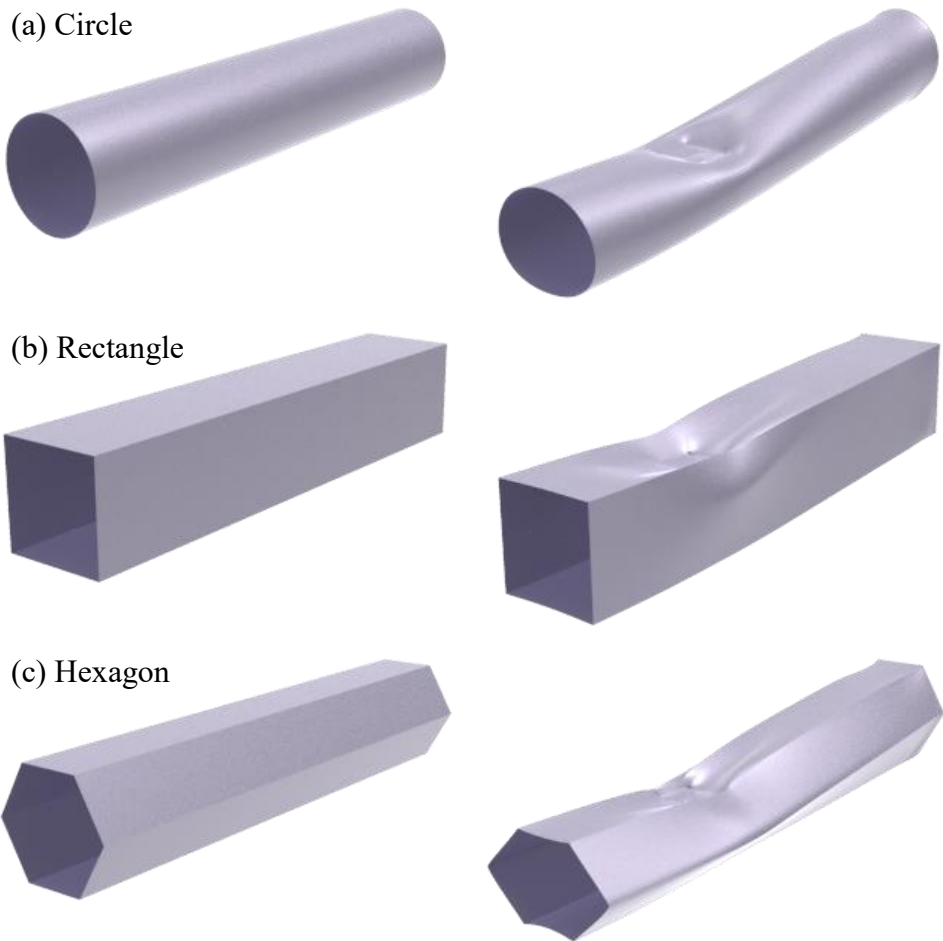


Figure 5.37. Undeformed and deformed shapes of un-patterned thin-walled tubes with different cross-section shapes subjected to transverse impact. (a) Circle. (b) Rectangle. (c) Hexagon.

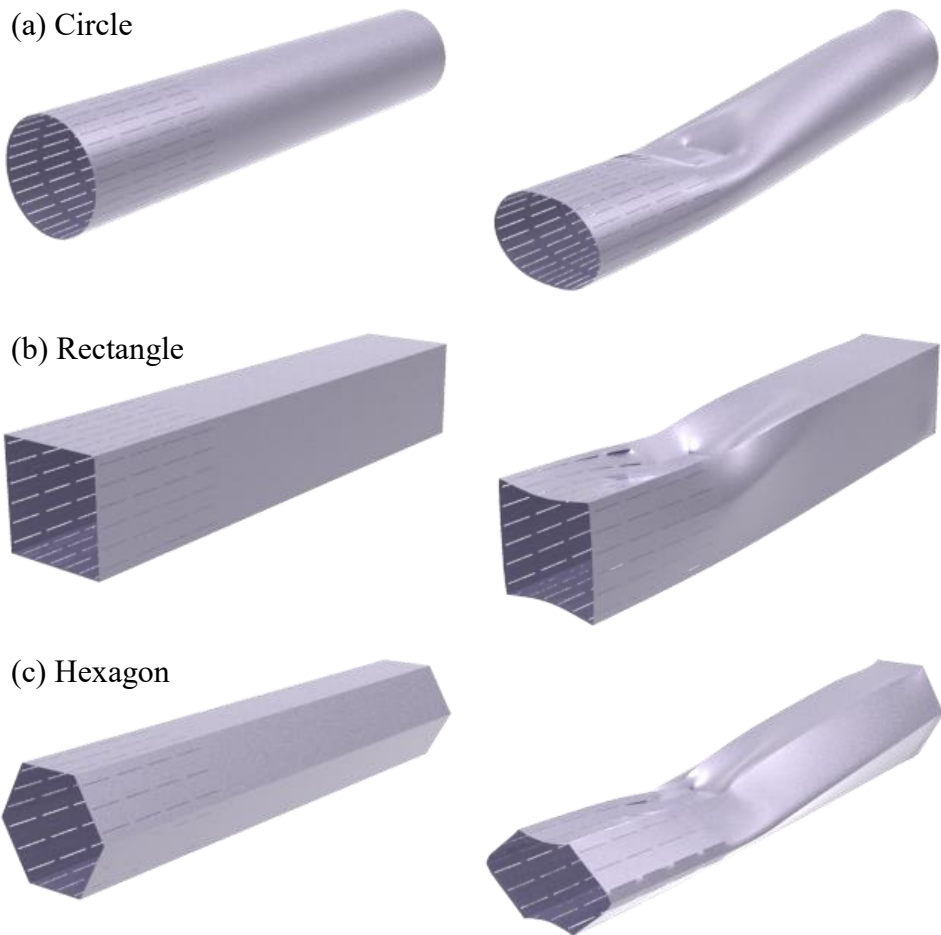


Figure 5.38. Undeformed and deformed shapes of patterned thin-walled tubes with different cross-section shapes subjected to transverse impact. (a) Circle. (b) Rectangle. (c) Hexagon.

5.7. Conclusion

In this chapter, we investigate the tube's deformation with multiple slit patterns on a sub-domain. First, we divided a longitudinal slit pattern in circumferentially and longitudinally to create more slit patterns, and we looked at the impact of the various division direction. Next, we select three longitudinal slit patterns with different heights, increase the quantity of slit patterns in circumferentially, and study the influence of different pattern height on deformation. In addition, we increase the number of slit patterns with different pattern ranges to make plastic deformation wider, and research the effect of dissimilar pattern ranges on the deformation. Considering the influences of multiple slit patterns on the deformation, arranging thin longitudinal slits in circumferentially on the tube is efficient in minimizing the tube's maximum center deflection. Also, it is advantageous in reducing the maximum center displacement because it induces more plastic deformation when the longitudinal slits are engraved to widen range.

Chapter 6

Concluding remark

We talked about the mechanism of tube plastic deformation under transverse loading, the design idea to minimize the maximum deflection, and the influence of the slit pattern. We proposed the design concept of engraving slits on the tube surface to reduce the maximum deflection. The reason for presenting this design concept is that the stiffness of the structure can be controlled by engraving patterns on the structure without patterns, and the deformation mode of the structure can be controlled by using this. Therefore, by engraving slit pattern on the tube to control the deformation mode, we tried to decrease tube maximum displacement. Additionally, we used simulation analysis to examine the deformation tube shape with slits in order to investigate the effect of slits on the displacement. The maximum center deflection could be decreased, according to finite element analysis, if the cross section deformation into an elliptic shape could absorb more of the impact energy. We added slits around the center to improve it more flexible during the cross section deformation in order to investigate this possibility. Our analysis shows that thin longitudinal slits are beneficial in lowering the tube's center displacement under transverse loading. By applying more and thinner slits in circumferentially for a larger range on the tube's surface, we can enhance this effect. It is noteworthy that adding slit patterns has little effect on the tube's bending stiffness. In conclusion, engraving longitudinal slits close to the center of the tube is a successful method of lowering the maximum deflection under transverse impact without adding to the weight. In other words, by engraving longitudinal slits around the center of the tube,

it distributes the concentrated effective stress and makes the local region of the structure more flexible. This effect makes the cross-section more elliptical and reduces the permanent deflection. We verified the proposed design concept by analyzing the slit effect on the tube deformation under transverse impact.

We present the limitation in that the slit effect on reducing maximum deflection has been verified when the transverse impact of the present conditions is applied to the thin-walled tube. However, even if the boundary and loading conditions are altered, we can reduce the maximum center displacement by applying the effects of width and height, quantity, and the pattern range of slit patterns. Therefore, we suggest that it is necessary to expand the study on the slit effect on the tube deformation according to the location and number of impact points, the thickness, and the change of slenderness ratio. By analyzing the deformation of the structure without slits in the suggested studies and regulating the plastic deformation mode of the structure by taking the effect of the slit patterns into account, we anticipate that the greatest center permanent deflection can be reduced.

Bibliography

1. Krishnamurthy, K., P. Mahajan, and R. Mittal, *A parametric study of the impact response and damage of laminated cylindrical composite shells*. Composites Science and Technology, 2001. **61**(12): p. 1655-1669.
2. Lim, T.S., *Mechanically fastened composite side-door impact beams for passenger cars designed for shear-out failure modes*. Composite structures, 2002. **56**(2): p. 211-221.
3. Hosseinzadeh, R., M.M. Shokrieh, and L.B. Lessard, *Parametric study of automotive composite bumper beams subjected to low-velocity impacts*. Composite Structures, 2005. **68**(4): p. 419-427.
4. Marzbanrad, J., M. Alijanpour, and M.S. Kiasat, *Design and analysis of an automotive bumper beam in low-speed frontal crashes*. Thin-walled structures, 2009. **47**(8-9): p. 902-911.
5. Ayhan, A.O., K. Genel, and S. Ekşi, *Simulation of nonlinear bending behavior and geometric sensitivities for tubular beams with fixed supports*. Thin-walled structures, 2012. **51**: p. 1-9.
6. Kong, B.S. and D.K. Park, *Design optimization of the cowl cross bar-light cowl cross bar satisfying 5 performances*. International Journal of Automotive Technology, 2018. **19**(3): p. 387-391.
7. Baroutaji, A., M. Sajjia, and A.-G. Olabi, *On the crashworthiness performance of thin-walled energy absorbers: recent advances and future developments*. Thin-Walled Structures, 2017. **118**: p. 137-163.
8. Ghadianlou, A. and S.B. Abdullah, *Crashworthiness design of vehicle side door beams under low-speed pole side impacts*. Thin-Walled Structures, 2013. **67**(2): p. 25-33.
9. Černiauskas, E., et al., *Investigation of anti-intrusion beams in vehicle side doors*. Mechanics, 2010. **86**(6): p. 11-16.

10. Guler, M.A., et al., *The effect of geometrical parameters on the energy absorption characteristics of thin-walled structures under axial impact loading*. International Journal of Crashworthiness, 2010. **15**(4): p. 377-390.
11. Ghamarian, A. and H. Zarei, *Crashworthiness investigation of conical and cylindrical end-capped tubes under quasi-static crash loading*. International journal of crashworthiness, 2012. **17**(1): p. 19-28.
12. Mohsenizadeh, S., et al., *Crashworthiness assessment of auxetic foam-filled tube under quasi-static axial loading*. Materials & Design, 2015. **88**: p. 258-268.
13. Yoon, T.H., et al., *An experiment and FE simulation for the development of a SPFC1180 AHSS one-body door impact beam about a car side collision*. International Journal of Precision Engineering and Manufacturing, 2016. **17**(1): p. 81-89.
14. Nichit, Y. and A. Battu, *Development of side door intrusion beam of passenger car for maximum bending load*. Int. J. Sci. Adv. Res. Technol., 2017. **3**(8): p. 1-6.
15. Tsang, H. and S. Raza, *Impact energy absorption of bio-inspired tubular sections with structural hierarchy*. Composite Structures, 2018. **195**: p. 199-210.
16. Gao, Q., et al., *Multi-objective crashworthiness optimization for an auxetic cylindrical structure under axial impact loading*. Materials & design, 2018. **143**: p. 120-130.
17. Zhou, G., et al., *Multi-objective reliability design optimization of a novel side door negative Poisson's ratio impact beam*. Proceedings of the Institution of Mechanical Engineers, Part D: Journal of automobile engineering, 2018. **232**(9): p. 1196-1205.
18. Cheon, S.S. and K.S. Jeong, *Composite side-door impact beams for passenger cars*. Composite structures, 1997. **38**(1-4): p. 229-239.
19. Feraboli, P., et al., *Crush energy absorption of composite channel section specimens*. Composites Part A: Applied Science and Manufacturing, 2009. **40**(8): p. 1248-1256.
20. Ben, G., N. Sugimoto, and Y. Aoki, *Development of simulation technology*

- for impact behavior of CFRP/Al alloy hybrid beams in side collision of automobiles. Advanced Composite Materials, 2010. 19(4): p. 363-379.*
21. Saraf, S. and P. Bajaj, *Design & experimentation of side impact beam for Hyundai Verna. IRJET, 2017. 4(06): p. 62-69.*
 22. Wu, C., et al., *Discrete topology optimization of ply orientation for a carbon fiber reinforced plastic (CFRP) laminate vehicle door. Materials & Design, 2017. 128: p. 9-19.*
 23. Gupta, N. and S. Gupta, *Effect of annealing, size and cut-outs on axial collapse behaviour of circular tubes. International journal of mechanical sciences, 1993. 35(7): p. 597-613.*
 24. Song, J., Y. Chen, and G. Lu, *Light-weight thin-walled structures with patterned windows under axial crushing. International Journal of Mechanical Sciences, 2013. 66: p. 239-248.*
 25. Taştan, A., et al., *Optimum crashworthiness design of tapered thin-walled tubes with lateral circular cutouts. Thin-Walled Structures, 2016. 107: p. 543-553.*
 26. Chen, L., et al., *Dynamic crushing behavior and energy absorption of graded lattice cylindrical structure under axial impact load. Thin-Walled Structures, 2018. 127: p. 333-343.*
 27. Guo, Y., et al., *Deformation behaviors and energy absorption of auxetic lattice cylindrical structures under axial crushing load. Aerospace Science and Technology, 2020. 98: p. 105662.*
 28. Hur, J.M., et al., *Harnessing distinct deformation modes of auxetic patterns for stiffness design of tubular structures. Materials & Design, 2021. 198: p. 109376.*
 29. Thomas, S., S. Reid, and W. Johnson, *Large deformations of thin-walled circular tubes under transverse loading—I: an experimental survey of the bending of simply supported tubes under a central load. International Journal of Mechanical Sciences, 1976. 18(6): p. 325-333.*
 30. Watson, A., et al., *Large deformations of thin-walled circular tubes under transverse loading—II: Experimental study of the crushing of circular tubes by centrally applied opposed wedge-shaped indenters. International Journal*

- of Mechanical Sciences, 1976. **18**(7-8): p. 387-397.
31. Mamalis, A., et al., *On the effect of shear when bending crashworthy thin-walled steel tubes*. Thin-walled structures, 1992. **14**(2): p. 153-165.
 32. Elchalakani, M., X.L. Zhao, and R.H. Grzebieta, *Plastic mechanism analysis of circular tubes under pure bending*. International Journal of Mechanical Sciences, 2002. **44**(6): p. 1117-1143.
 33. Mamalis, A., et al., *Bending of cylindrical steel tubes: numerical modelling*. International Journal of Crashworthiness, 2006. **11**(1): p. 37-47.
 34. Poonaya, S., C. Thinwongpituk, and U. Teeboonma, *An Analysis of collapse mechanism of thin-walled circular tubes subjected to bending*. Proceedings of WASET, 2007. **26**: p. 329.
 35. Liu, Y. and M.L. Day, *Bending collapse of thin-walled circular tubes and computational application*. Thin-Walled Structures, 2008. **46**(4): p. 442-450.
 36. Thinwongpituk, C., et al. *The ovalisation of thin-walled circular tubes subjected to bending*. in *World Congress on Engineering*. 2008. Citeseer.
 37. Zhang, Z., S. Liu, and Z. Tang, *Design optimization of cross-sectional configuration of rib-reinforced thin-walled beam*. Thin-walled structures, 2009. **47**(8-9): p. 868-878.
 38. Poonaya, S., U. Teeboonma, and C. Thinwongpituk, *Plastic collapse analysis of thin-walled circular tubes subjected to bending*. Thin-walled structures, 2009. **47**(6-7): p. 637-645.
 39. Khedmati, M.R. and M. Nazari, *A numerical investigation into strength and deformation characteristics of preloaded tubular members under lateral impact loads*. Marine Structures, 2012. **25**(1): p. 33-57.
 40. Xu, F., X. Tian, and G. Li, *Experimental study on crashworthiness of functionally graded thickness thin-walled tubular structures*. Experimental Mechanics, 2015. **55**(7): p. 1339-1352.
 41. Boreanaz, M. and G. Belingardi, *Development of crash box for automotive application*. Politecnico di Torino, Italy, 2018.
 42. Tugcu, P. and J. Schroeder, *Plastic deformation and stability of pipes exposed to external couples*. International Journal of Solids and Structures, 1979. **15**(8): p. 643-658.

43. Zhang, L. and T. Yu, *An investigation of the brazier effect of a cylindrical tube under pure elastic-plastic bending*. International journal of pressure vessels and piping, 1987. **30**(2): p. 77-86.
44. Wierzbicki, T. and M. Suh, *Indentation of tubes under combined loading*. International Journal of Mechanical Sciences, 1988. **30**(3-4): p. 229-248.
45. Kecman, D., *Bending collapse of rectangular and square section tubes*. International Journal of Mechanical Sciences, 1983. **25**(9-10): p. 623-636.
46. Corona, E., L.-H. Lee, and S. Kyriakides, *Yield anisotropy effects on buckling of circular tubes under bending*. International Journal of Solids and Structures, 2006. **43**(22-23): p. 7099-7118.
47. Hilditch, T., et al., *Performance of wrought aluminium and magnesium alloy tubes in three-point bending*. Materials & Design, 2009. **30**(7): p. 2316-2322.
48. Ungureanu, V., et al., *Plastic mechanisms database for thin-walled cold-formed steel members in compression and bending*. Thin-walled structures, 2010. **48**(10-11): p. 818-826.
49. Sadowski, A.J. and J.M. Rotter, *Solid or shell finite elements to model thick cylindrical tubes and shells under global bending*. International Journal of Mechanical Sciences, 2013. **74**: p. 143-153.
50. Sun, G., et al., *Dynamical bending analysis and optimization design for functionally graded thickness (FGT) tube*. International Journal of Impact Engineering, 2015. **78**: p. 128-137.
51. Tang, T., et al., *Crushing analysis of thin-walled beams with various section geometries under lateral impact*. Thin-Walled Structures, 2016. **102**: p. 43-57.
52. Zhang, J., et al., *A theoretical study of low-velocity impact of metal foam-filled circular tubes*. Thin-Walled Structures, 2020. **148**: p. 106525.
53. Estrada, Q., et al., *Bending crashworthiness of elliptical tubes with different aspect ratio and stiffeners*. The International Journal of Advanced Manufacturing Technology, 2022: p. 1-20.
54. Do, Y. and D.-N. Kim, *Investigating the effect of slit patterns on the deformation of thin-walled tubes under side impact*. Journal of Mechanical Science and Technology, 2022. **36**(11): p. 5649-5655.

국 문 초 록

최근 교통수단의 점진적인 발달로 인하여 도로 위의 차량이 증가하고 있으며 교통사고 또한 증가하고 있다. 이에 따라 탑승객의 충돌 안정성 확보 문제가 핵심 이슈로 급부상하고 있다. 승객의 안전을 확보하기 위해서는 충격을 받는 구조물이 충격 에너지를 흡수하고 승객의 안전을 위협하는 구조적 변형을 최소화하는 것이 필요하다. 충격 하중을 받는 구조에는 박판 구조들이 가장 널리 사용되며 비행기, 자동차, 기차와 같은 곳에도 사용되어오고 있다. 그 중에서도 본 연구에서는 차량에 사용되는 카울 크로스 바의 박판 튜브에 대해 초점을 맞추고 있으며 충돌로 인해 발생하는 변형에 대해 분석한다. 카울 크로스 바의 박판 튜브 구조는 횡방향 충격으로 인해 변형이 발생하고 이 변형이 탑승객 쪽을 향하게 되며 탑승객의 상해를 야기하게 된다. 이러한 구조는 충격으로 인해 발생하는 영구적인 변형을 줄임으로써 탑승객의 안전을 확보할 수 있다.

영구적인 변형을 감소시키기 위한 선행 연구들은 재료를 개선하거나 기하학적 구조를 개선하는 방식으로 진행되어오고 있다. 하지만 기존의 방식들은 고비용, 추가적인 무게 증가라는 문제점이 존재한다. 이에 본 연구에서는 슬릿 패턴을 이용하여 변형 모드를 조절하여 추가적인 무게 증가 없이 박판 튜브의 영구적인 변형을 감소시키고자 한다.

본 연구에서는 유한요소해석을 통해 횡방향 충격을 받는 박판 튜브 구조의 변형에 대해 분석한다. 충격으로 인해 박판 튜브의 중앙부에 발생하는 최대 처짐을 감소시키기 위해 양쪽의 충돌부 사이에 슬릿 패턴을 새긴다. 슬릿 패턴의 종횡비, 두께, 개수 및 새겨지는 범위를 조절하여 슬릿 패턴이 박판 튜브의 최대 처짐에 미치는 영향에 대해 연구한다. 본 연구를 통해 종방향 슬릿이 충격 에너지를 소모하여 박판 튜브의 단면 형상을 타원형으로 변형시키는데 효과적이며 박판 튜브의 최대 처짐을 감소시킬 수 있는데 효과적이라는 사실을 도출하였다. 또한, 패턴을 새김으로써 박판 튜브의 굽힘강성이 크게 감소하지 않는다는 점과 추가적인 무게 증가가 없다는 장점이 존재한다.

주요어 : 박판 튜브, 유한요소법, 횡방향 충격, 슬릿 패턴

학 번 : 2014-21878